USGS
science for a changing world

Volcanic Aquifers of Hawai‘i—Construction and Calibration of Numerical Models for Assessing Groundwater Availability on Kaua‘i, O‘ahu, and Maui

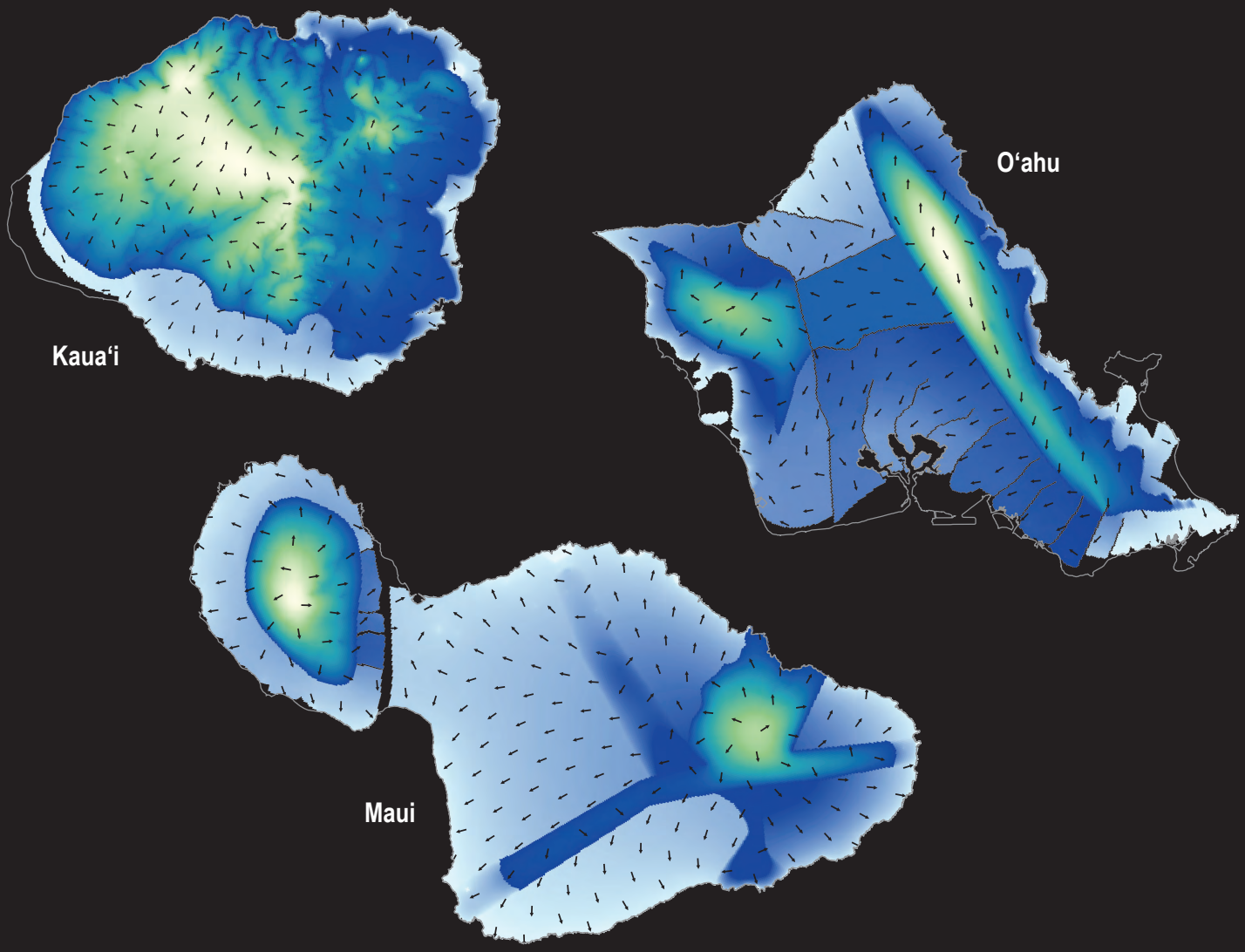

Scientific Investigations Report 2020–5126

U.S. Department of the Interior
U.S. Geological Survey

Cover. Images of simulated head and groundwater flow in the calibrated numerical groundwater models of Kaua‘i, O‘ahu, and Maui.

Volcanic Aquifers of Hawai‘i—Construction and Calibration of Numerical Models for Assessing Groundwater Availability on Kaua‘i, O‘ahu, and Maui

By Scot K. Izuka, Kolja Rotzoll, and Tracy Nishikawa

Scientific Investigations Report 2020–5126

U.S. Department of the Interior
U.S. Geological Survey

U.S. Geological Survey, Reston, Virginia: 2021

For more information on the USGS—the Federal source for science about the Earth, its natural and living resources, natural hazards, and the environment—visit https://www.usgs.gov or call 1–888–ASK–USGS.

For an overview of USGS information products, including maps, imagery, and publications, visit https://store.usgs.gov.

Suggested citation:
Izuka, S.K., Rotzoll, K., and Nishikawa, T., 2021, Volcanic Aquifers of Hawai‘i—Construction and calibration of numerical models for assessing groundwater availability on Kaua‘i, O‘ahu, and Maui: U.S. Geological Survey Scientific Investigations Report 2020-5126, 63 p., https://doi.org/10.3133/sir20205126.

Associated data for this publication:
Rotzoll, K., and Izuka, S.K., 2021, MODFLOW-2005 and SWI2 models for assessing groundwater availability in volcanic aquifers on Kaua‘i, O‘ahu, and Maui, Hawai‘i: U.S. Geological Survey data release, https://doi.org/10.5066/P9K4DK2P.

ISSN 2328-0328 (online)

Geographic and Geologic Names

Geographic names in this report are largely consistent with the U.S. Board on Geographic Names (http://geonames.usgs.gov), including the use of the ʻokina (ʻ) and kahakō (¯) diacritical marks in Hawaiian names. The diacritical marks are not used in anglicized derivations from Hawaiian names (for example, the ʻokina appears in the name "Hawaiʻi" but not in the derivation "Hawaiian"), or where a place name appears without the diacritical marks in an established proper noun or title in a cited reference. Names of geologic formations and features are consistent with the State geologic map by Sherrod and others (2007).

The entire group of Hawaiian Islands and the largest island in the group are named "Hawaiʻi." To avoid confusion, the island group is referred to as "Hawaiʻi" and the largest island is referred to as "Hawaiʻi Island." Other islands (for example, Oʻahu, Maui, and Kauaʻi) are simply referred to by their names because there is no potential for confusion with other geographic entities.

Acknowledgments

This report is a product of the Hawaiʻi Volcanic Aquifer Study, one of the regional groundwater-availability studies supported by the U.S. Geological Survey (USGS) Water Availability and Use Science Program. The authors are grateful to the following people and organizations that contributed expertise and data to this study: Robert Whittier (Hawaiʻi State Department of Health), Chris Langevin (USGS), Joseph Hughes (USGS), Michael Fienen (USGS), Delwyn Oki (USGS), Lisa Miller (USGS), and Stephen Gingerich (USGS). Jason Bellino (USGS) and William Souza (USGS, retired) provided helpful technical reviews.

Contents

Figures

Tables

Conversion Factors

U.S. customary units to International System of Units

Multiply	By	To obtain
inch (in.)	2.54	centimeter (cm)
foot (ft)	0.3048	meter (m)
mile (mi)	1.609	kilometer (km)
square foot (ft^2)	0.09290	square meter (m^2)
square mile (mi^2)	2.590	square kilometer (km^2)
gallon (gal)	3.785	liter (L)
cubic foot (ft^3)	0.02832	cubic meter (m^3)
million gallons per day (Mgal/d)	0.04381	cubic meter per second (m^3/s)
inch per year (in/yr)	25.4	millimeter per year (mm/yr)

Temperature in degrees Celsius (°C) may be converted to degrees Fahrenheit (°F) as °F = (1.8 × °C) + 32.

Temperature in degrees Fahrenheit (°F) may be converted to degrees Celsius (°C) as °C = (°F – 32) / 1.8.

Datum

Horizontal coordinate information is referenced to the North American Datum of 1983 (NAD 83).

Altitude, as used in this report, refers to distance above mean sea level.

Volcanic Aquifers of Hawai‘i—Construction and Calibration of Numerical Models for Assessing Groundwater Availability on Kaua‘i, O‘ahu, and Maui

By Scot K. Izuka, Kolja Rotzoll, and Tracy Nishikawa

Abstract

Steady-state numerical groundwater-flow models were constructed for the islands of Kaua‘i, O‘ahu, and Maui to enable quantification of the hydrologic consequences of withdrawals and other stresses that can place limits on groundwater availability. The volcanic aquifers of Hawai‘i supply nearly all drinking water for the islands’ residents, freshwater for diverse industries, and natural discharge to springs, streams, and nearshore areas that support ecosystems, cultural practices, aesthetics, and recreation. Increases in groundwater withdrawal and changes in climate can cause water-table depression, saltwater rise, and reduction of natural groundwater discharge—all of which can limit fresh groundwater availability. The numerical models described in this report are designed to quantify these consequences. Separate models were created for each island using MODFLOW-2005 with the Seawater Intrusion package, which allows simulation of freshwater and saltwater in ocean-island aquifers. Calibration resulted in models that generally replicate observed water-level, stream base-flow, and spring-flow data, and simulate groundwater-flow directions and fresh groundwater thicknesses that are consistent with conceptual models. The calibrated models use hydraulic properties that are consistent with the ranges reported in previous studies. The models show that the relative distribution of fresh groundwater discharge to the ocean, streams, and springs and withdrawals for human use differ substantially among the three islands studied here. These differences indicate that consequences that limit the availability of fresh groundwater for human use are likely to differ among the three islands.

Introduction

Kaua‘i, O‘ahu, and Maui are among the eight main islands of Hawai‘i (fig. 1). These islands are the tops of immense basaltic shield volcanoes that rise from the floor of the Pacific Ocean. The volcanoes form aquifers that supply nearly all of the drinking water for Hawai‘i’s 1.4 million residents (U.S. Census Bureau, 2011)—including a large component of U.S. military presence in the Pacific region—and freshwater for diverse industries. Natural groundwater discharge to springs, streams, and submarine seeps near the coast support aquatic ecosystems, cultural practices, aesthetics, and recreation.

Hawai‘i’s volcanic aquifers are considered among the principal regional aquifers in the United States (Reilly and others, 2008), but their capacity to store freshwater is limited. The islands of Hawai‘i are small and each is surrounded by saltwater. No fresh groundwater can flow naturally between islands, so high withdrawals on one island cannot be mitigated by lower withdrawals on another. Also, many aquifers contain saltwater that permeates from the ocean (fig. 2). Because of the limited storage capacity, fresh groundwater resources are vulnerable to increases in groundwater withdrawal and to reductions in groundwater recharge that result from changes in land cover, short-term climate cycles, and long-term climate change.

Limits to Groundwater Availability

Any withdrawal of groundwater affects the hydrologic system. Effects of withdrawing fresh groundwater from Hawai‘i’s aquifers include (1) water-table decline, (2) saltwater rise, (3) reduction in the natural discharge rate to springs, streams, and submarine seeps, and (4) reduction in flow to adjacent groundwater bodies. For a given area of an island, the type and magnitude of the effect depend on the rates and distribution of recharge and withdrawals, and the geologic structure and distribution of hydraulic properties of the aquifer. The availability of fresh groundwater for human use is limited by the magnitude of the consequences that are deemed acceptable by the community and water-resource managers. For example, availability of fresh groundwater may be limited by the desire to constrain saltwater rise to protect existing freshwater wells or maintain minimum streamflows for

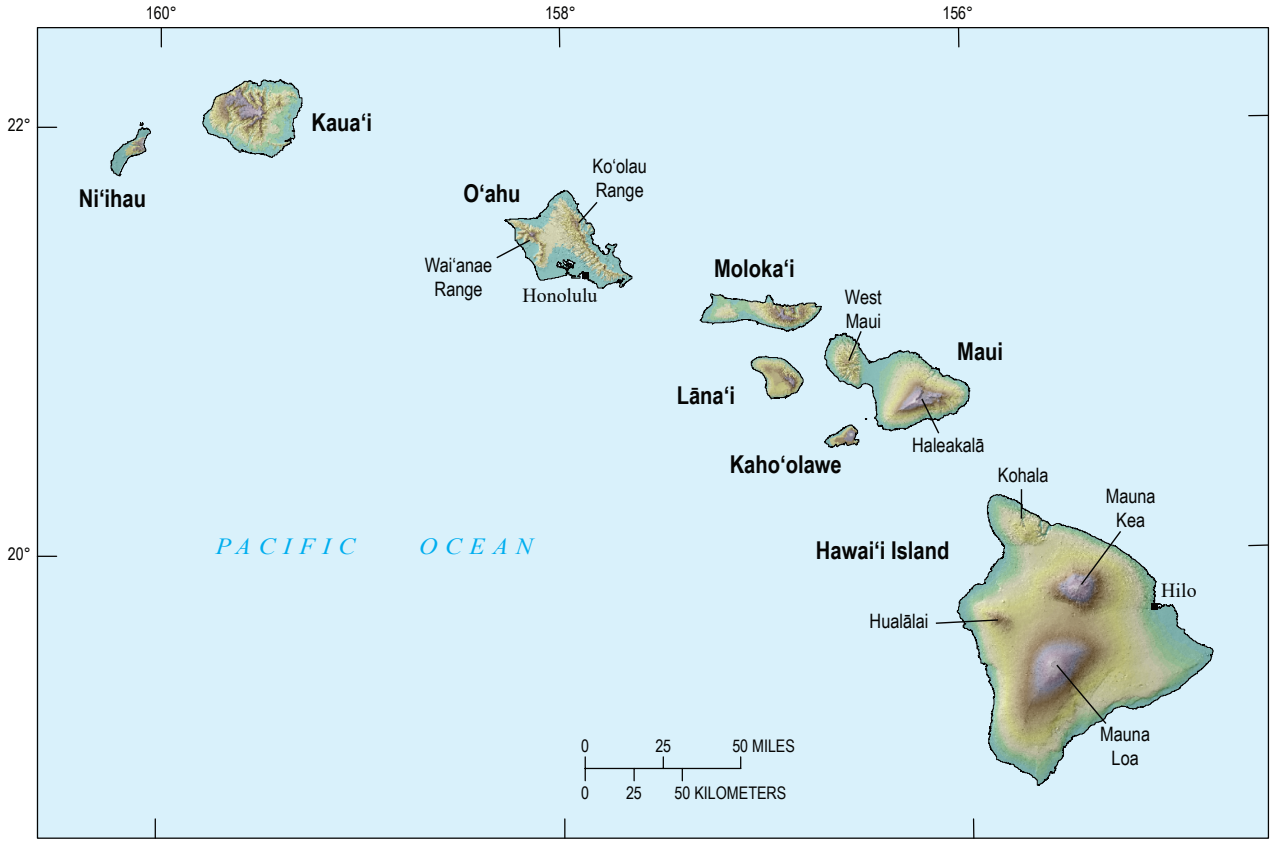

Base modified from U.S. Geological Survey 10-meter digital elevation model
Universal Transverse Mercator zone 4 north
North American Datum of 1983

Figure 1. Map of the Hawaiian Islands.

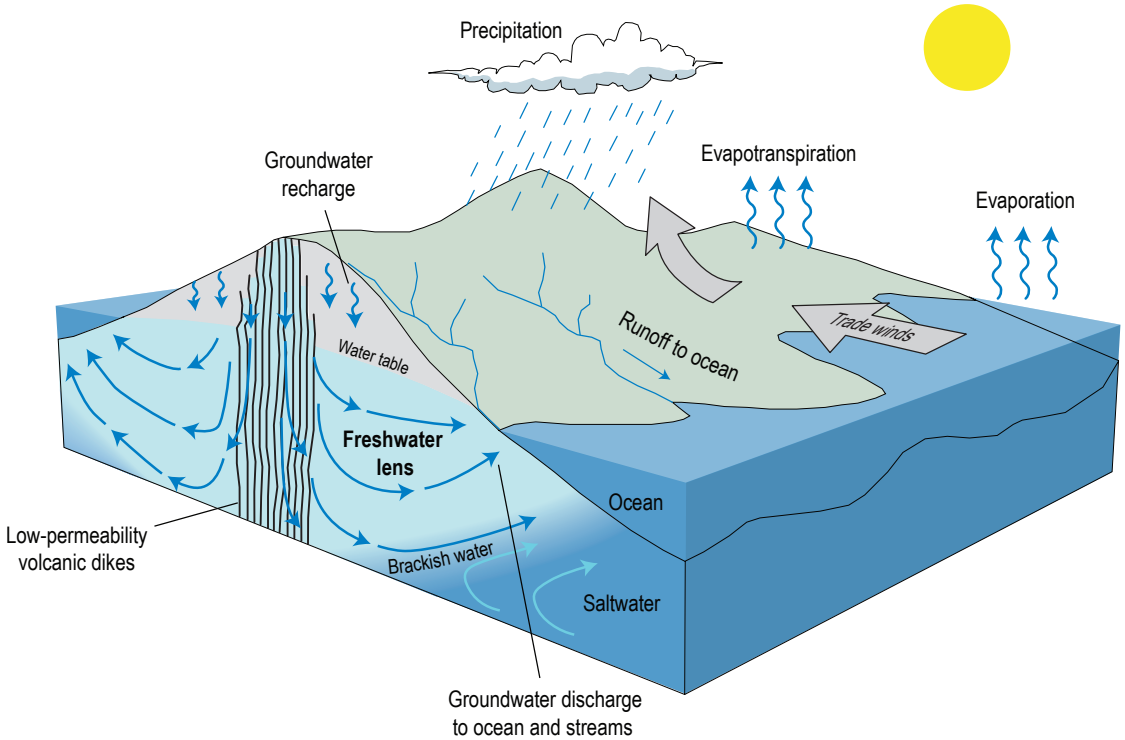

Figure 2. Three-dimensional illustration showing the relation of fresh groundwater in oceanic islands to precipitation, evapotranspiration, runoff, and saltwater. Modified from Izuka and others (2018).

aquatic habitats. The consequences of groundwater withdrawals therefore can translate to limits on groundwater availability.

Quantification of the consequences of groundwater withdrawals, including exacerbation by climate change, provides key decision-support information for groundwater management. Numerical modeling is currently the most comprehensive approach to analyzing the many factors that determine the consequences of groundwater withdrawal. Although any approach is limited by data availability, numerical modeling can consider more of the relevant data, particularly spatially variable data such as distribution of hydraulic properties. Other approaches require broader simplifying assumptions, ignore some available data, or are limited to generic geometries.

Numerical models can be used to simulate various scenarios of withdrawal, such as predevelopment (no-withdrawal) conditions, current withdrawal rates, or future projected rates. Comparing the water-table altitude, transition-zone altitude, and the natural discharge rates for different scenarios allows quantification and assessment of the spatial distribution of the consequences of groundwater withdrawals. Similarly, the effects of changing groundwater recharge—as might result from climate or land-use changes—can be quantified by comparing model scenarios that represent different recharge conditions. Key to quantifying effects related to changes in withdrawals or recharge for Hawaii's volcanic aquifers is the construction and calibration of numerical models that represent the hydrogeology of the islands.

Purpose and Scope

The purpose of the numerical groundwater models is to assess availability of fresh groundwater in the volcanic aquifers of Hawai‘i. To meet this objective, the models were designed to quantify the consequences of groundwater withdrawal that can lead to limits on the amount of groundwater available from Hawai‘i's volcanic aquifers: (1) water-table decline, (2) saltwater rise, (3) reduction of natural discharge to springs, streams, and submarine seeps, and (4) reduction in flow to adjacent groundwater bodies.

This report describes the construction and calibration of numerical groundwater models of the volcanic aquifers in three islands in Hawai‘i: Kaua‘i, O‘ahu, and Maui. These islands have 86 percent of the population and the bulk of the groundwater demand in Hawai‘i. O‘ahu has 70 percent of Hawaii's population, Maui has 11 percent, and Kaua‘i has 5 percent (Izuka and others, 2018). Hawai‘i Island also has a considerable fraction of Hawai‘i's population (14 percent), but it was not included in this study because its hydrogeology is not known well enough to meet the purposes of this study. The other main islands of Hawai‘i (Ni‘ihau, Moloka‘i, Lāna‘i, and Kaho‘olawe) together constitute only 8.1 percent of the land area and have less than 1 percent of the population.

Overview of the Regional Setting

Kaua‘i, O‘ahu, and Maui lie in the trade-wind belt of the tropical North Pacific Ocean. The climate for most areas in the islands is characterized by mild temperatures, moderate humidity, and prevailing northeasterly trade winds (Giambelluca and Schroeder, 1998). Precipitation distribution is influenced by the northeasterly trade winds and orographic effect—trade winds blow against the mountain slopes, forcing air to rise and cool and water to condense (fig. 2). As a result, rainfall amounts are high on northeast-facing (windward) slopes and on most mountain crests. Rainfall ranges from less than 10 inches per year (in/yr) on some leeward coasts to more than 400 in/yr on some windward slopes and can vary by more than an order of magnitude within 5 horizontal miles (Giambelluca and others, 1986, 2013). The peaks of the tallest mountains—such as Haleakalā on Maui—are arid because the orographic effect is limited to an altitude of about 7,200 feet (ft) by the trade-wind inversion (Giambelluca and others, 2013). Occasional migratory storm systems can bring rain to any part of an island, and are the main form of precipitation in areas that do not receive substantial orographic rain (Giambelluca and others, 2013). Fog interception by vegetation is another source of water for high-altitude forests in Hawai‘i (Juvik and Nullet, 1995).

Human activity has affected Hawai‘i's groundwater resources for centuries, not only by groundwater withdrawals from wells, but also as a result of changes in groundwater recharge related to changes in land use, such as expanding urbanization, deforestation and reforestation, displacement of native forests by nonnative species, and agricultural irrigation. More recently, the decline and ultimate closure of large sugarcane (and to a lesser extent pineapple) plantations set an important point of change in groundwater use and recharge in the islands. These plantations had dominated Hawai‘i's agriculture and industry from the late 19th century and used hundreds of millions of gallons of surface water and groundwater per day for irrigation and processing. The plantations began declining in the later decades of the 20th century and most were closed by the early 21st century. Some former sugarcane and pineapple fields have been converted to other forms of agriculture and some have been urbanized, but much of the former agricultural land is currently covered by grass and shrub.

Hydrogeologic Overview

Although the hydrogeology of each island in Hawai‘i is unique in detail, the islands share some similarities owing to their common origin as basaltic shield volcanoes. The hydrogeology and conceptual models of Hawai‘i's volcanic aquifers were described in detail by Izuka and others (2018). This section summarizes their description, particularly

aspects relevant to construction of numerical models to assess groundwater availability on Kaua‘i, O‘ahu, and Maui. Summaries of hydrogeology and conceptual models for individual islands discussed later in this report are also largely based on descriptions by Izuka and others (2018).

Eruptive Stages

The shield volcanoes that form the islands of Hawai‘i were built from the ocean floor by mid-plate hot-spot volcanism (Macdonald and others, 1983; Clague and Dalrymple, 1987). As a result of the northwestward motion of the Pacific Plate over the relatively stationary Hawaiian Hot Spot, the islands are successively younger toward the southeastern part of the chain. The shield volcanoes along the island chain are also at different stages of geologic development. Four stages are recognized in the life of Hawaiian volcanoes; in order of occurrence these are preshield, shield, postshield, and rejuvenation (Clague and Dalrymple, 1987; Clague and Sherrod, 2014). Only the last three stages form aquifers containing freshwater resources presently used by humans in Hawai‘i (fig. 3).

The shield stage is the principal stage of growth for Hawai‘i’s shield volcanoes (fig. 3*A*) and forms 90 percent or more of the subaerial volume of each shield volcano (Clague and Dalrymple, 1987). The stage is characterized by highly fluid lava erupted near the volcano’s summit and rift zones (Macdonald and Katsura, 1964; Macdonald and others, 1983). Most shield volcanoes also have, or are presumed to have had, a summit caldera, but the caldera can be alternately filled and reformed during the life of the shield volcano (Wolfe and Morris, 1996). Shield-stage lava erupted above sea level typically forms thin lava flows with an average thickness of about 15 ft (Macdonald and others, 1983). These thin lava flows accumulate to create the immense dome-shaped mountains that characterize shield volcanoes. Shield-volcano islands sink as they grow; as a result, lavas that were formed subaerially can occur thousands of feet below sea level (Moore, 1987).

Postshield-stage volcanism is characterized by eruptions that are less frequent than in the shield stage, and the lava is more viscous, lava flows are thicker and shorter, and tephra deposits are more common (Stearns, 1946, 1966; Macdonald and others, 1983). Although postshield-stage rocks can be areally extensive, they only form a thin cap on Hawai‘i’s shield volcanoes (fig. 3*B*). Some shield volcanoes in Hawai‘i do not have postshield-stage rocks.

Some shield volcanoes in Hawai‘i have rejuvenation-stage volcanism. This stage is characterized by eruptions that are even less frequent than those of the postshield stage (Stearns, 1946, 1966; Macdonald and others, 1983). Rejuvenation-stage eruptions form small edifices and lava flows that overlie, commonly unconformably, the much more voluminous shield-stage lavas (fig. 3*C*). Rejuvenation-stage deposits vary widely in character from ash to lava flows. Lava-flow thickness can vary depending on lava viscosity and preexisting topography.

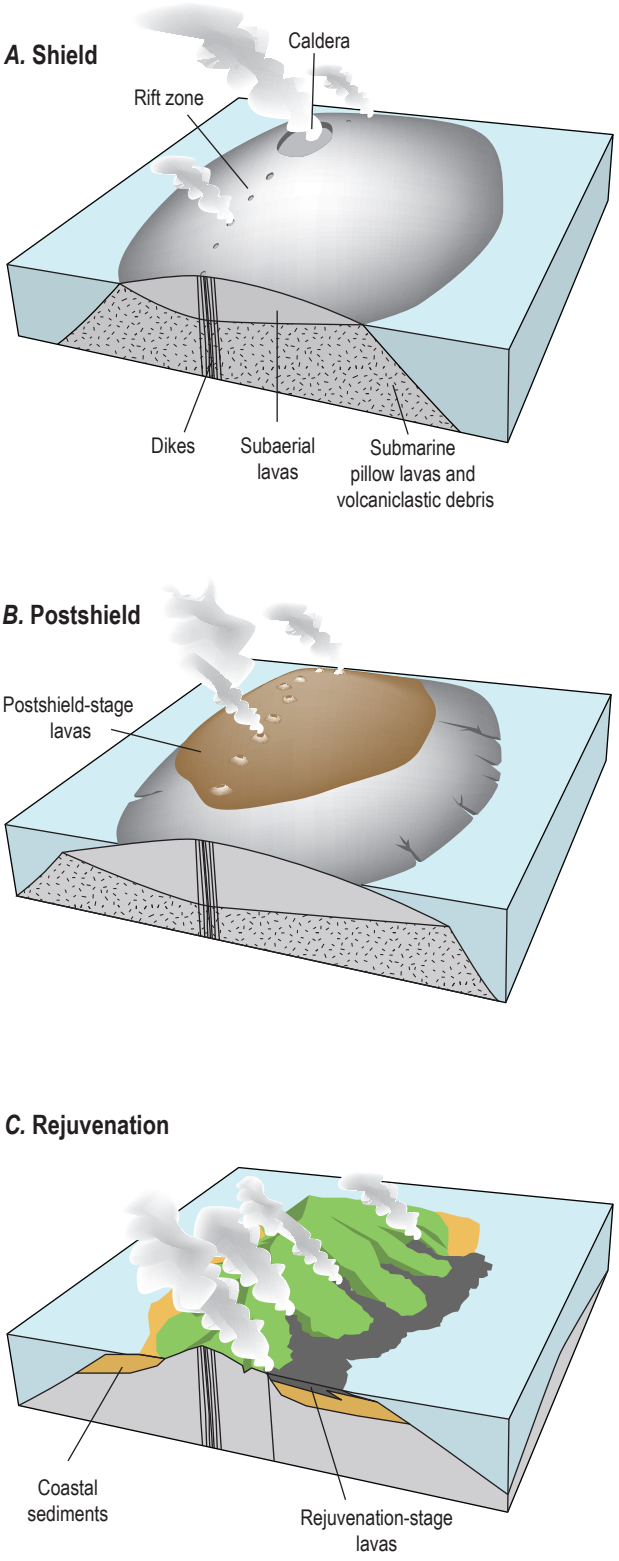

Figure 3. Three-dimensional illustrations showing three eruptive stages of Hawaiian shield volcanoes: (*A*) shield, (*B*) postshield, and (*C*) rejuvenation.

Faulting, Erosion, and Sedimentation

Faulting, erosion, and sedimentation modify the hydrogeologic framework of Hawai‘i’s volcanic aquifers. Faults are common in and near the summit and rift zones and on the volcano’s flanks (Macdonald and others, 1983). Although the hydraulic properties of faults themselves are poorly known, faults can juxtapose rocks of contrasting hydraulic properties—for example, low-permeability caldera-fill lavas and high-permeability flank lava flows. Faulting can also form depressions that are filled by subsequent lava flows that accumulate to form low-permeability aquifers.

Stream erosion and mass wasting have created valleys in the flanks of the shield volcanoes (Stearns and Vaksvik, 1935; Macdonald and others, 1983). On older shield volcanoes, such as those on Kaua‘i, O‘ahu, and West Maui, deeply incised streams cut into the upper parts of the volcanic aquifers, resulting in substantial groundwater discharge to streams. Such stream incision is particularly important in affecting the location of groundwater discharge and shaping the water table where the aquifers are saturated nearly to the surface (see additional discussion below in the Groundwater Settings section).

The upper parts of many stream valleys have only a very narrow ribbon of alluvium, but the lower parts of larger valleys have substantial deposits of alluvium and, in some cases, rejuvenation-stage volcanic rocks and marine sediments (Stearns and Vaksvik, 1935). Owing to sea-level fluctuations and island subsidence, the valley fill in some places extends below present sea level (Palmer, 1927; Stearns, 1946; Macdonald and others, 1983). Terrigenous and marine sediments are also deposited along the coast—these sediments, together with rocks from rejuvenation-stage volcanism, can form extensive coastal plains that partly surround some islands (fig. 3*C*), such as O‘ahu.

Rocks and Their Hydrologic Significance

Most groundwater in Hawai‘i is stored in lava-flow aquifers. The thin lava flows characteristic of Hawaiian shield volcanoes typically form highly permeable aquifers, with horizontal hydraulic conductivity (K_h) values ranging from hundreds to tens of thousands of feet per day (Soroos, 1973; Oki, 1999; Lau and Mink, 2006; Rotzoll and El-Kadi, 2008). In a few places, K_h can be several orders of magnitude lower where thick rejuvenation-stage lava flows formed by ponding in preexisting depressions (Izuka and Gingerich, 1998, 2003). Little direct information exists on the hydraulic anisotropy of lava-flow aquifers in Hawai‘i, but vertical hydraulic conductivity (K_v) has been estimated to be one to three orders of magnitude less than K_h (Souza and Voss, 1987).

Dikes are dense, near-vertical, sheet-like intrusive bodies formed by magma that congeals as it rises to the surface in fractures when the volcano is active. Dikes cut across the pile of gently dipping lava flows and are usually much less permeable than most lava-flow aquifers of Hawai‘i (Hunt, 1996). Dikes impede horizontal groundwater flow and reduce the bulk permeability and storage of aquifers into which they intrude and can cause groundwater to accumulate to high altitudes (fig. 2, 4*A*). However, a few dikes widely spaced in a large area of permeable lava-flow aquifers can impound groundwater and increase storage; groundwater in the dike-intruded lava flows is commonly referred to as dike-impounded groundwater (Takasaki and Mink, 1985).

Weathering of the basalts in Hawai‘i reduces rock porosity (Wentworth, 1928; Macdonald and others, 1983; Mink and Lau, 1980). The thickness of weathering depends on climate, vegetation, slope, and time since the basalt became exposed to surface weathering agents. Low-permeability weathered volcanic rock can impede the flow of groundwater. Weathered layers have been found above or buried among less-altered lava flows of shield volcanoes, and commonly lie beneath the alluvium in stream valleys (Oki, 2005).

Sedimentary rocks in Hawai‘i include alluvium and marine deposits. Valley-filling alluvium consists mostly of consolidated to unconsolidated, poorly sorted gravel with clasts ranging in size from boulders to clay. As a whole, alluvium has hydraulic conductivities several orders of magnitude lower than that of lava-flow aquifers (Hunt, 1996; Lau and Mink, 2006). Most marine sediment consists of carbonates; consolidation of carbonate sediment forms limestone. The permeability of limestone can be as high as, or higher than, that of lava-flow aquifers (Lau and Mink, 2006).

Sedimentary rocks can form semiconfining units that affect the flow and storage of water in volcanic aquifers. For example, sediments (with some rejuvenation-stage volcanic rocks) of the extensive coastal plain that fringes O‘ahu form a low-permeability semiconfining layer, locally known as caprock (fig. 4*A*), that overlies parts of the high-permeability lava-flow aquifer. The caprock impedes the natural coastal discharge of groundwater from the volcanic aquifers, allowing groundwater storage in the volcanic aquifers to be greater than it would be without the caprock. Much of O‘ahu’s extensive groundwater resources is the result of the island’s well-developed coastal-plain caprock (Stearns and Vaksvik, 1935).

Groundwater Settings

The fresh groundwater system of each island is dynamic—groundwater flows from the wet inland areas, where most recharge occurs, toward the coast, where the groundwater naturally discharges to springs, streams, and submarine seeps (fig. 2). Most of the water that recharges the volcanic aquifers comes from precipitation (primarily rainfall, but also fog and snow). Irrigation contributes to recharge in some places.

Izuka and others (2018) describe four principal “hydrogeologic settings” that encompass most of the groundwater on the three islands in this study. This report refers to these as “groundwater settings” to distinguish them from terminology that is used to describe hydrogeologic characteristics of the volcanic aquifers, although each groundwater setting typically occurs in aquifers that have

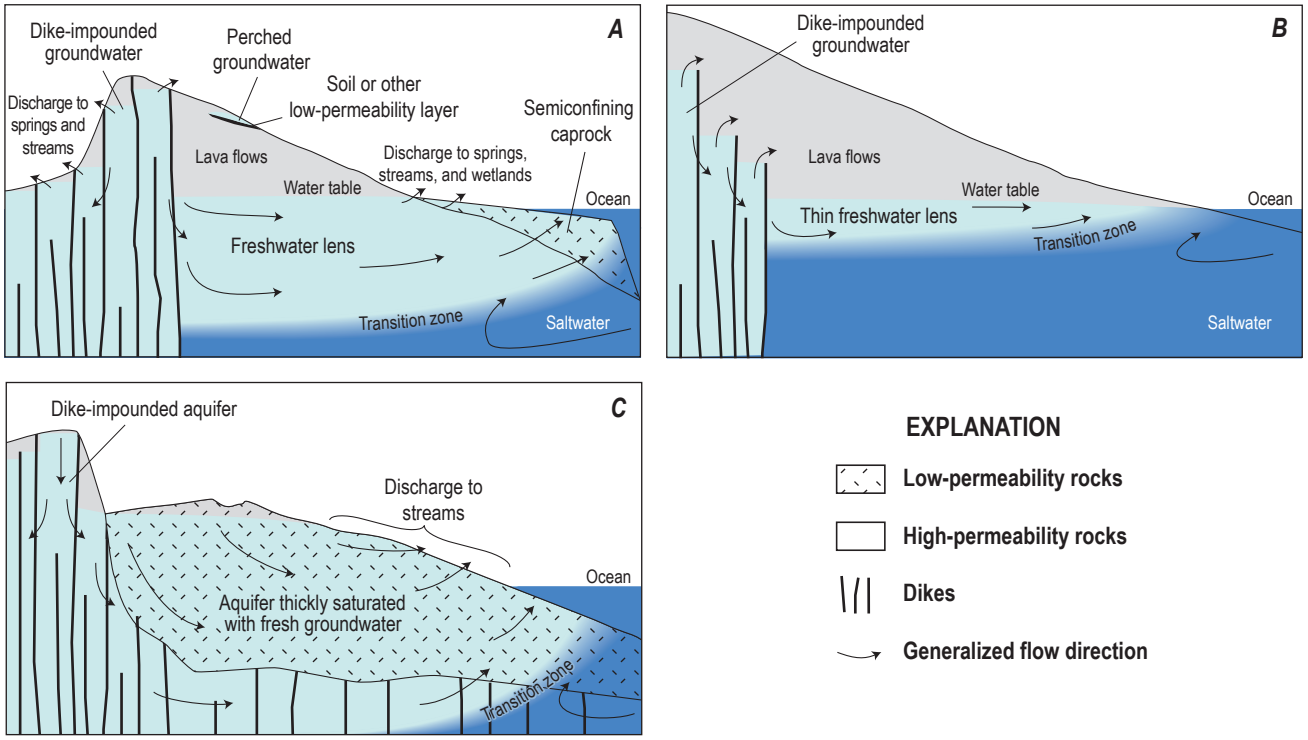

Figure 4. Schematic diagrams showing the principal groundwater settings in the volcanic aquifers of Hawai‘i. Modified from Izuka and others (2018).

a certain type of hydrogeology. The principal groundwater settings in Hawai‘i are the: (1) freshwater-lens setting, (2) dike-impounded-groundwater setting, (3) thickly saturated setting, and (4) perched-groundwater setting.

Freshwater-Lens Setting

Aquifers consisting of thin, high-permeability lava flows occur on all islands in this study and are a primary source of fresh groundwater for human use in Hawai‘i. Fresh groundwater in these aquifers exists as a freshwater lens that buoyantly overlies saltwater (fig. 4*A*, *B*). Between the freshwater and saltwater is a brackish transition zone. The water table of the freshwater lens typically is no higher than a few tens of feet above sea level and slopes gently toward the coast. Inflow to the freshwater lens comes from groundwater recharge through the land surface and subsurface flow from adjacent groundwater systems, such as dike-impounded or perched groundwater. Water in the lens generally flows from inland areas toward discharge areas at or near the coast.

Where little or no caprock exists, the only resistance to groundwater flow is the minimal resistance offered by the high-permeability aquifer itself. As a result, the freshwater lens is thin (fig. 4*B*) and most of the groundwater discharge near the coast happens below sea level. Where substantial caprock resists coastal discharge from the high-permeability aquifer (fig. 4*A*), the freshwater lens is thicker. Some groundwater discharges to the ground surface where the caprock pinches out above sea level, and some flows through the caprock and discharges to the caprock surface above or below sea level.

Dike-Impounded-Groundwater Setting

Near the center of a shield volcano and along its rift zones, the lava flows are commonly intruded by low-permeability dikes that resist horizontal groundwater flow. The system of dikes that intrudes high-permeability lava flows can be conceptualized as compartments. Groundwater stored in compartments of high-permeability rock between the low-permeability dikes is commonly referred to as dike-impounded groundwater and can accumulate to hundreds of feet above sea level (fig. 4) (Takasaki and Mink, 1985). Groundwater flows from one compartment to another and from dike-impounded groundwater to adjacent down-gradient groundwater bodies such as freshwater lenses. Some water seeps through the dike rock itself, but most of the water probably flows over the top or around the dikes (Macdonald and others, 1960). Where erosion has exposed the dikes (fig. 4*A, C*), groundwater commonly discharges to the surface and feeds springs and streams or the ocean. In some shield volcanoes, such as the Ko‘olau volcano on O‘ahu, dikes are aligned in linear trends that result in preferential flow in the direction of the dikes (Hirashima, 1962).

Regional permeability of a dike-intruded area depends on the characteristics of the dikes and how closely spaced the dikes are. Permeability is lower where dikes are abundant and closely spaced. Dikes are more abundant at the center of dike-intruded

complexes, such as those associated with rift zones, and are less abundant toward the margin (Macdonald and others, 1983; Walker, 1987). Dike abundance increases with depth, and at some point, effective porosity of the aquifer probably approaches zero (Takasaki and Mink, 1985; Kauahikaua, 1993; Moore and Trusdell, 1993). Although the depth to which fresh groundwater extends in dike compartments is largely unknown, most conceptualizations presume that freshwater in most dike compartments extends through the entire depth that groundwater is significantly mobile.

Thickly Saturated Setting

In the thickly saturated setting, the water table can be hundreds of feet above sea level, but not as a result of dike intrusion. In this setting, a condition herein referred to as a thickly saturated setting, a thick part of the aquifer is saturated with fresh groundwater because the aquifer is formed primarily by low-permeability volcanic rocks, such as massive lava flows (fig. 4*C*). An extensive thickly saturated low-permeability aquifer covers much of eastern Kaua‘i. The low permeability probably results from thick lava flows that formed by ponding in preexisting depressions, interbedded with low-permeability sediment (Izuka and Gingerich, 1998, 2003). An area near Nāhiku on the northeastern coast of Haleakalā volcano on Maui also has a thickly saturated low-permeability lava-flow aquifer (Gingerich, 1999a; Meyer, 2000; Scholl and others, 2002). In these low-permeability aquifers, head gradients in both the horizontal and vertical directions are steep, and groundwater saturates to hundreds of feet above sea level. The water table is kept just below most of the land surface by the draining action of streams. Indeed, most of the groundwater in this setting discharges above sea level to streams; less discharges to submarine seeps (Izuka and Gingerich, 1998, 2003). Saltwater and a transition zone probably underlie the fresh groundwater body near the coast, but whether these exist farther inland is not known.

Perched-Groundwater Setting

Perched groundwater is a body of saturated groundwater that accumulates on a low-permeability layer embedded within a body of higher permeability rock (fig. 4*A*). Perched groundwater is not simulated in the models in this study. Although some perched groundwater may discharge to streams, this study assumes that most groundwater temporarily stored in perched bodies eventually continues downward to the freshwater lens. Gingerich (1999a, b) postulated the existence of perched groundwater near Ha‘ikū, Maui, but suggested that more than 90 percent of the recharge in the general area moves downward to the freshwater lens, although in some basins the percentage may be less. Perched groundwater bodies on O‘ahu and Kaua‘i are small and considered insignificant at the whole-island scale of the models in this study.

Numerical Groundwater Models

Three separate numerical models were created to simulate the volcanic aquifers of Kaua‘i, O‘ahu, and Maui (Rotzoll and Izuka, 2020). Creation of separate models is consistent with each island’s isolation—in terms of fresh groundwater availability—by seawater. Also, each model reflects the unique combination of hydrogeology and groundwater flow of the island it represents. All three models, however, were created using consistent methods to yield comparable results to meet the common purpose of this study. The first subsection below describes aspects of construction and calibration that are common to all three models. Later subsections describe the details that are unique to the individual models.

Aspects Common to the Three Numerical Models

The three models were created using the U.S. Geological Survey’s (USGS) finite-difference groundwater-modeling program MODFLOW-2005 (Harbaugh, 2005). The models used the same boundary conditions and horizontal cell dimensions and were calibrated in steady-state mode for the same stress period. The models also used consistent sources for topographic, bathymetric, recharge, and withdrawal datasets. Consistency was facilitated by using Python scripts incorporating FloPy3, a Python package developed for MODFLOW-based models (Bakker and others, 2016). The scripts automated the creation of model input files, allowed easy adjustment of parameter values during calibration, and provided post-processing tools for consistent model evaluation.

The Layered Property Flow package was used to specify aquifer parameter values and the Preconditioned Conjugate-Gradient solver was used to numerically solve the finite-difference groundwater-flow equation. Head-dependent boundary packages in MODFLOW-2005 allowed simulation of groundwater discharge to springs, streams, submarine seeps, and withdrawals from free-flowing groundwater-development tunnels. Conventional vertical wells were simulated using the Well package (details are given below in the section on Flow Boundaries). All altitudes in the models are referenced to sea level.

The Seawater Intrusion package (SWI2) (Bakker and others, 2013) of MODFLOW-2005 was used to simulate saltwater and freshwater in the island aquifers. The saltwater and freshwater bodies are simulated as two immiscible fluids with different densities. SWI2 models can simulate aspects related to the density difference between saltwater and freshwater, such as the formation of a freshwater lens overlying saltwater, but because the two fluids cannot mix, the boundary between them is simulated as a sharp interface rather than a transition zone (fig. 5). SWI2 refers to the altitude of the sharp interface as *ZETA*.

Fluid densities used in the models for this study correspond to those of freshwater (1.000 gram per cubic centimeter [g/cm^3])

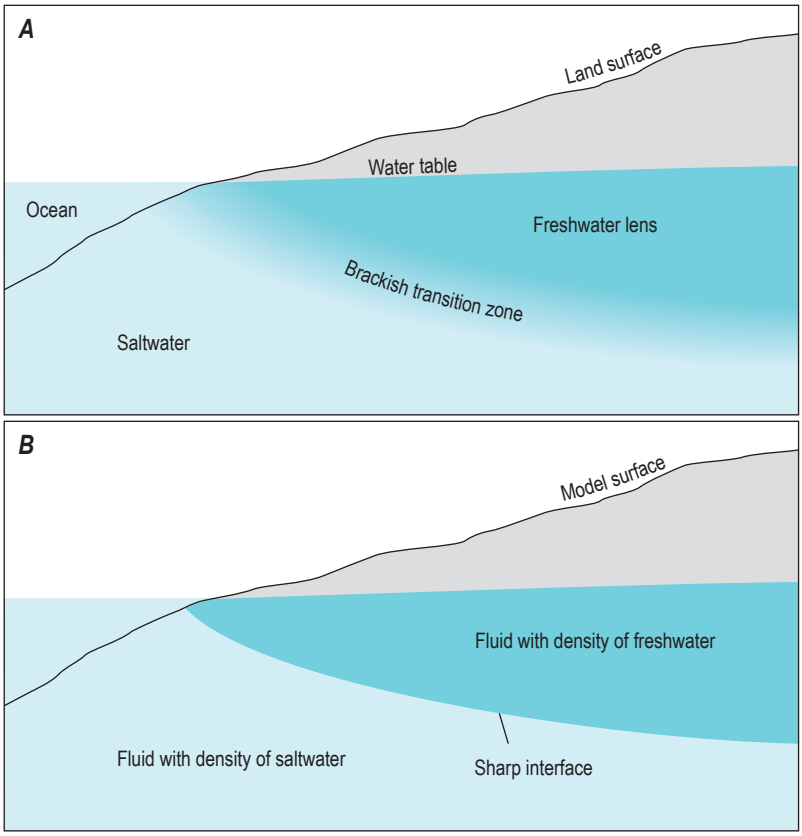

Figure 5. Diagram showing the boundary between freshwater and saltwater in an aquifer. *A*, In reality, the boundary is a zone transitioning gradually from freshwater above to saltwater below. *B*, In the model, the Seawater Intrusion package (SWI2) represents the boundary as a sharp interface (surface) between immiscible fluids that have different densities; the altitude of the boundary is referred to as *ZETA*.

and seawater (1.025 g/cm^3); in this study, the freshwater-saltwater interface approximates the altitude of the part in the transition zone where the brackish water is a mixture of 50 percent freshwater and 50 percent seawater. The modeled *ZETA* and simulated head can be used to assess the size of the freshwater lens, but the size will be overestimated because the thickness of the brackish water in the transition zone above the 50-percent freshwater-seawater mixture is not represented. Despite this limitation, the sharp-interface approach is useful for simulating fresh and saline groundwater for island-scale models because it is less computationally demanding than the alternative solute-transport approach yet provides a means to assess the flow of freshwater and saltwater at the island scale. The dimensionless control variables *TIPSLOPE*, *TOESLOPE*, *ALPHA*, and *BETA*, which govern the horizontal movement of the interface (Bakker and others, 2013), were set to 0.4, 0.4, 0.1, and 0.1, respectively.

The models in this study were calibrated in the steady-state mode using 2001–2010 average conditions (with some exceptions for recharge, which are described in the Recharge section below). Simulations using the steady-state models indicate the groundwater storage and natural-discharge rates that would ultimately exist if recharge and withdrawal rates remained constant indefinitely. Comparing results of steady-state models for different groundwater-withdrawal rates can quantify the effects of changing groundwater use by humans; comparing results for different recharge rates can quantify the effects of changing climate and land cover.

Implicit in the steady-state approach is the assumption that inflows and outflows are at a reasonably steady state during the calibration period. The 2001–2010 period was selected for the steady-state calibration of the models in this study because it represents a time of relative stasis following the rapid and substantial changes related to the closure of large plantations in the last few decades of the 20th century (Izuka and others, 2018). The plantations affected the groundwater budgets of Kaua‘i, O‘ahu, and Maui not only by withdrawing groundwater, but also by enhancing groundwater recharge by irrigating with stream water. Most of the substantial changes in surface-water and groundwater use took place between 1980 and 2000 (fig. 6), prior to the calibration period. Some wells show downward or upward trends in water levels during the calibration period, but the trends are gradual, and several wells show virtually flat trends (fig. 7). Given the history of changes that have affected Hawai‘i’s aquifers, and the availability of more data after rather than before the changes, the 2001–2010 period was considered to be the best period for steady-state calibration in this study.

Model Domains and Discretization

The periphery of each model’s domain was set far enough beyond the islands’ coasts that fresh-groundwater flow in the

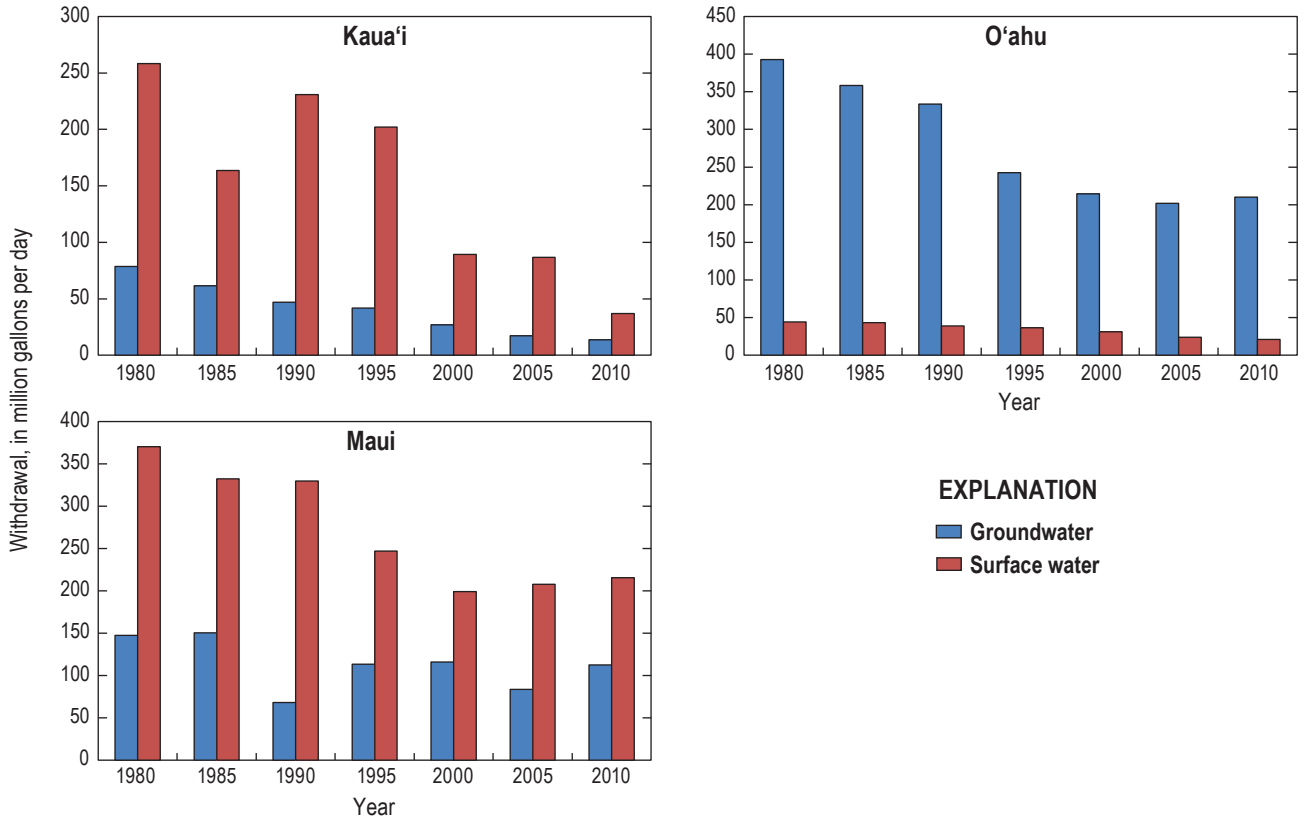

Figure 6. Graphs of freshwater withdrawals from 1980 to 2010 for Kaua'i, O'ahu, and Maui, Hawai'i. The graphs show a snapshot of water use every fifth year (not an average over a 5-year period). Modified from Izuka and others (2018).

model was not limited by no-flow boundaries. The no-flow boundary at the bottom of the model domains for all islands was set at an altitude of –5,906 ft on the basis of a seismic velocity discontinuity (Furumoto and others, 1970), and indications are that below this depth, porosity becomes nearly zero as a result of secondary mineralization (Kauahikaua, 1993).

The altitude of the top of each model cell in the upper layer represents the altitude of the surface of the volcanic aquifer within the model cell. Some nonvolcanic units, such as valley-fill alluvium, were also simulated by active cells with aquifer properties. Caprock and streambed sediment were not included as aquifer units in the models, but their effect on groundwater in the volcanic aquifers was simulated using head-dependent boundaries (see the sections on Caprock and Streams, Tunnels, and Springs below). The surfaces of the volcanic aquifers are based largely on the surface of the volcanic hydrogeologic units reported by Izuka and others (2018), with some exceptions discussed below in the sections that describe the individual models.

The active domains of all models were horizontally divided (discretized) into 500-ft by 500-ft cells. Each model was discretized vertically into one or two layers, depending on how hydraulic properties are distributed in that island (see the section on Zones of Hydraulic Properties below). Most volcanic aquifers in Hawai'i are vertically extensive, with major hydrogeologic units extending from the surface to thousands of feet below sea level. Although hydraulic properties probably vary with depth, the models assume homogeneity with depth in a hydrogeologic unit. Hydraulic properties can, however, vary sharply in the horizontal direction. An island typically has areas with sharply contrasting properties, positioned side-by-side. For example, aquifers formed by a pile of thin lava flows having K_h values of hundreds of feet per day are commonly adjacent to dike-intruded aquifers where bulk K_h values are less than a foot per day. Layering of one aquifer on another is limited to a few areas; thus, objectives of this study can be achieved with single-layer models for O'ahu and Maui. The Kaua'i model was created with two layers to allow simulation of two hydrogeologically distinct units that overlie part of the island (more details are given in the description of the Kaua'i model, below).

Time discretization is irrelevant for steady-state models, but numerical simulation of flow involving two fluids having different densities cannot be solved in a single time step. Steady state in SWI2 is achieved by running in the transient mode until *ZETA* stops changing or changes very slowly (Bakker and others, 2013). In SWI2, time-step length is computed from user-defined stress-period length and number of time steps per stress period. The time-step length has no bearing on the steady-state results, but it affects computer execution time and numerical stability. The ideal time-step length differed among the three models, but was typically between 1 and 30 simulated days.

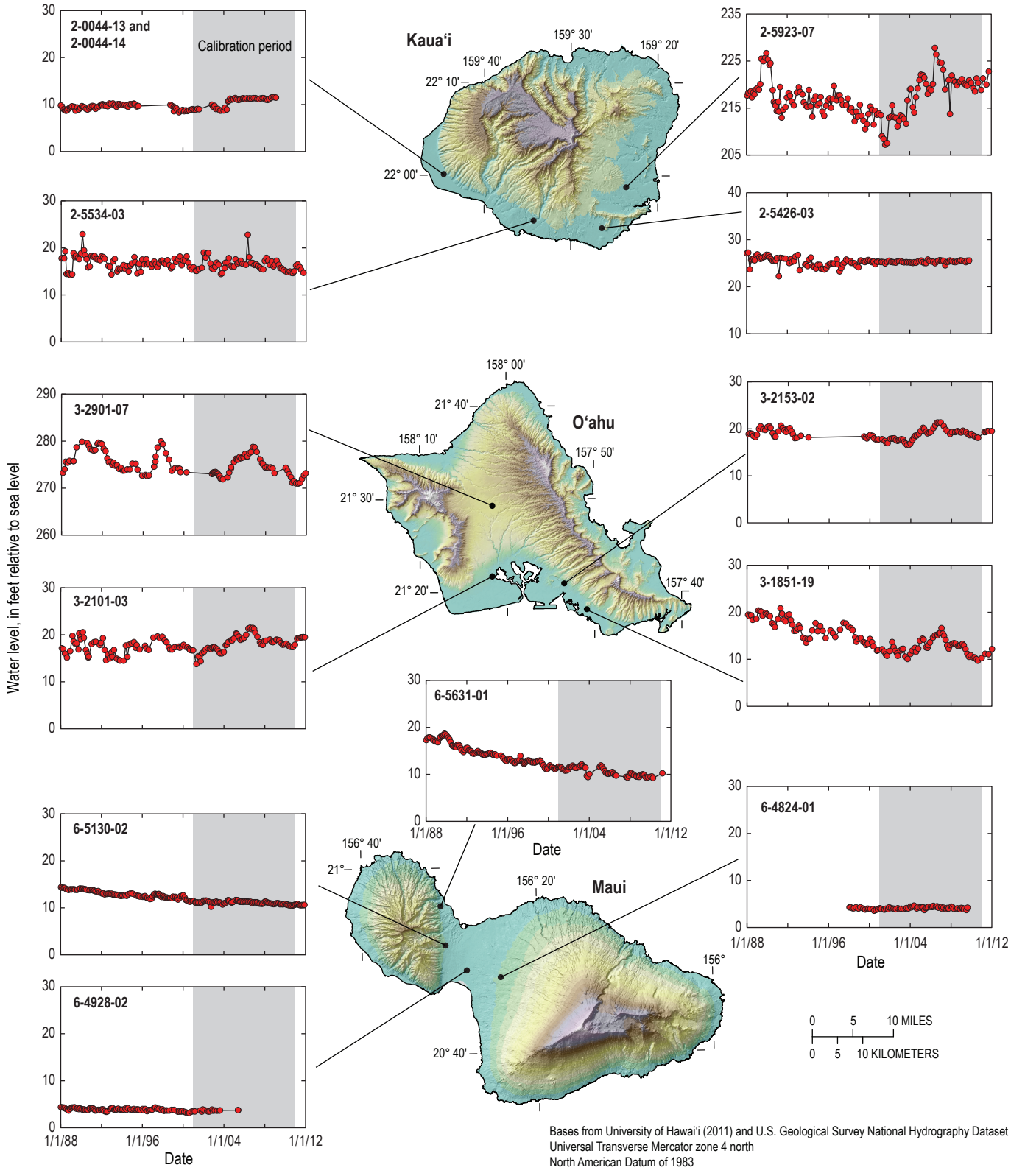

Figure 7. Graphs of water levels measured at selected wells on Kaua‘i, O‘ahu, and Maui, Hawai‘i.

Flow Boundaries

Flow boundaries in the numerical groundwater models are boundaries through which water flows in and out of the models. The only freshwater inflow to the groundwater models is recharge, whereas outflow occurs at wells, tunnels, and shafts, and where groundwater discharges to streams, springs, and the ocean. In the volcanic aquifers of Hawai‘i, flow boundaries include locations where groundwater (1) is withdrawn through wells and other groundwater-development systems, (2) flows through caprock, (3) discharges to streams and springs, and (4) is recharged. Hawai‘i does not have large natural lakes, and seepage from irrigation reservoirs has already been incorporated in the groundwater-recharge estimates for each island (Izuka and others, 2018).

Withdrawals

Groundwater in Hawai‘i is withdrawn by conventional vertical wells, and by tunnels and shafts with galleries (fig. 8). A shaft is a large facility that consists of a vertical or inclined boring excavated down to the water table, with one or more nearly horizontal borings (galleries) designed to skim water from near the surface of a fresh groundwater lens; these facilities are the largest individual producers of fresh groundwater from Hawai‘i’s volcanic aquifers. Tunnels are large borings driven nearly horizontally into dike-impounded or other shallow groundwater systems.

Only withdrawals from volcanic aquifers were simulated in the models of this study; withdrawals from the caprock were excluded. Vertical wells, shafts, and some tunnels were simulated using the Well package of MODFLOW-2005 (Harbaugh, 2005). Locations, depths, and open intervals were determined from information in the USGS National Water Information System (NWIS) database (U.S. Geological Survey, 2019). Draft rates were determined on the basis of water use reported to the State of Hawai‘i Commission on Water Resource Management (CWRM) for the period 2001–2010. The average draft for each well in operation in 2001–2010 was computed from reported values if available. Draft rates were assumed to be zero before the well permit was approved, if that information is available, or prior to the well-construction date. Underreported wells are those that were in operation in 2001–2010, but part of the withdrawal record for that period is missing. Unreported wells are those that were in operation in 2001–2010 but no withdrawals were reported. Methods for estimating underreported and unreported withdrawals for wells are described below in the sections on each model.

Most tunnels were simulated using the Drain package of MODFLOW-2005 (Harbaugh, 2005). Most tunnels in the model behave more like streams than pumped vertical wells or shafts—groundwater flows freely from the tunnels, driven by the head difference between the tunnel and the aquifer. Although water in some tunnels is collected in a shallow sump and pumped to the location of its use, flow from the aquifer to the tunnel is driven by the head difference between the aquifer

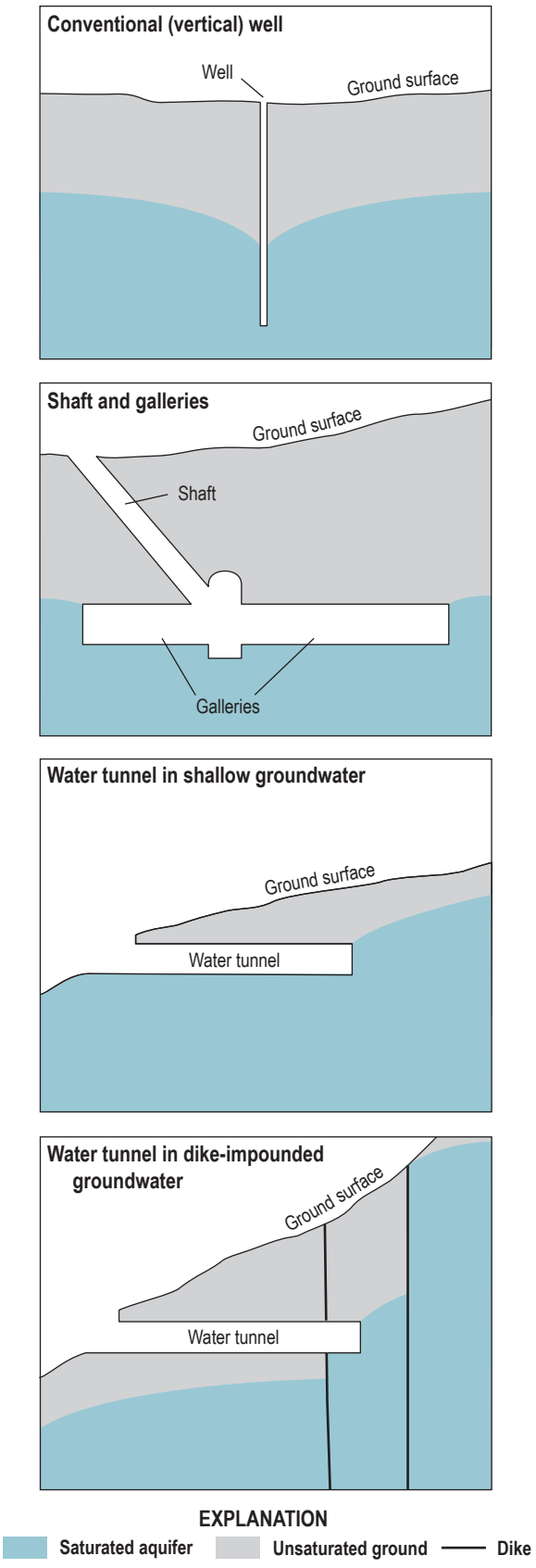

Figure 8. Diagrams showing wells, shafts, and tunnels used to withdraw groundwater from the volcanic aquifers of Hawai‘i.

and the tunnel, not by drawdown caused by the pump. Six tunnels on O‘ahu were simulated with the Well package rather than the Drain package during calibration (see the O‘ahu section below for more information), but the calibration procedure was eventually able to match satisfactorily the tunnel flows and nearby water levels, so the effect on the model is the same as if the tunnels were simulated as drains.

Caprock

Caprock consists mostly of sediments, but it has a substantial effect on fresh groundwater storage in the volcanic aquifers because it impedes groundwater discharge to the ocean. For the models in this report, caprock is defined as the largely nonvolcanic units that lie above areas where the top of the volcanic aquifers is below sea level (fig. 9). Where the top of the caprock lies above sea level, its extent is assumed to correspond with coastal sediments and rejuvenation-stage volcanic rocks shown in the geologic maps of Sherrod and others (2007). Onshore areas of caprock are assumed to extend offshore, although most offshore caprock extents in Hawai‘i have not been mapped.

Caprock units are not simulated as aquifer units in the numerical groundwater models in this study; instead, their effect on discharge from the volcanic aquifers is simulated using head-dependent boundaries. Head-dependent boundaries assume that flow between an aquifer and an overlying surface-water body is vertical and is a function of (1) the vertical hydraulic conductance of the material at the boundary and (2) the difference between the head in the aquifer and the water level of the surface-water body (Harbaugh, 2005). Where groundwater discharges through caprock, the caprock conductance contributes to (and commonly dominates) the conductance at the head-dependent boundaries.

Where the top of the caprock lies below sea level, the effect of the caprock was simulated using general-head boundaries (GHBs) (fig. 9). Groundwater exchange between the aquifers and ocean is a function of (1) the difference between the model-computed head in the aquifer and the head assigned to the ocean and (2) the caprock conductance. This relation, notationally modified from Harbaugh (2005), is given by:

$$Q_{cpr} = C_{cpr}\,(H_{ocean} - H_{aq}) \qquad (1)$$

where

Q_{cpr} is the flow across the caprock; negative values indicate flow out of the aquifer [L^3/T],[1]
C_{cpr} is the caprock conductance [L^2/T],
H_{ocean} is the head in the ocean [L], and
H_{aq} is the freshwater head in the volcanic aquifer [L].

[1]Expressions in brackets give the dimensions of the variable, where L is length and T is time.

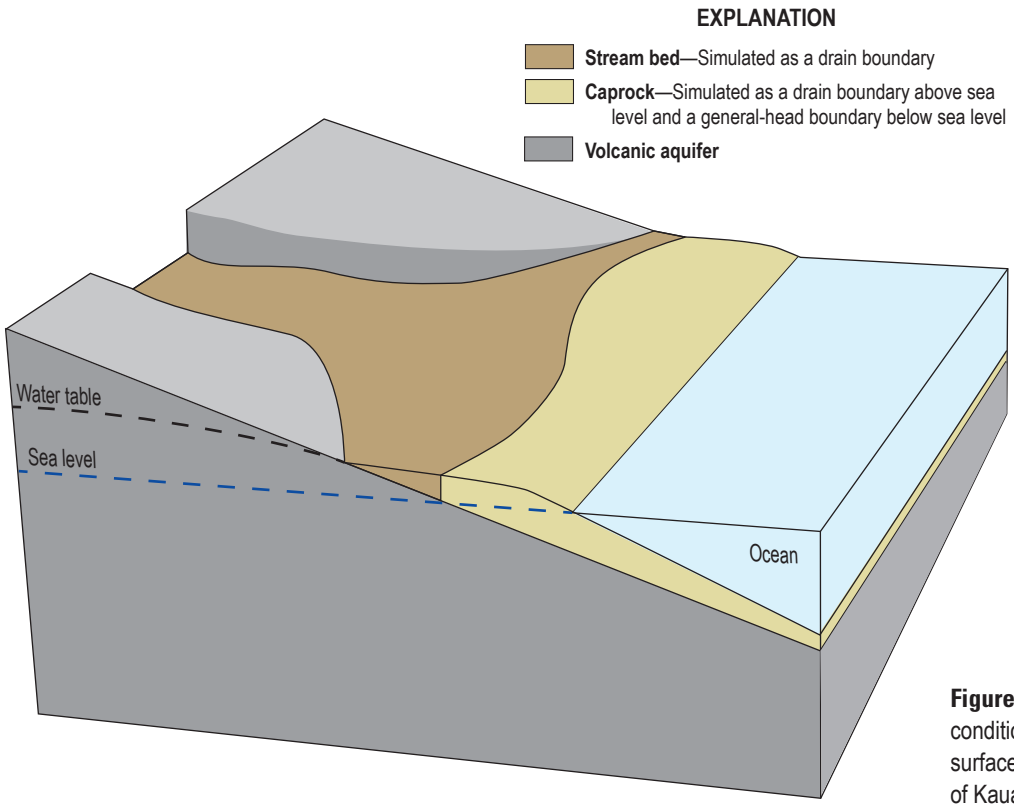

Figure 9. Diagram showing the boundary conditions used to simulate flow through the surface of the numerical groundwater models of Kaua‘i, O‘ahu, and Maui, Hawai‘i.

Because the ocean contains seawater, H_{ocean} must account for the density difference between seawater and freshwater. Assuming seawater is 1.025 times denser than freshwater, and that all heads are measured relative to sea level,

$$H_{ocean} = D_{volc}/40, \quad (2)$$

where D_{volc} is the depth of the surface of the volcanic aquifer below sea level [L].

D_{volc} was equated to the depth of the volcanic-aquifer surface for SWI2 (rather than bathymetry, which is typical for most coastal models [for example, Bakker and others, 2013]).

For a cell with caprock, the caprock conductance, C_{cpr}, is given by (Harbaugh, 2005):

$$C_{cpr} = K_{vc}(A)/T_{cpr}, \quad (3)$$

where

K_{vc} is the vertical hydraulic conductivity of the caprock [L/T],
A is the area of the cell [L^2], and
T_{cpr} is the thickness of the caprock [L].

For the models in this study, C_{cpr} was computed externally (from MODFLOW) on the basis of K_{vc} and the thickness of the overlying caprock. Caprock thickness was computed by subtracting the altitudes of the top surface of the volcanic aquifers from that of the topographic/bathymetric surface (Izuka and others, 2018). A minimum caprock thickness of 1 ft was assumed on the premise that even where sediments may be thin or absent, discharge from the volcanic aquifer to the ocean will meet some resistance from the volcanic aquifer itself. Values for K_{vc} were determined during model calibration.

Caprock inland of the shoreline and overlying the areas where the top of the volcanic aquifer is below sea level was simulated using drains (fig. 9). This part of the caprock typically contains fresh to brackish groundwater, with the water table below land surface but generally not much above sea level. The equation, notationally modified from Harbaugh (2005), for flow across caprock simulated as drains is:

$$Q_{cpr} = C_{cpr}(H_{cpr} - H_{aq})$$

for $H_{aq} > H_{cpr}$ and

$$Q_{cpr} = 0$$

for $H_{aq} \leq H_{cpr}$ (4)

where H_{cpr} is the head in the caprock [L].

Water discharges from the volcanic aquifer through the caprock only when the head in the volcanic aquifer is greater than the head in the caprock ($H_{aq} > H_{cpr}$). When the head in the volcanic aquifer is less than or equal to the head in the caprock ($H_{aq} \leq H_{cpr}$), no water flows through the caprock. This one-way-flow (out of the aquifer) feature of drains allows the simulation of groundwater discharge through the caprock and prevents the head-dependent boundary from being an unlimited artificial source of fresh groundwater if H_{aq} falls below H_{cpr}. Analogous to the part of the caprock simulated with GHBs, C_{cpr} for these drains is a function of K_{vc} and caprock thickness (eq. 3), minimum caprock thickness is assumed to be 1 ft, and values for K_{vc} are determined during model calibration. Available data indicate that H_{cpr} is within a few feet of sea level. For the models of this study, H_{cpr} was assumed to be zero (sea level) except in southern O‘ahu, where H_{cpr} was based on previous studies (see the section on O‘ahu below).

Streams, Tunnels, and Springs

Streams, springs, and tunnels were simulated as drains. The equation describing groundwater seepage to drains representing streams, springs, and tunnels is identical to eq. 4 except that terms for the caprock are replaced by terms for the stream or spring:

$$Q_{str} = C_{str}(H_{str} - H_{aq})$$

for $H_{aq} > H_{str}$ and

$$Q_{str} = 0$$

for $H_{aq} \leq H_{str}$ (5)

where

Q_{str} is the flow across the stream bed, spring bed, or tunnel bottom [L^3/T],
C_{str} is the spring- or stream-bed or tunnel-bottom conductance [L^2/T], and
H_{str} is the head in the stream, spring, or tunnel [L].

For streams and springs, drains allow groundwater to discharge when the head in the aquifer is above the head in the stream or spring, but water does not flow into the aquifer when the head in the cell is below the stream or spring bed. The one-way groundwater exchange is consistent with the nature of groundwater seepage for most streams and springs in Hawai‘i. Where the water table is below the stream channel in Hawai‘i, the channels commonly are dry except during direct-runoff peaks. Direct runoff from Hawai‘i’s small, steep stream basins is flashy (Wu, 1969, Wong, 1994); this study assumes that stream stage does not stay elevated long enough to impel substantial flow from the stream to the underlying aquifer. Any seepage of direct runoff has been indirectly accounted for in the recharge described by Izuka and others (2018) that was applied to the models. Similarly, if the water table drops below the altitude of a spring, the spring simply goes dry—there is no surface-water head in the spring to cause flow into the aquifer.

In the models for this study, cells coinciding with stream channels and springs in the National Hydrologic Dataset (NHD) (U.S. Geological Survey, 2012) were designated as

drain cells. The head above the drain cell (H_{str} in eq. 5) was set to the stream-channel or spring altitude at that location. The stream-channel and spring altitudes are considered a close approximation of the heads in these settings because streams and springs in Hawai‘i are shallow during the base-flow conditions represented by the models. Theoretically, C_{str} depends on the thickness and K_v of the sediments in the stream or spring bed (similar to C_{cpr} for caprock [eq. 3]), but for calibrating the models in this study, C_{str} was varied rather than the separate parameters of thickness and K_v.

Most tunnels constructed for withdrawing fresh groundwater were also simulated as drains. Where a model cell coincided with the trace of tunnels, the cells were designated as drain cells, H_{str} (eq. 5) was set at the altitude of the tunnel invert, and C_{str} was varied during calibration (rather than the separate parameters of thickness and K_v). As described in the Withdrawals section above, six tunnels on O‘ahu were simulated as pumped wells, not drains (see the O‘ahu section below for additional discussion).

Recharge

The models were calibrated using recharge extracted from the datasets of average recharge for 1978–2007 and 2001–2010 computed by Izuka and others (2018). Their recharge estimates were computed using a soil water-balance model, and are independent of the processes simulated by the groundwater models—recharge to the model is unaffected by the altitude of the water table relative to the land surface. The recharge datasets consisted of irregular polygons of varying sizes, which are converted to 100-ft raster datasets using the maximum-combined-area method in ArcGIS. Recharge for a given cell in the groundwater model is the interpolated nearest neighbor of the 100-ft raster to the model-cell centroid. Total recharge from the rasterized dataset used for each model is within 0.5 percent of the corresponding recharge computed by Izuka and others (2018). Recharge was applied only to cells whose tops were above sea level. No recharge was applied, however, to cells covered by caprock; these areas are assumed to be zones of discharge.

The 1978–2007 recharge rates were applied to areas of the models that represent zones of dike intrusion. Because groundwater flows slowly through these low-permeability aquifers, the earlier and longer term 1978–2007 average is a better representation of the source of the water that was flowing through the dike-intruded setting and into adjacent downgradient settings during the 2001–2010 calibration period. The 2001–2010 recharge rates were applied to all other areas of the models (marginal dike zones, caldera, and high-permeability aquifers). This recharge period corresponds with the 2001–2010 period for withdrawal and observation data used for calibration.

Zones of Hydraulic Properties

The active cells in each model were grouped into zones that have uniform hydraulic properties. Two types of zones were used in the models: (1) hydraulic-conductivity zones (*K* zones), and (2) caprock-conductance zones (*C* zones). *K* zones delineate sectors of relatively uniform hydraulic conductivity within an island; thus, all model cells in a *K* zone are given the same K_h value. In most *K* zones, the K_h value was the same in the x and y directions, but in *K* zones that represent dike-intruded areas on O‘ahu, K_h in the x direction (K_{hx}) differs from K_h in the y direction (K_{hy}) because the dikes have subparallel alignments that impart horizontal anisotropy. Extents of *K* zones are generally consistent with structural and stratigraphic relations described by Izuka and others (2018) and other studies cited in the sections that describe the individual models below. The hydrogeologic units are presumed to extend offshore; *K* zones representing these units likewise extend offshore. For the two-layer Kaua‘i model, all cells in a *K* zone were also given the same K_v values, and in all cases, the K_v values are lower than the corresponding K_h values, which is consistent with the layered characteristic of lava flows (Nichols and others, 1996).

C zones delineate sectors where the caprock has relatively uniform vertical hydraulic conductivity; thus, all model cells in a *C* zone are given the same K_{vc} value, which is used to compute caprock conductance, C_{cpr} (eq. 4). The values for the hydraulic properties in the groundwater models were determined during model calibration and are discussed in the sections for each model below.

Calibration

The objective of calibration is to create models that represent the groundwater systems being studied. This objective is met by adjusting the models’ physical parameters until the models match observations of the hydrologic system for the set of groundwater withdrawal and recharge conditions specified for the models. Model parameters are typically the physical properties of the geologic materials through which groundwater flows (for example, aquifer hydraulic conductivity) because their values are not known precisely, although they may fall within a known range (Wang and Anderson, 1982). Observations are field measurements (or averages computed from these measurements). In a well-calibrated model, residuals (differences between model-simulated values and measured observations) are minimized and the model is considered, for the objectives of the study, to be a reasonable representation of the real-word system.

Calibration parameters for the models in this study were K_h, K_v, K_{hx}, K_{hy}, K_{vc}, C_{cpr}, and C_{str} for each *K* zone, *C* zone, or stream reach for which they were appropriate (table 1). The

Table 1. Calibration parameters for the numerical groundwater models of Kauaʻi, Oʻahu, and Maui, Hawaiʻi.

[*K* zones, zones of uniform hydraulic conductivity; *C* zones, zones of uniform caprock conductance; NA, not applicable]

Symbol in report	Applied to	Parameter description	Number of model parameters		
			Kauaʻi	Oʻahu	Maui
K_h	*K* zones	Horizontal hydraulic conductivity of volcanic aquifers	12	31	19
K_v	*K* zones	Vertical hydraulic conductivity of volcanic aquifers	12	NA	NA
K_{hx}	*K* zones	Horizontal hydraulic conductivity in the x direction for dike-intruded aquifers	NA	6	NA
K_{hy}	*K* zones	Horizontal hydraulic conductivity in the y direction for dike-intruded aquifers	NA	6	NA
K_{vc}	*C* zones	Vertical hydraulic conductivity used to compute general-head boundary and drain conductances for caprock	17	36	8
C_{str}	Streams	Conductance of drains simulating streams, tunnels, and springs	70	57	39
		Total number of parameters	111	136	66

parameter K_v is only needed in the Kauaʻi model, the only model with more than one layer. The parameters K_{hx} and K_{hy} are only used for the *K* zones that represent certain dike-intruded areas of the Oʻahu model where horizontal anisotropy was simulated.

Observations included groundwater levels measured in wells, the altitude of transition-zone midpoints determined from salinity profiles of deep monitoring wells (DMWs), base flows and spring flows estimated from stream-gage records, and tunnel flows (table 2). Average groundwater levels during the 2001–2010 calibration period were computed from data in the USGS NWIS database. In areas with few or no water-level observations during 2001–2010, measurements outside the calibration period were used to supplement the dataset, but these observations were given lower consideration during calibration. Additionally, on Oʻahu, some water-level measurements in DMWs collected by the Honolulu Board of Water Supply and CWRM during 2001–2010 were used to supplement the observations. Observations of transition-zone midpoints were based on a study by Rotzoll and others (2010), who defined the midpoint as the point in a DMW salinity profile where the concentration is equivalent to a mixture of 50-percent saltwater and 50-percent seawater.

Stream base-flow estimates used as observations for calibrating the models were computed by Izuka and others (2018) using continuous-record stream-gage data and a hydrograph-separation computer program by Wahl and Wahl (1995). Base-flow averages used for calibration of a given region of a model corresponded with the recharge period used (1978–2007 or 2001–2010, as described in the Recharge section above). For Oʻahu, Kauaʻi, and West Maui, average base flow was computed for the 1978–2007 period because the streams gain mostly from dike-impounded groundwater. Base flow in streams on Haleakalā was calculated for the 2001–2010 period because the streams gain water entirely from areas outside the dike-impounded-groundwater setting, where the 2001–2010 recharge rate was applied. For a gage that did not have data in the calibration period, base flow was estimated for the period available and adjusted to the 1978–2007 or 2001–2010 period using data from a long-term index gage:

$$G_{cal} = G_{con} (I_{cal} / I_{con}) \quad (6)$$

where

G_{cal} is the estimated base flow at gage *G* for the calibration period [L^3/T],

G_{con} is the base flow at gage *G* computed by hydrograph separation for the period when gages *G* and *I* operated concurrently [L^3/T],

I_{cal} is the base flow at index gage *I* for the calibration period computed by hydrograph separation [L^3/T], and

I_{con} is the base flow at index gage *I* for the concurrent period of gages *G* and *I*, computed by hydrograph separation [L^3/T].

Flow observations for tunnels simulated with the Drain package were averaged from reported withdrawal data as described previously for wells (see section on Withdrawals above).

During calibration, groundwater-level observations were compared to model-simulated heads at model cells representing the location of the wells. Where hydraulic gradients are steep, real-world water levels can vary substantially within the area

Table 2. Summary of observations used to calibrate the numerical groundwater models of Kaua‘i, O‘ahu, and Maui, Hawai‘i.

[*ZETA*, altitude of freshwater-saltwater interface]

Observation type	Representation in models	Number of observations		
		Kaua‘i model	O‘ahu model	Maui model
Water level in well	Head in cells representing location of well	57	257	67
Altitude of transition-zone midpoint	*ZETA* in cells representing location of deep monitor wells	0	35	4
Stream base flow at gage	Sum of discharge from drain cells representing stream reaches upstream of gage	18	19	31
Spring flow	Sum of discharge from drain cells representing spring	0	5	1
Tunnel flow	Sum of discharge from drain cells representing trace of tunnel	3	13	0
Total number of observations		78	329	103

represented by a model cell. A model cell, however, can only have one head value; this value is an integration of real-world water levels in the cell's area. To assist in calibration, the Groundwater Data Utility MOD2OBS (Watermark Numerical Computing, 2014) was used to interpolate the simulated water level to the coordinates of the well. Transition-zone-midpoint depth observations were compared to the model-simulated *ZETA* for model cells at the location of DMWs. Stream base-flow observations were compared to the sum of discharges from model drain cells representing stream reaches upstream of gages (the possibility that non-gaining model reaches could potentially lose water in reality was assumed negligible). Tunnel and spring flows were compared to the sum of discharges from drain cells representing the tunnel or the spring.

As discussed above, steady state in the models of this study was achieved by running in the transient mode until *ZETA* stopped changing from one time step to the next. However, at some model cells, particularly those at boundaries between two *K* zones that have sharply contrasting hydraulic properties (for example, between dike-intruded aquifers and dike-free lava-flow aquifers), *ZETA* oscillated about an average value as the model approached steady state. To mitigate the effect of the oscillation, model results (*ZETA*, head, and discharge through drains and GHBs) from the last two time steps of the final runs for each model were averaged and the averages were used for the purposes of calibration and comparing the numerical models to their respective conceptual models in this report.

Calibration workflow.—The models in this study were calibrated using a hybrid of manual parameter adjustments and the parameter-estimation program (PEST) by Doherty (2010). Manual calibration uses a series of model runs that adjust the values of one or a few parameters at a time to achieve a match between modeled and observed values. Prior knowledge of the hydrology of each island is used to select the parameters to be adjusted and the range of values to test. Each time a model run is submitted manually, the investigator can set simulation times to be as long as necessary to achieve steady state for a given set of parameter values. This approach is ideal for targeting a few key parameters whose values are at least partly known, but can be difficult to use in systems with many poorly known parameters. PEST is helpful for estimating multiple parameters whose values are poorly known. PEST automates the adjustment of parameter values and execution of hundreds of model runs to find the combination of parameter values that minimizes weighted residuals. However, because SWI2 runs in transient mode until steady state is achieved, individual SWI2 model runs may be long. Using PEST with long-running SWI2 models can be impractical because a single PEST run can require hundreds of model runs and many PEST runs are typically needed to calibrate a model. Additionally, the length of all SWI2 model runs in a given PEST run must be the same, and must be specified at the onset, yet it is difficult to know in advance how long a given SWI2 model run will take to reach steady state when PEST alters parameter values.

The hybrid approach used in this study started with manual calibration of each numerical model to ensure validity of the conceptual model and achieve a steady-state result that matched observations (fig. 10). Parameter values, model heads, and *ZETA* from the manual calibration were then used as initial conditions for model runs with PEST. PEST finds the combination of parameter values that minimizes residuals, but residuals may not represent steady state. After a PEST run, the parameter values that yielded the lowest residuals and were consistent with the conceptual model were used in a manual run until steady state was achieved. If necessary, additional adjustments were made to selected parameters using manual-calibration methods. The model was passed iteratively between manual and PEST methods, each time using the output (final head and *ZETA*) from the previous step (if it resulted in an improved calibration) as the starting conditions for the next, until satisfactory model calibration was achieved. In this report, "calibrated model" refers to the model that has the set

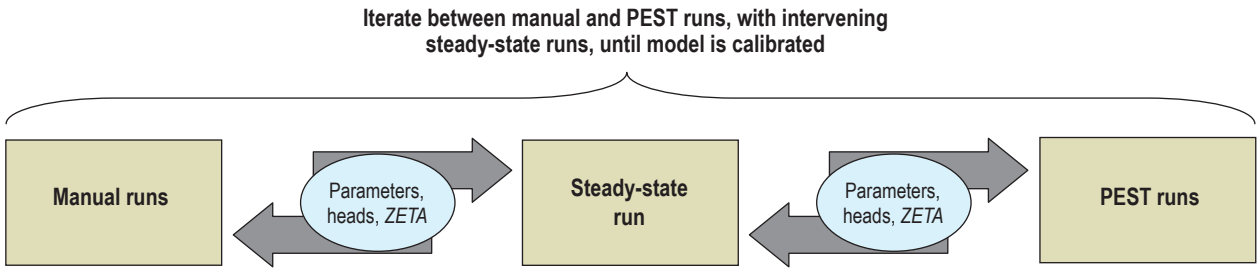

Figure 10. Diagram of the workflow used to calibrate the numerical groundwater models described in this report. *ZETA* is the altitude of the freshwater-saltwater interface.

of parameter values, determined by calibration, that resulted in satisfactory matches between simulated and measured observations for each model while remaining consistent with the conceptual models and available data on the range of hydraulic properties characteristic of the volcanic aquifers of Hawai‘i.

Parameter weighting.—A larger number of observations will generally drive calibration toward a model that more accurately represents the real-world system, but not all observations are equally reliable or matched by the model to the same level of precision. Some observations may have substantial measurement error, may not adequately represent the steady-state conditions being modeled, or may reflect hydrogeologic complexities that cannot be represented given the groundwater models' discretization or the simplified hydraulic-conductivity zonation. These observations are less useful for model calibration because they introduce residuals that cannot be ameliorated by adjusting parameters while staying true to the conceptual model and known hydrogeology. Some observations, such as water levels in areas where head gradients are steep, are inherently difficult to match precisely in a model, but a larger residual may be acceptable during calibration. In this study, average water levels and base flows computed from measurements made within the calibration period were generally weighted highest during calibration; observations computed from data measured outside this period were used where better data were not available, but these observations were given lower weight during calibration. Weights were further adjusted to account for differences in hydrologic setting and how reliable or representative each observation was deemed to be.

Sensitivity analysis.—After the models were calibrated, the sensitivity of simulated values for observations to the parameters adjusted during calibration was analyzed for each of the three models from the composite sensitivities provided by PEST. A parameter's composite sensitivity reflects the sensitivity of the model's weighted observations to the parameter. Composite sensitivities for the Kaua‘i, O‘ahu, and Maui models were generated by executing a single run of PEST using the parameter values, final heads, and final *ZETA* from the calibrated model as starting conditions. Relative composite sensitivities, which allow comparison of different types of parameters, were computed by multiplying the composite sensitivity by the parameter value in the calibrated model (Doherty, 2010). The relative sensitivity values were normalized for each model by dividing the values from the model by the highest relative sensitivity value of the model.

Error statistics.—For each groundwater setting (freshwater-lens, dike-impounded-groundwater, or thickly saturated setting) on each island, error statistics were calculated, including the (1) range of values in observations, (2) average absolute residual between simulated and observed values, and (3) standard deviation of residuals (table 3). Another useful statistic is the ratio of standard deviation of residuals and the range of observations. This statistic should generally be less than one, and a good fit to the data would be reflected if the ratio was equal to or less than about 0.1 (Kuniansky and others, 2004).

Residuals between modeled and observed values were evaluated using a 5-percent tolerance for each groundwater setting on each island (table 3). The 5-percent tolerance is ±5 percent of the overall range of observed values in each groundwater setting. For example, observed water levels in the freshwater-lens settings on O‘ahu spanned a 25-ft range from 0.6 to 25.6 ft relative to mean sea level; the 5-percent tolerance was computed as 5 percent of 25 ft, or ±1.25 ft. The 5-percent tolerance is thus scaled to the range of expected water levels in a given groundwater setting—the 5-percent tolerance may be tens of feet for settings where water tables are steep and water levels vary over hundreds of feet (for example, in the dike-impounded-groundwater setting), whereas tolerance may be less than a few feet for settings with gentle water-table gradients and a narrow range of water levels (such as the freshwater-lens setting). This statistic is more meaningful for evaluating the fit of a model than simply computing the residual as a percentage of the water-level value. For *ZETA*, the 5-percent tolerance was based on the Ghyben-Herzberg principle (range of observed water levels in that setting multiplied by 40). For drain discharge, all types (streams, springs, and tunnels) were included in the range of values used to compute the 5-percent tolerance for each island.

Table 3. Summary of error statistics for the numerical groundwater models of Kaua'i, O'ahu, and Maui, Hawai'i.

[*ZETA*, altitude of freshwater-saltwater interface. Range is the differrence between maximum and minimum values for the observation for a given island and hydrogeologic setting. The 5-percent tolerance is defined as 5 percent of the overall range of observed values in each hydrogeologic setting]

Comparison between		Hydrogeologic setting	Observations		5-percent tolerance[1]	Average absolute residual[1]	Standard deviation of residuals[1]	Percent of simulated values within 5-percent tolerance	Standard deviation of residuals divided by range of observations (dimensionless)
Model simulated	Observed		No.	Range[1]					
				Kaua'i					
Head	Water level	Freshwater lens	29	51.3	2.6	4.3	6.5	48	0.13
Head	Water level	Thickly saturated	23	577.6	28.9	33.4	52.0	70	0.09
Head	Water level	Dike-impounded groundwater	5	3,530.3	176.5	80.9	110.9	80	0.03
Discharge	Discharge	Streams and tunnels	21	67.0	3.4	0.5	0.9	95	0.01
				O'ahu					
Head	Water level	Freshwater lens	147	25.0	1.2	1.3	1.9	69	0.08
Head	Water level	Schofield high-level groundwater, caldera, and dike-impounded groundwater	110	1,209.5	60.5	69.6	158.5	76	0.13
ZETA	Transition-zone midpoint	Freshwater lens	35	798.0	49.9	79.1	106.5	51	0.13
Discharge	Discharge	Streams, springs, and tunnels	37	13.4	0.7	0.1	0.3	97	0.02
				Maui					
Head	Water level	Freshwater lens	55	12.9	0.6	0.7	0.9	49	0.07
Head	Water level	Dike-impounded groundwater and thickly saturated	12	1,161.4	58.1	96.5	189.2	75	0.16
ZETA	Transition-zone midpoint	Freshwater lens	4	820.0	25.8	226.0	199.3	0	0.24
Discharge	Discharge	Streams and springs	32	30.1	1.5	0.1	0.4	97	0.01

[1]Values are in units of feet for heads and *ZETA* or in million gallons per day for discharge.

Kaua‘i

Kaua‘i is the oldest of the three islands modeled in this study. The emergent part of Kaua‘i was formed by a single shield volcano that has been modified by erosion and collapse (fig. 11). Depressions in the shield volcano, carved by erosion and faulting, have been partly filled by sediment and rejuvenation-stage rocks. The bulk of the Kaua‘i massif, however, is composed of shield-stage volcanic rocks, which form the base on which younger units lie.

Much of Kaua‘i has low permeability as a result of dike intrusion (fig. 12). Near the center of the dike-intruded lavas is a region of low-permeability caldera-filling lava flows and dikes (Macdonald and others, 1960). Dike abundances decrease (and bulk aquifer permeability increases) away from the caldera. Water levels are highest in this low-permeability interior region of the island. The dike-impounded-groundwater setting (fig. 4*C*) is predominant in this part of the island (fig. 13). Groundwater saturates the rocks and emerges as a wetland near the center of the island. From there, the water table descends steeply toward the coast and is largely shaped by streams that incise and drain

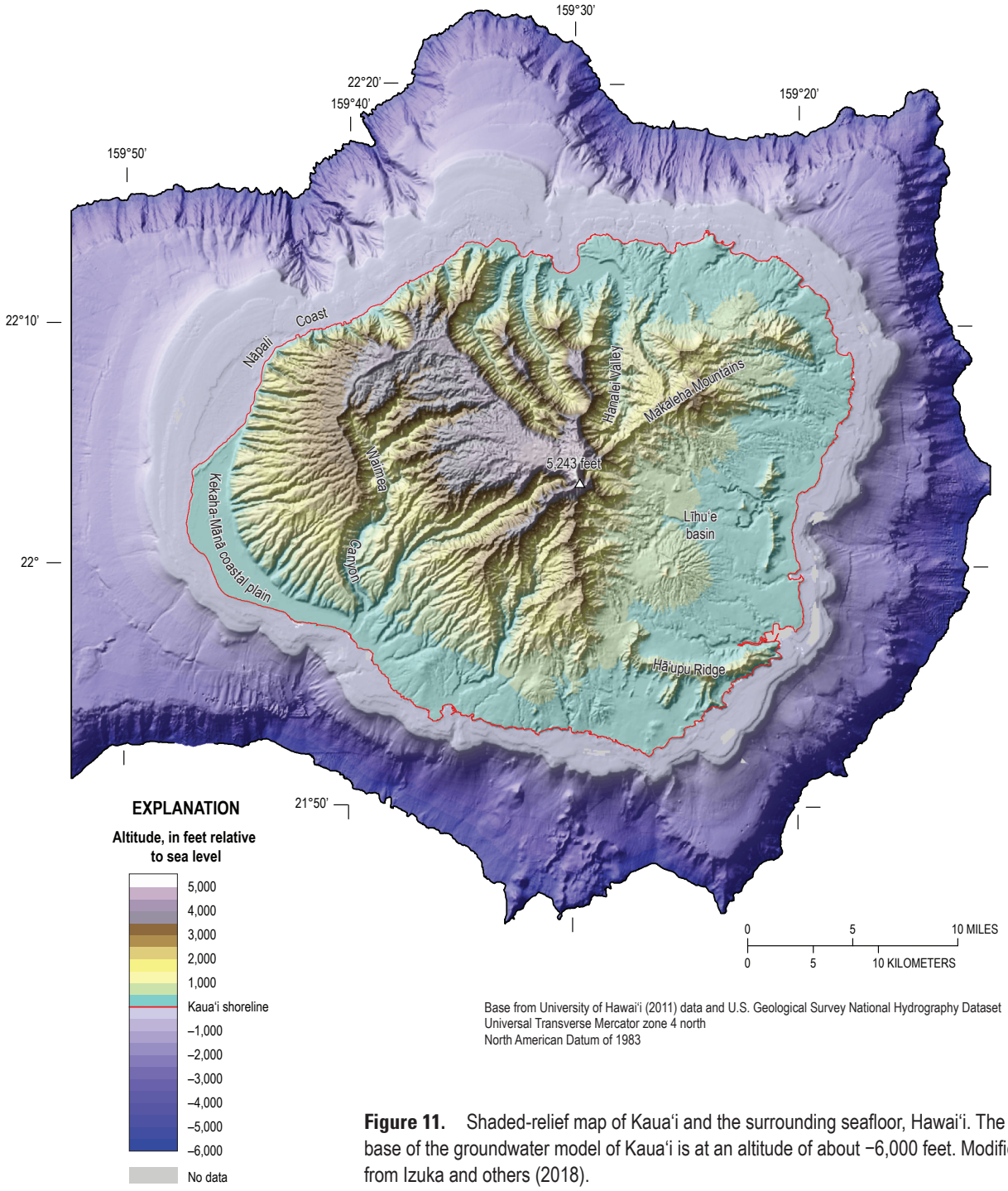

Figure 11. Shaded-relief map of Kaua‘i and the surrounding seafloor, Hawai‘i. The base of the groundwater model of Kaua‘i is at an altitude of about −6,000 feet. Modified from Izuka and others (2018).

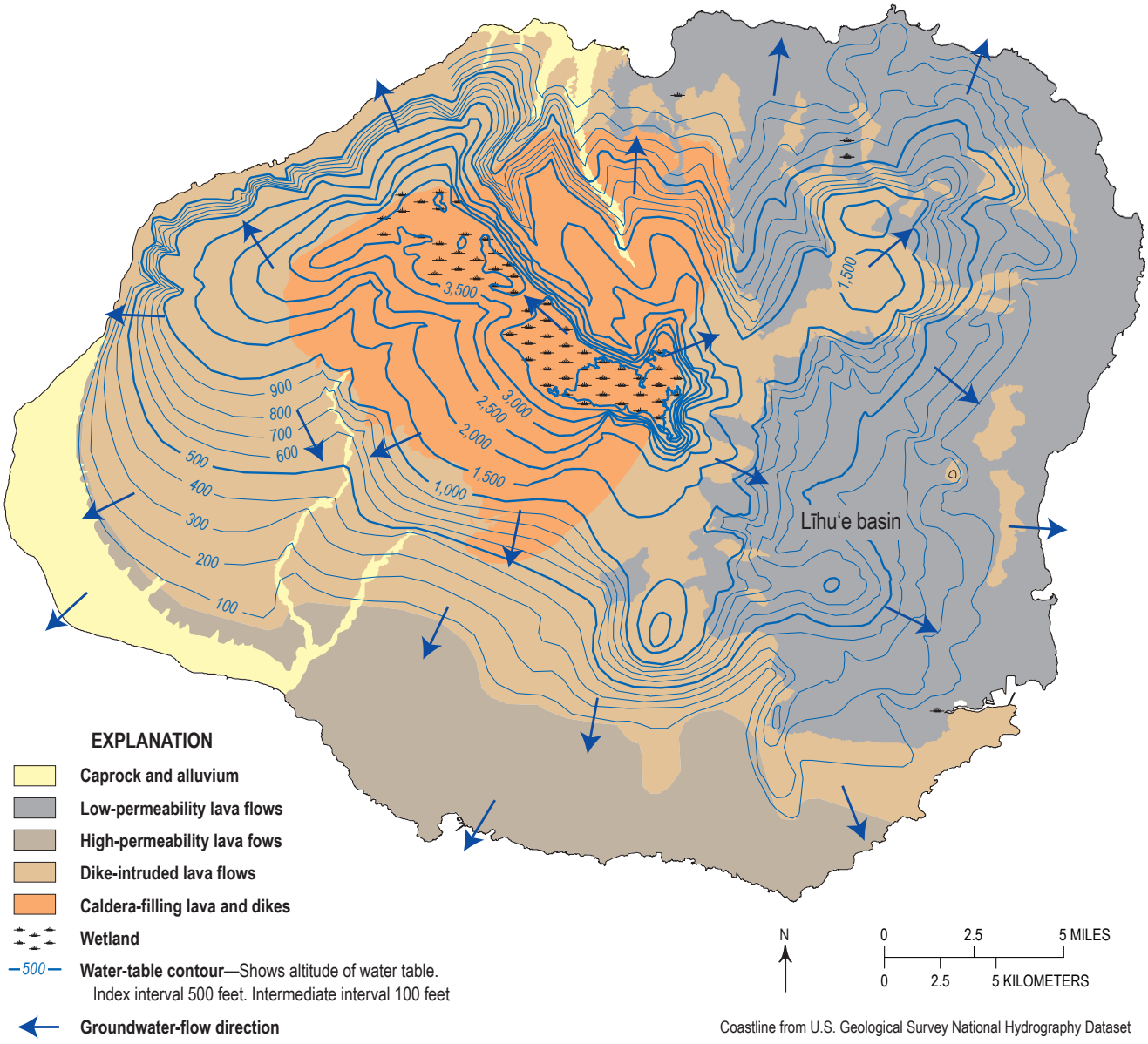

Figure 12. Map showing the water table and its relation to the hydrogeology of Kaua‘i, Hawai‘i. Modified from Izuka and others (2018) with information from Sherrod and others (2007); water table from Izuka and others (2018).

the upper parts of the dike compartments. Stream gages in this area indicate that flow persists 95 percent of the time or more (Cheng, 2016), which is consistent with groundwater discharges to streams from the dike-impounded-groundwater setting. Groundwater that does not discharge to streams flows through the subsurface either to other groundwater bodies that have lower water levels or to coastal discharge.

In eastern Kaua‘i, thick rejuvenation-stage lava flows and sediments overlie the shield volcano’s eroded surface. These rocks that partly fill depressions in the shield volcano form a low-permeability, although largely dike free, aquifer (fig. 12) (Izuka and Gingerich, 1998, 2003). The low-permeability lava flows resist groundwater flow, which results in steep horizontal and vertical head gradients and the predominance of the thickly saturated setting (fig. 4*C*, 13). Estimates of K_h for the low-permeability aquifer vary widely, but the regional K_h is probably less than 1 ft/d; estimates of K_v are about three orders of magnitude lower (Izuka and Gingerich, 1998; Gingerich, 1999c; Izuka and Oki, 2002; Izuka, 2006; Izuka and others, 2018). The low-permeability aquifers receive subsurface flow from the dike-impounded-groundwater settings of central Kaua‘i and through the surface from recharge. Streams provide the primary means by which groundwater discharges naturally from the aquifer (Izuka and Gingerich, 1998).

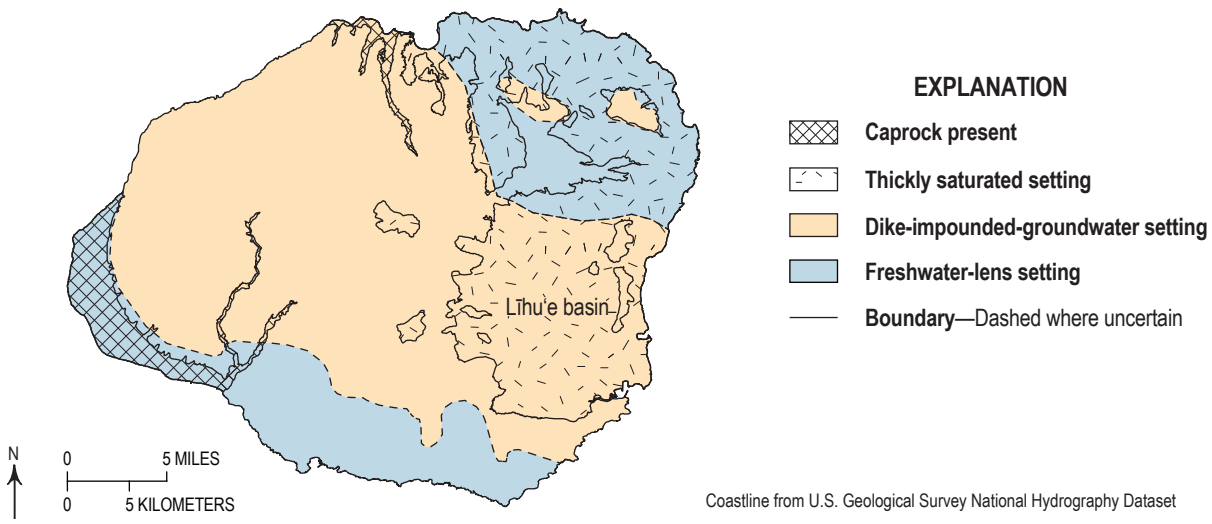

Figure 13. Map showing the principal groundwater settings on Kaua'i, Hawai'i. Modified from Izuka and others (2018).

The freshwater-lens setting (fig. 4*A*, *B*) predominates in the high-permeability lava-flow aquifers along the southern coast of Kaua'i (fig. 12, 13). The lava flows are mostly from the shield stage, but some are from the rejuvenation stage (Izuka and others, 2018). Estimates of K_h range from about 200 to 800 ft/d; estimates for K_v are about 1.0 ft/d (Izuka and Gingerich, 1998; Izuka and Oki, 2002; Izuka, 2006; Rotzoll and El-Kadi, 2008). The freshwater lenses receive subsurface flow from upgradient dike-impounded-groundwater settings and through the surface from recharge. In the southwest, the high-permeability aquifer is overlain by caprock that resists groundwater discharge from the volcanic aquifers and causes the freshwater lens to be thicker than it would be without the caprock (fig. 4*A*). Caprock is less well developed along the rest of the southern Kaua'i coast.

Model Structure

The Kaua'i numerical model consists of two layers with 341 rows and 421 columns. The model has 191,399 active cells, 76,304 of which are in the upper layer and 115,095 in the lower layer. The model grid is rotated 10 degrees clockwise relative to the cardinal geographic directions to facilitate efficient discretization of the hydrogeologic features (fig. 14). The model was divided into 12 *K* zones that represent Kaua'i's principal generalized hydrogeologic units (fig. 12). The boundary between the upper and lower layers is a horizontal surface at –500 ft, which is about the mean altitude of the contact between shield- and rejuvenation-stage rocks in eastern Kaua'i (Izuka and others, 2018).

A total of 871 million gallons per day (Mgal/d) of groundwater recharge was applied to the upper layer of the Kaua'i model, wherever surfaces of the volcanic aquifers were above sea level (fig. 15). A total withdrawal of 49.4 Mgal/d from wells and shafts was simulated in the model (fig. 16). The withdrawals were computed from reported drafts for the calibration period, as described in the Withdrawals section above; if no draft was reported but CWRM records indicated that a well was in operation during the calibration period, withdrawal was estimated to be 34 percent of the pump capacity (the 34-percent value is based on wells that have reported data, and is equivalent to about 8 hours of runtime per day). Altitudes for drains that simulate streams and tunnels (H_{str} in eq. 5) and for heads used in offshore GHBs (H_{ocean} in eq. 2) (fig. 17) were computed as previously described. The altitude for drains that simulate areas where the top of the caprock is above sea level and the top of the volcanic aquifer is below sea level (H_{cpr} in eq. 4) was set to zero. A high-altitude marsh on Kaua'i (fig. 12) is conceptualized as part of the saturated groundwater system; its altitude is used as a general indication of water-table altitude and simulated water exchange with the model is represented in the discharge to streams.

Hydraulic Properties

In the calibrated model of Kaua'i, *K* zones that represent aquifers composed of dike-free shield-stage lavas in the model have a K_h value of 2,000 ft/d and K_v value of 6.0 ft/d (fig. 14). These values are consistent with the high K_h and the horizontal-to-vertical anisotropy typically associated with shield-stage lava-flow aquifers in Hawai'i. Although much of Kaua'i is intruded by dikes, a substantial part of the volcanic massif at some distance offshore is likely composed of dike-free lava flows. In the Kaua'i model, the wide areas covered by the *K* zone that represents dike-free shield-stage lava-flow aquifers are consistent with this premise.

Near the center of the Kaua'i model, a low-permeability region corresponds to caldera-filling lava flows and dikes (fig. 14). Values for K_h and K_v for this zone in the calibrated model are 0.10 and 0.050 ft/d, respectively. These low hydraulic

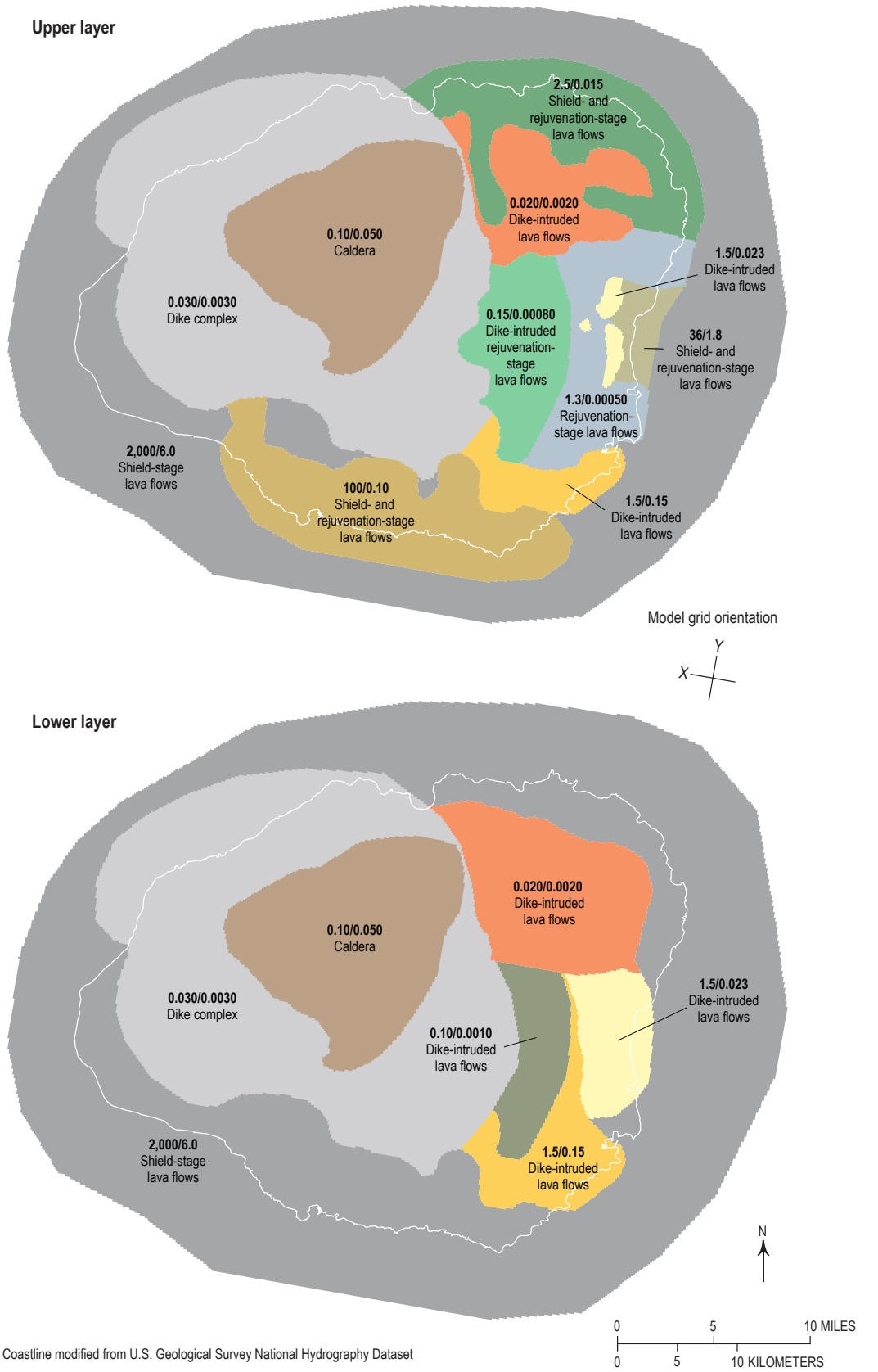

Figure 14. Map of hydraulic-conductivity zones (*K* zones) and values in the numerical groundwater model of Kaua‘i, Hawai‘i. Numbers show hydraulic conductivity in feet per day: values to the left of the slash are horizontal conductivity, values to the right are vertical conductivity. White line shows the Kaua‘i coastline.

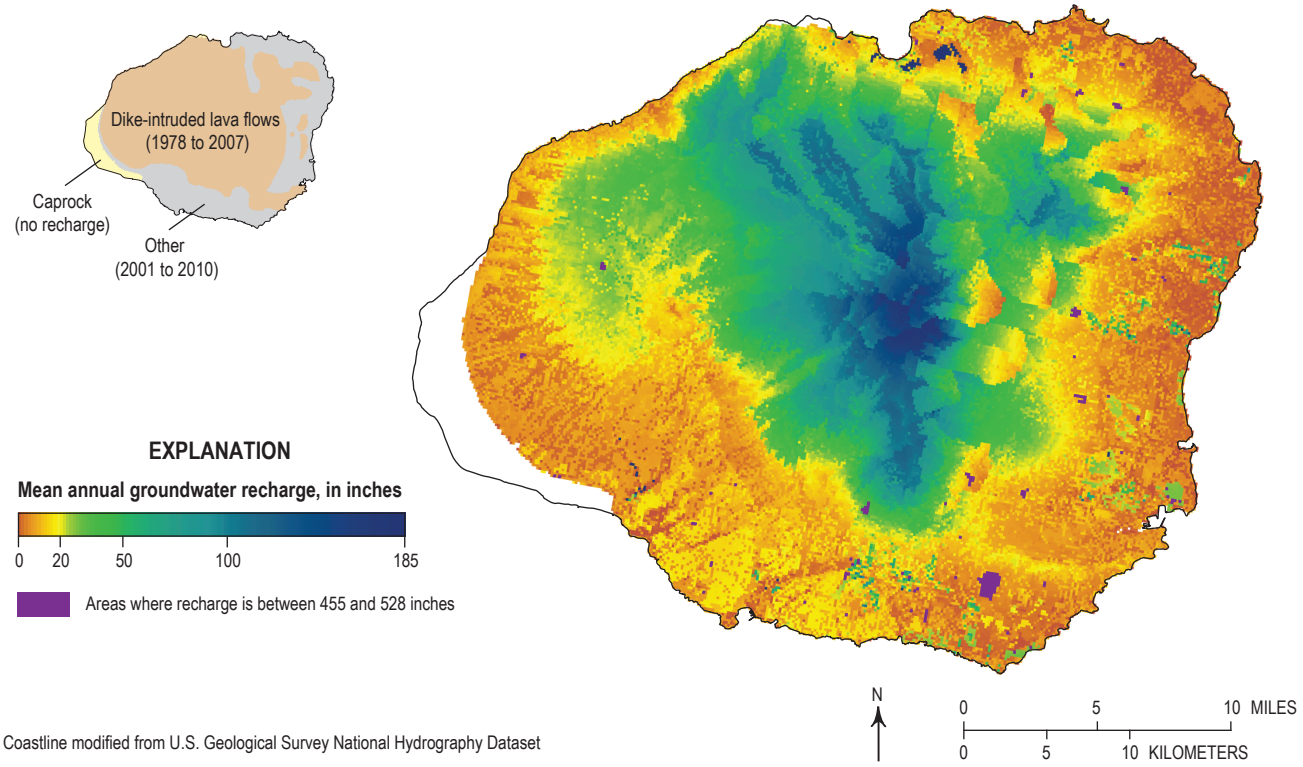

Figure 15. Map showing the distribution of groundwater recharge in the numerical groundwater model of Kauaʻi, Hawaiʻi. Recharge is based on averages computed by Izuka and others (2018) for periods shown on the inset map.

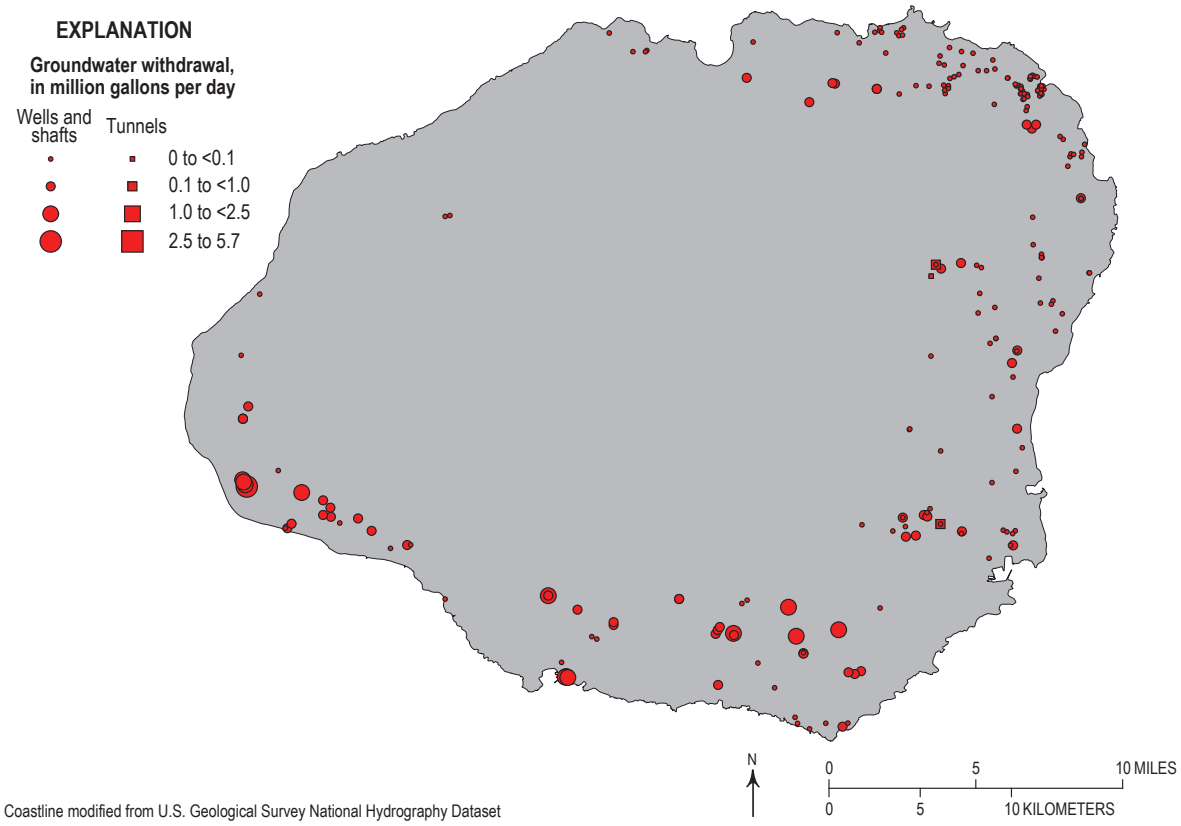

Figure 16. Map showing the distribution of groundwater withdrawals in the numerical groundwater model of Kauaʻi, Hawaiʻi.

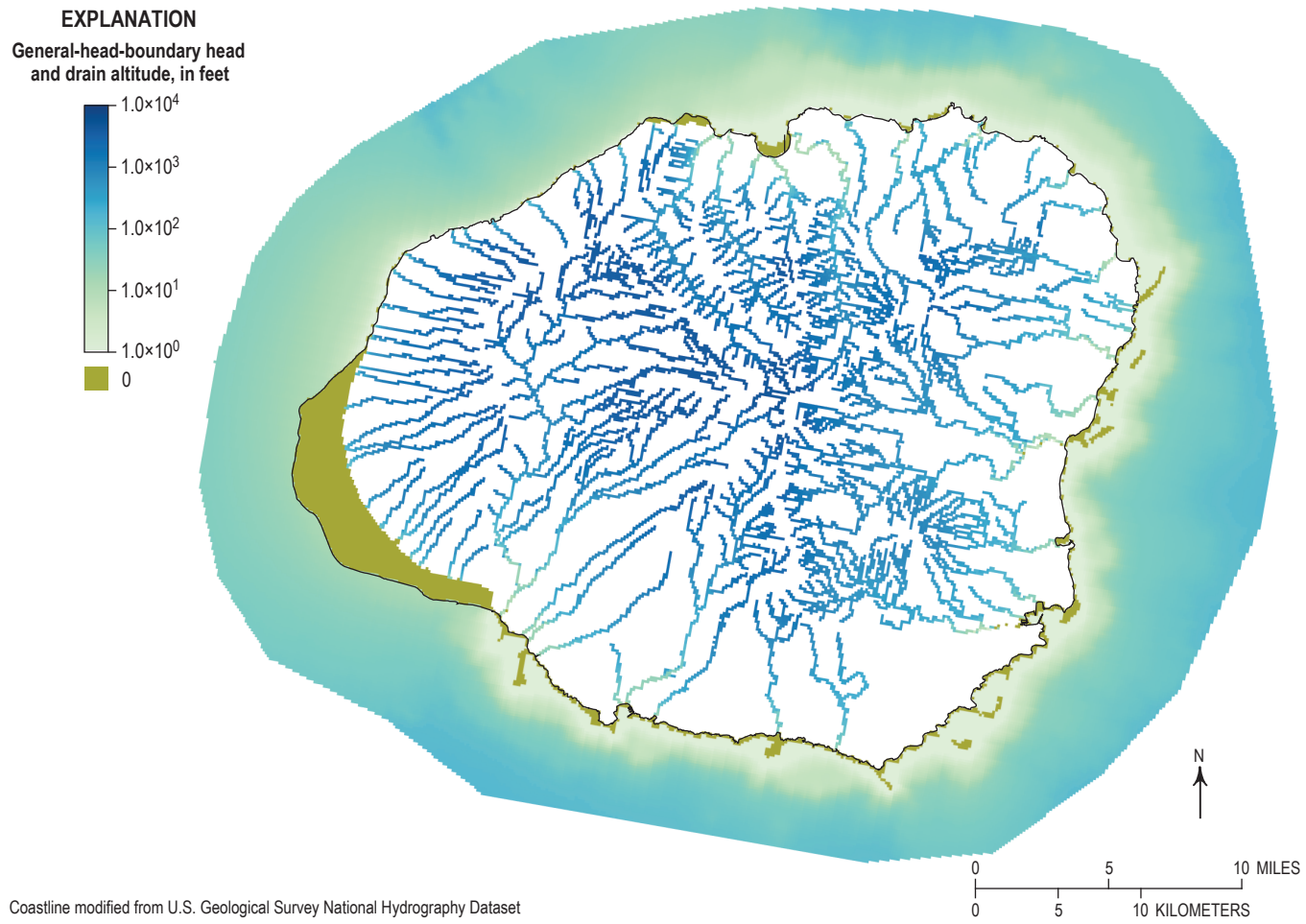

Figure 17. Map of general-head-boundary heads and drain altitudes in the numerical groundwater model of Kaua‘i, Hawai‘i. Black line shows the Kaua‘i coastline.

conductivities are consistent with the conceptualization that caldera fill consists of thick, massive lava flows intruded by dikes.

Surrounding the caldera fill are six *K* zones that represent dike-intruded areas. The dike complex represents the area of high dike concentration; in the calibrated model this zone has a K_h value of 0.030 ft/d (fig. 14), which is comparable to estimates of low bulk hydraulic conductivities in dike complexes in Hawai‘i. The K_v value for this *K* zone is 0.0030 ft/d; this zone is expected to be less anisotropic (K_h to K_v) than zones that consist of dike-free lava flows because dike sheets that cut vertically across lava flows reduce K_h more than K_v. A *K* zone that represents a northeast extending rift zone (described by Macdonald and others [1960]), also presumed to have a high dike concentration, has a K_h value of 0.020 ft/d and K_v value of 0.0020 ft/d in the calibrated model. An upper-layer *K* zone with K_h value of 0.15 ft/d and K_v value of 0.00080 ft/d in the calibrated model represents dike intrusion into thick, rejuvenation-stage lava flows that already have low permeability. Four *K* zones represent parts of the shield-stage rocks where dike abundances are likely to be lower and hydraulic conductivities higher than the dike complex; these areas have K_h values of 0.10 to 1.5 ft/d and K_v values of 0.0010 to 0.023 ft/d. The lowest of these values is in a *K* zone that represents an area that was intruded by dikes during both the shield and rejuvenation stages.

Two *K* zones in the upper layer represent low-permeability rejuvenation-stage lavas that accumulated in the Līhu‘e basin (fig. 12). Where the low-permeability rejuvenated-stage lava flows are dike free, values of K_h and K_v in the calibrated model are 1.3 and 0.00050 ft/d, respectively (fig. 14). These values are similar to low hydraulic-conductivity values reported in previous studies and consistent with the conceptualization that thick lava flows and interlayered sediments accumulated in a preexisting depression have low permeability. Hydraulic conductivities are lower where the rejuvenation-stage lava flows are intruded by dikes—values of K_h and K_v in the calibrated model are 0.15 and 0.00080 ft/d, respectively.

Outside the Līhu‘e basin, the rejuvenation-stage rocks have not accumulated to as great a thickness as within the basin. In these areas, the upper layer of the model represents a combination of rejuvenation-stage and shield-stage rocks.

Three K_h zones in the upper-layer of the Kaua‘i model outside the Līhu‘e basin represent a combination of shield- and rejuvenation-stage lava flows (fig. 14). In the calibrated model, K_h in these zones ranges from 2.5 to 100 ft/d and K_v ranges from 0.015 to 1.8 ft/d. The highest horizontal hydraulic conductivity among these K zones is in the south where, as described in the conceptual model for Kaua‘i, available data indicate that the area is more permeable than other areas that are covered by rejuvenation-stage lava flows.

In the calibrated model, values of C_{str} for stream and tunnel cells range from 1.9 to 10,000 square feet per day (ft^2/d) (fig. 18). The wide range of values is consistent with the concept that stream-bed thickness and hydraulic properties vary widely among streams on Kaua‘i, but measured values for this parameter are lacking. Values of C_{cpr} in the calibrated model also range widely from 2.0 to 1,000,000 ft^2/d, but no measured values for C_{cpr} are available for comparison. The wide range is due to the wide variation in hydraulic properties and caprock thicknesses in the calibrated model of Kaua‘i. The sharp contrast in C_{cpr} between east and west offshore areas is mostly an artifact of the value of T_{cpr} used in computing C_{cpr}. Along the west coast, where caprock thickness varies substantially, T_{cpr} was computed as described in the Flow Boundaries section; in the east, the minimum value of 1 ft was used for T_{cpr}.

Groundwater Levels and Flow

The calibrated model of Kaua‘i generally replicates the different ranges of observed water levels among the different groundwater settings that are present on Kaua‘i (figs. 13 and 19). Model-simulated head in the high-permeability aquifers on the south coast of Kaua‘i replicate the gentle water-level gradient characteristic of freshwater-lens settings, where observed water levels are less than a few tens of feet above sea level (figs. 19*A* and 20). The average absolute residual in the freshwater-lens settings of Kaua‘i was 4.3 ft, the standard deviation of residuals was 6.5 ft, and the ratio between standard deviation of residuals and range of values was 0.13 (table 3). Observed levels spanned a range of 51.3 ft; 48 percent of the simulated heads were within 5 percent of this range. The

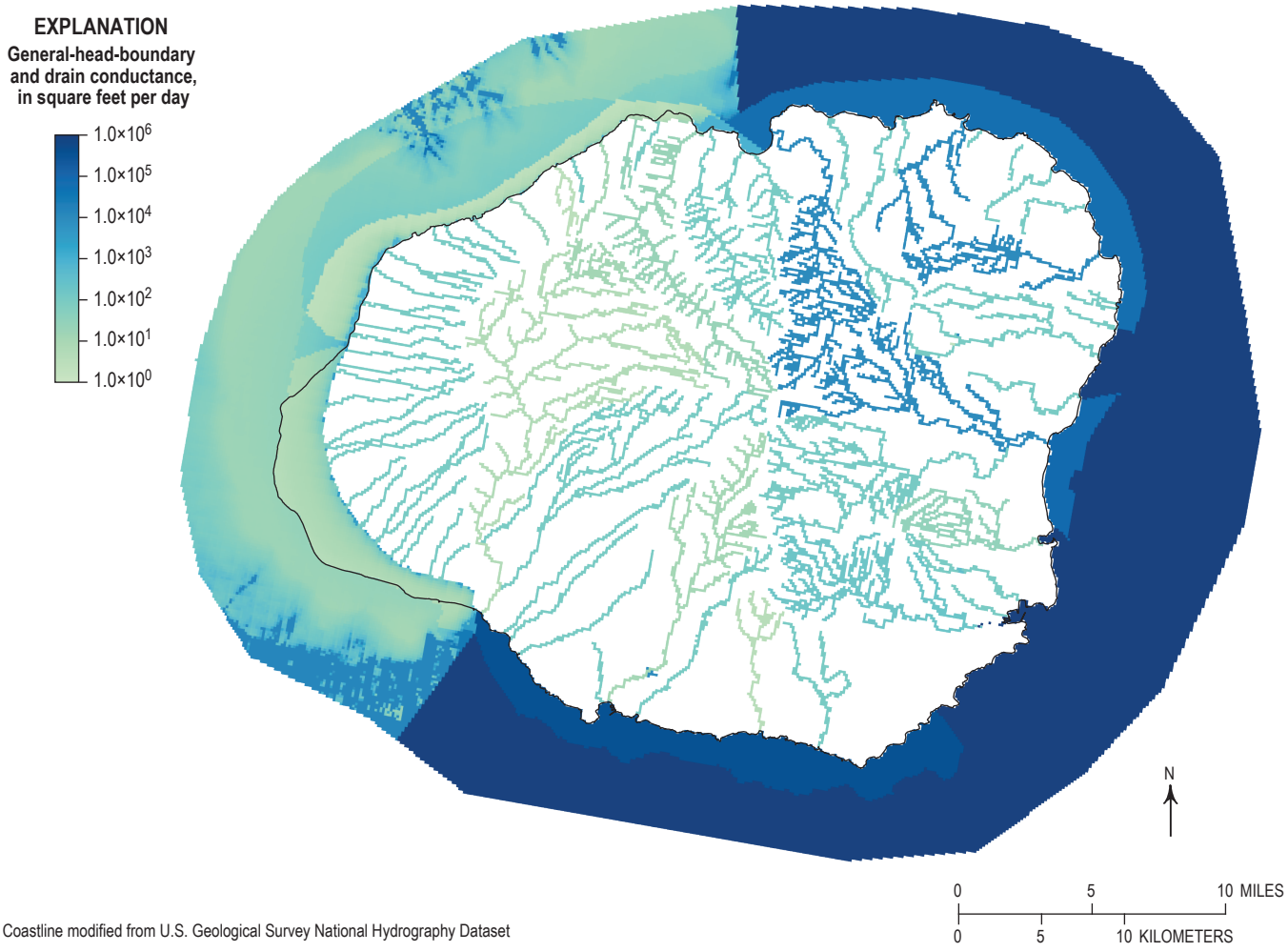

Figure 18. Map showing the distribution of conductance values for head-dependent boundary cells that represent caprock, streams, and tunnels in the calibrated numerical groundwater model of Kaua‘i, Hawai‘i. Black line shows the Kaua‘i coastline.

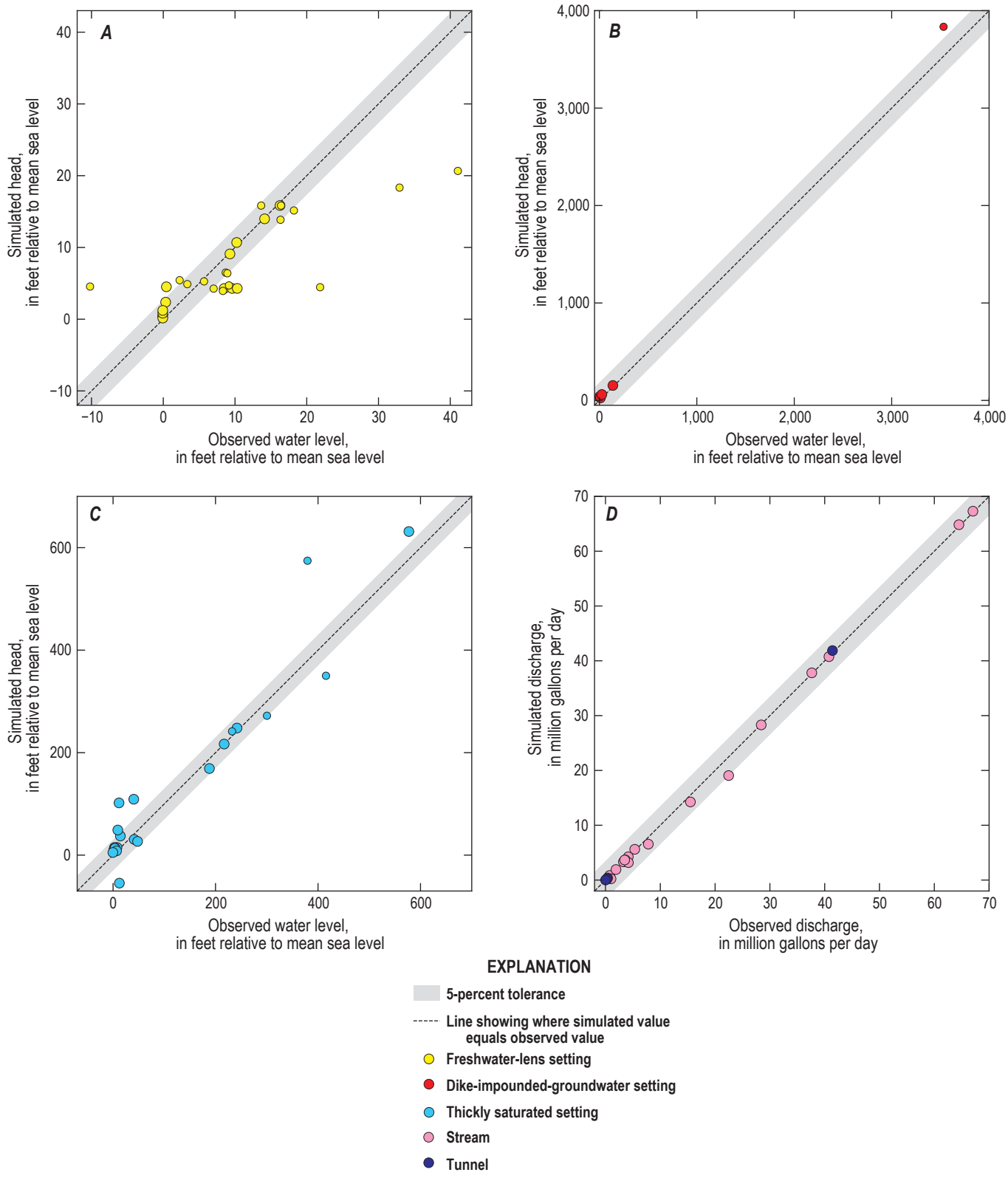

Figure 19. Plots comparing observed and model-simulated values in the calibrated numerical groundwater model of Kaua‘i, Hawai‘i. Symbol diameter indicates relative weight during calibration.

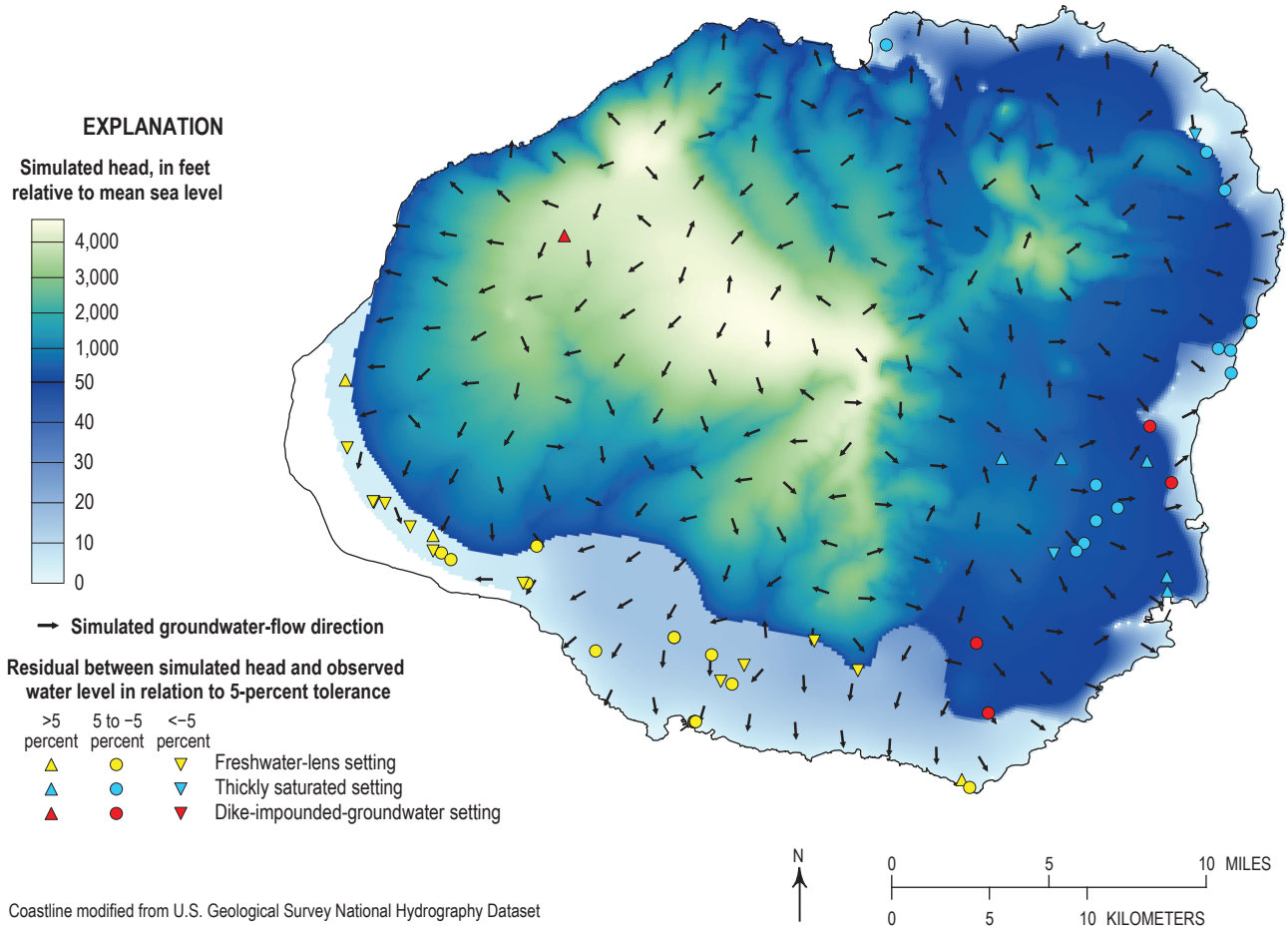

Figure 20. Map of simulated head and groundwater flow in the upper layer of the calibrated numerical groundwater model of Kaua‘i, Hawai‘i.

calibrated Kaua‘i model replicates the low-altitude, low-gradient water table and the general flow direction toward discharge at the coast.

Observed water levels from the dike-impounded-groundwater setting (fig. 13), which includes caldera fill for the purposes of this discussion, span a wide range of altitudes from a few tens to thousands of feet above sea level (fig. 19*B*). Heads in the calibrated Kaua‘i model generally match the water-level observations for this setting, although few reliable observations are available and a substantial data gap exists between about 400 and 3,600 ft altitude. Model-simulated heads match available observed water levels within the 5-percent tolerance (as described in “error statistics” of the Calibration section above), except for one observation near 3,600 ft. However, the areal distribution of model heads replicates the key characteristics of this setting, such as the high, steeply sloping water table and flow toward discharge at incised streams (figs. 11 and 20). The average absolute residual for observations in the dike-impounded-groundwater setting was 80.9 ft and the standard deviation of residuals was 110.9 ft (table 3).

Observed water levels from the thickly saturated setting in eastern Kaua‘i (fig. 13) range from about 0 to 600 ft (fig. 19*C*). The wide range of water levels results from the steep horizontal and vertical head gradients characteristic of this low-permeability setting (Izuka and Gingerich, 1998, 2003). Simulated heads in the calibrated Kaua‘i model generally replicate this range of observed water levels and the overall steep gradient. The average absolute residual in the low-permeability aquifers was 33.4 ft and the standard deviation of residuals was 52.0 ft. Differences between simulated heads and observed water levels stem in part from limitations in the model’s ability to precisely represent steep head gradients in both the horizontal and vertical directions. Wells that are close together but penetrate to different depths can have substantially different observed water levels that cannot always be replicated in a model with only two layers. Discrepancies between simulated heads and observed water levels are small, however, compared to the 600-ft range of water-level altitudes in this setting—70 percent of the simulated heads in this setting fall within the 5-percent tolerance. The ratio between standard

deviation of residuals and range of values was 0.09. The model-simulated heads generally reproduce the elevated, stream-incised water table in this low-permeability aquifer (figs. 13 and 20).

The distribution of head in the calibrated model of Kaua‘i results in groundwater flow (fig. 20) that is generally consistent with the conceptual model (fig. 12). Groundwater in the dike-impounded-groundwater setting in the interior of the island (fig. 13) flows radially toward the coast, but much of it discharges to streams before it can flow to down-gradient aquifers. Some of the groundwater flows into the thickly saturated setting in the low-permeability aquifers of eastern Kaua‘i; much of this groundwater also discharges to streams and the remainder discharges to the ocean. Some of the groundwater from the interior of Kaua‘i flows into the freshwater-lens settings in the high-permeability aquifers in the south of the island. Most of the groundwater flowing through freshwater lenses ultimately discharges to the ocean, either directly from the volcanic aquifers or through the caprock. Groundwater flowing from the interior to the northwest discharges to the ocean directly from the dike-impounded-groundwater setting.

Freshwater-Saltwater Interface

No direct measurements of the altitude of the transition zone in Kaua‘i’s aquifers are available to compare to the model-simulated freshwater-saltwater interface, but the simulated interface (figs. 21 and 22) is consistent with the conceptual model of groundwater in oceanic islands (figs. 2 and 4). In the dike-impounded-groundwater setting that dominates the center of the island, fresh groundwater extends down to the bottom of the model. A relatively thin simulated freshwater lens exists in the high-permeability aquifers in the southern part of the Kaua‘i model. Fresh groundwater forms a thicker body in the thickly saturated setting in eastern Kaua‘i.

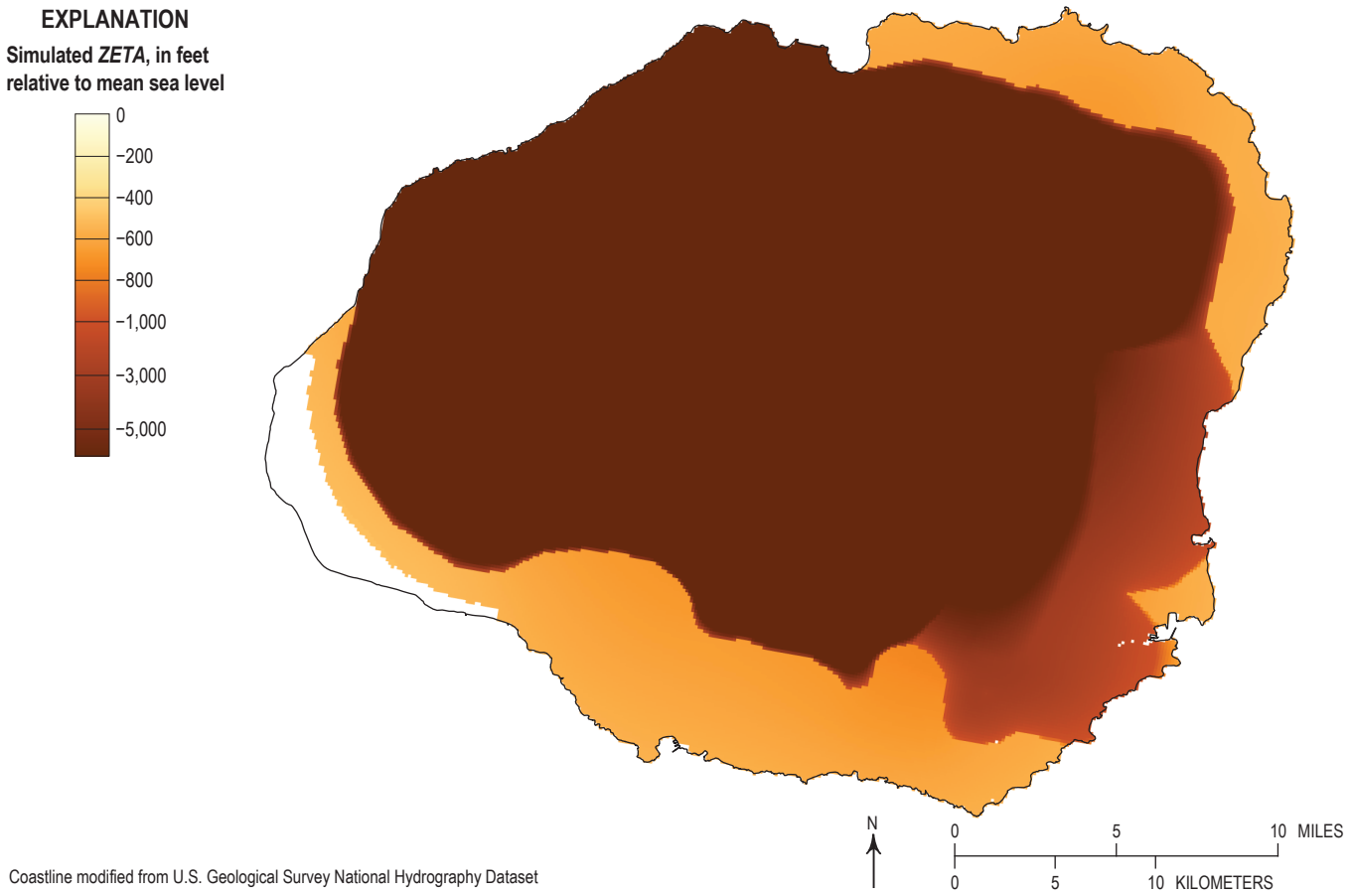

Figure 21. Map of the simulated altitude of the freshwater-saltwater interface (*ZETA*) in the numerical groundwater model of Kaua‘i, Hawai‘i.

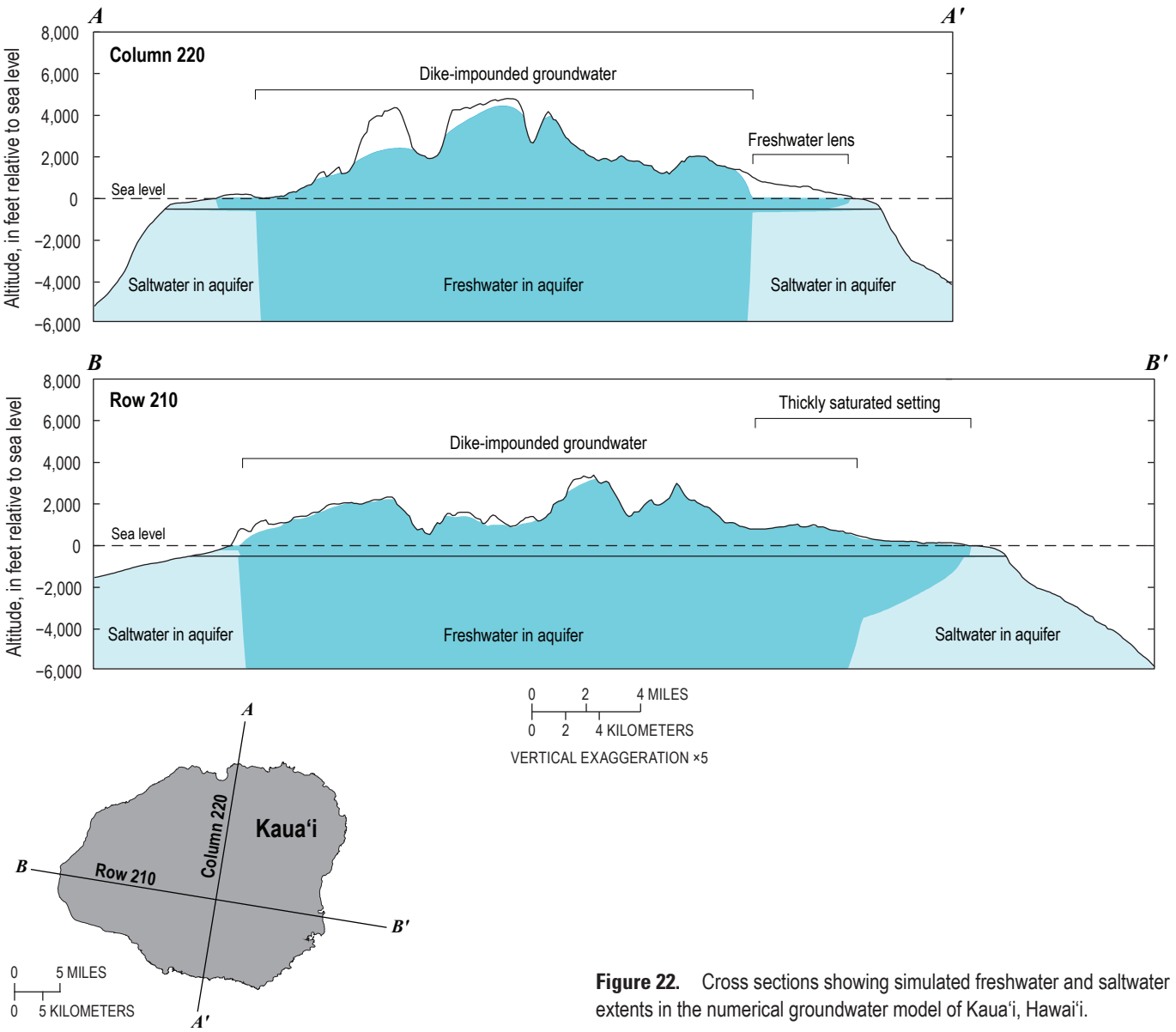

Figure 22. Cross sections showing simulated freshwater and saltwater extents in the numerical groundwater model of Kaua‘i, Hawai‘i.

Discharge to Streams, Tunnels, and the Ocean

Base-flow observations for all but one stream gage were computed using the hydrograph separation method described in the Calibration section above. A base-flow estimate by Izuka and Gingerich (1998) for Hanamā‘ulu Stream in the Līhu‘e basin (adjusted for period as described in eq. 6), was also used as an observation during calibration. Although this gage was operated for only a very short time between 1911 and 1913, it provided information where no better data exist. Simulated drain discharge to tunnels and streams in the calibrated Kaua‘i model agree closely with tunnel draft data and base-flow estimates from analyses of stream-gage data (fig. 19*D*). The average absolute residual was 0.5 Mgal/d, the standard deviation of residuals was 0.9 Mgal/d, the ratio between standard deviation and range of values was 0.01, and 95 percent of residuals between simulated and observed drain discharge were within the 5-percent tolerance (table 3).

Most of the discharge to streams (fig. 23) occurs in the dike-impounded-groundwater setting in the center of Kaua‘i and the thickly saturated setting in eastern Kaua‘i (figs. 12 and 13). This result is consistent with the conceptual model for Kaua‘i in which stream incision plays an important role in draining the aquifer and shaping the water table in these low-permeability aquifers. In contrast, stream reaches that traverse high-permeability aquifers in southern Kaua‘i receive little or no

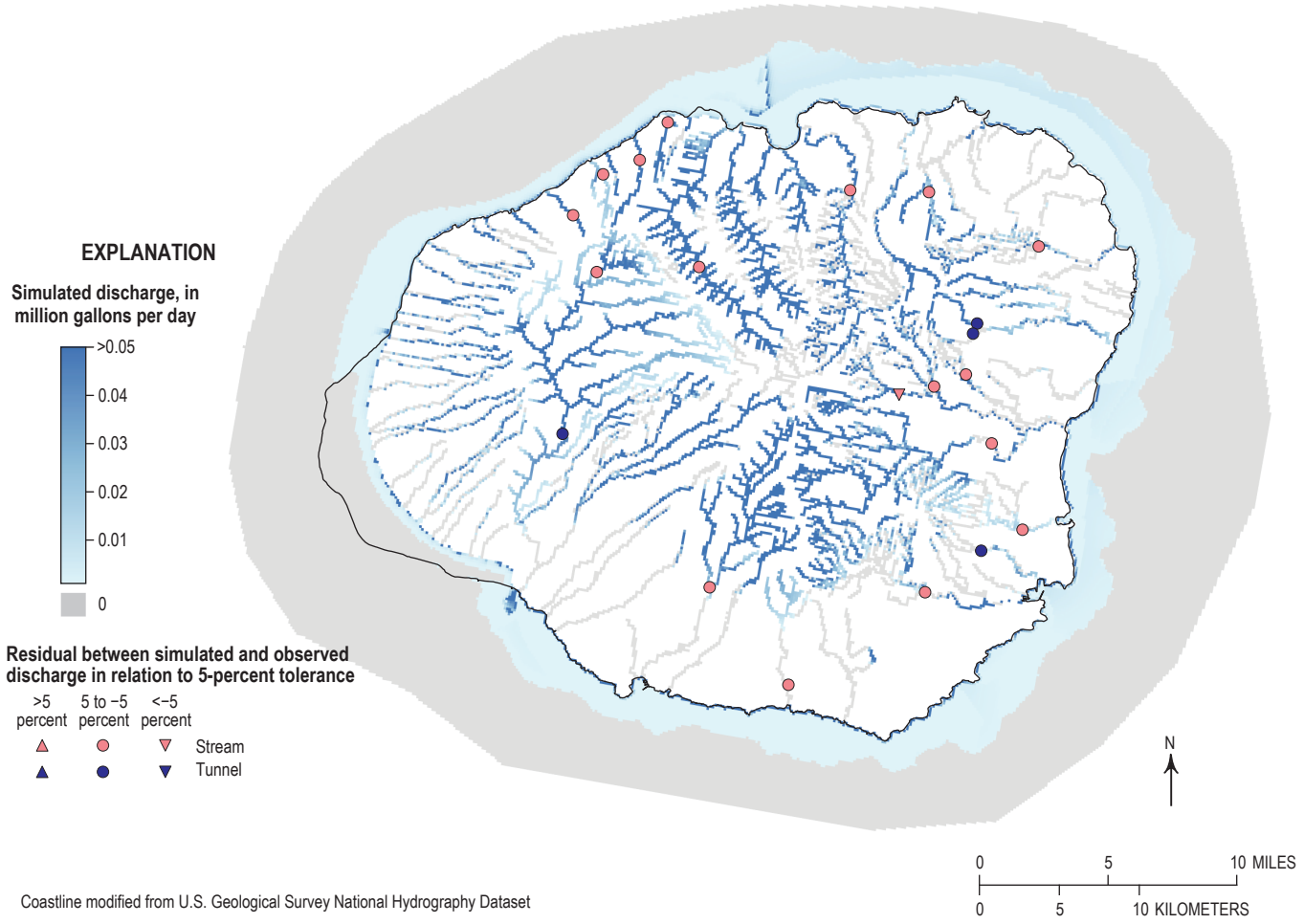

Figure 23. Map of simulated groundwater discharge to streams, tunnels, and the ocean in the calibrated numerical groundwater model of Kaua‘i, Hawai‘i. Black line shows the Kaua‘i coastline.

groundwater discharge because the stream channels are mostly above the water table.

Groundwater discharge to the ocean occurs diffusely over broad areas of cells as well as in narrow bands of cells that have high discharge rates (fig. 23). One of the narrow bands of high discharge corresponds with the intersection of the volcanic aquifer with sea level, which is consistent with the conceptual model. A second smaller band of high discharge occurs at the intersection of the volcanic aquifer and the boundary between the upper and lower layers of the model. This second band is an artifact of the numerical model and discretization. Other areas of high discharge to the ocean are artifacts of other aspects of the numerical modeling approach, such as whether caprock thickness was computed or set to the minimum value (see the Flow Boundaries section above). Although these artifacts of the numerical model cause imprecision in the simulated location of groundwater discharge to the ocean, the overall partitioning of simulated groundwater discharge between streams and the ocean is consistent with the conceptual model.

Model Sensitivity to Parameters

The parameters to which the calibrated groundwater model of Kaua‘i was most sensitive (fig. 24) were K_h of the caldera fill and K_h of the dike-intruded interior of the island (fig. 14). Because groundwater generally flows from these interior areas toward the coast, model-simulated heads and stream base flows throughout the island are affected when the values of these parameters are varied during calibration. The model is also sensitive to C_{str} for streams that drain the caldera fill and dike-intruded interior. Not only do the C_{str} values affect the model's match of base flows for these streams, but the draining of groundwater by these streams affects the flow of groundwater from the interior of the island to adjacent aquifers and plays a principal role in shaping the water table (Izuka and others, 2018). Model calibration was much less sensitive to hydraulic properties of aquifers downgradient of the dike-impounded-groundwater setting (particularly those that have few observations), the caprock (C_{cpr}), and streams draining the coastal aquifers.

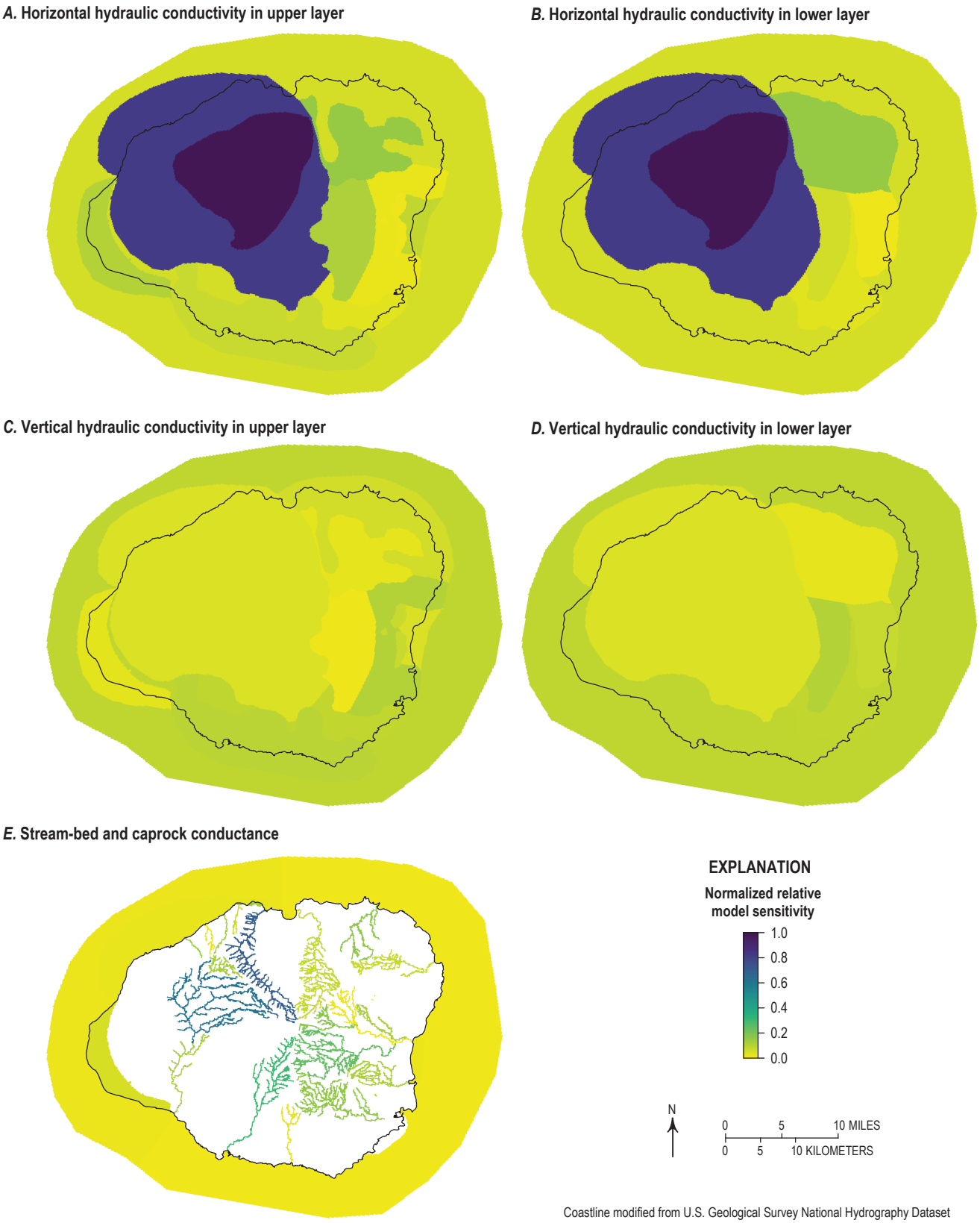

Figure 24. Maps showing normalized relative composite sensitivities of parameters adjusted during calibration of the numerical groundwater model of Kaua‘i, Hawai‘i. *A*, Horizontal hydraulic conductivity in the upper layer of the model; *B*, horizontal hydraulic conductivity in the lower layer of the model; *C*, vertical hydraulic conductivity in the upper layer of the model; *D*, vertical hydraulic conductivity in the lower layer of the model; and *E*, stream-bed conductance and parameters related to caprock conductance. Black line shows the Kaua‘i coastline.

O‘ahu

O‘ahu is the second oldest of the islands modeled in this study. It has two prominent mountain ranges, the Wai‘anae and Ko‘olau Ranges, the remnants of two shield volcanoes (fig. 25). Rocks of the younger Ko‘olau volcano partly overlap the eroded flank of the Wai‘anae volcano beneath the Schofield Plateau. Soil, weathered basalt, and alluvium separate the Ko‘olau and Wai‘anae rocks in some places. The Wai‘anae and Ko‘olau volcanoes are built mostly of thick accumulations of thin lava flows that form high-permeability aquifers (fig. 26). Estimates of K_h for dike-free lava-flow aquifers on O‘ahu range from a few to several thousand feet per day, but most estimates are between 500 and 5,000 ft/d. In these high-permeability aquifers, freshwater exists primarily in the freshwater-lens setting with extensive caprock that resists groundwater discharge to the ocean (figs. 4*A* and 27). Large volumes of freshwater accumulate in the lenses as a result of the caprock, forming some of the most productive groundwater sources in Hawai‘i.

The freshwater lenses receive much of their water from subsurface flow from upgradient aquifers (fig. 26) but also some inflow from recharge through the surface. The water tables of the freshwater lenses are less than about 50 ft above sea level and slope gently toward the coast. Fresh groundwater in the lenses generally flows toward the ocean, and discharges naturally to springs along the inland margin of the caprock or seeps through the caprock to discharge offshore. Low-permeability structures within the freshwater-lens settings result

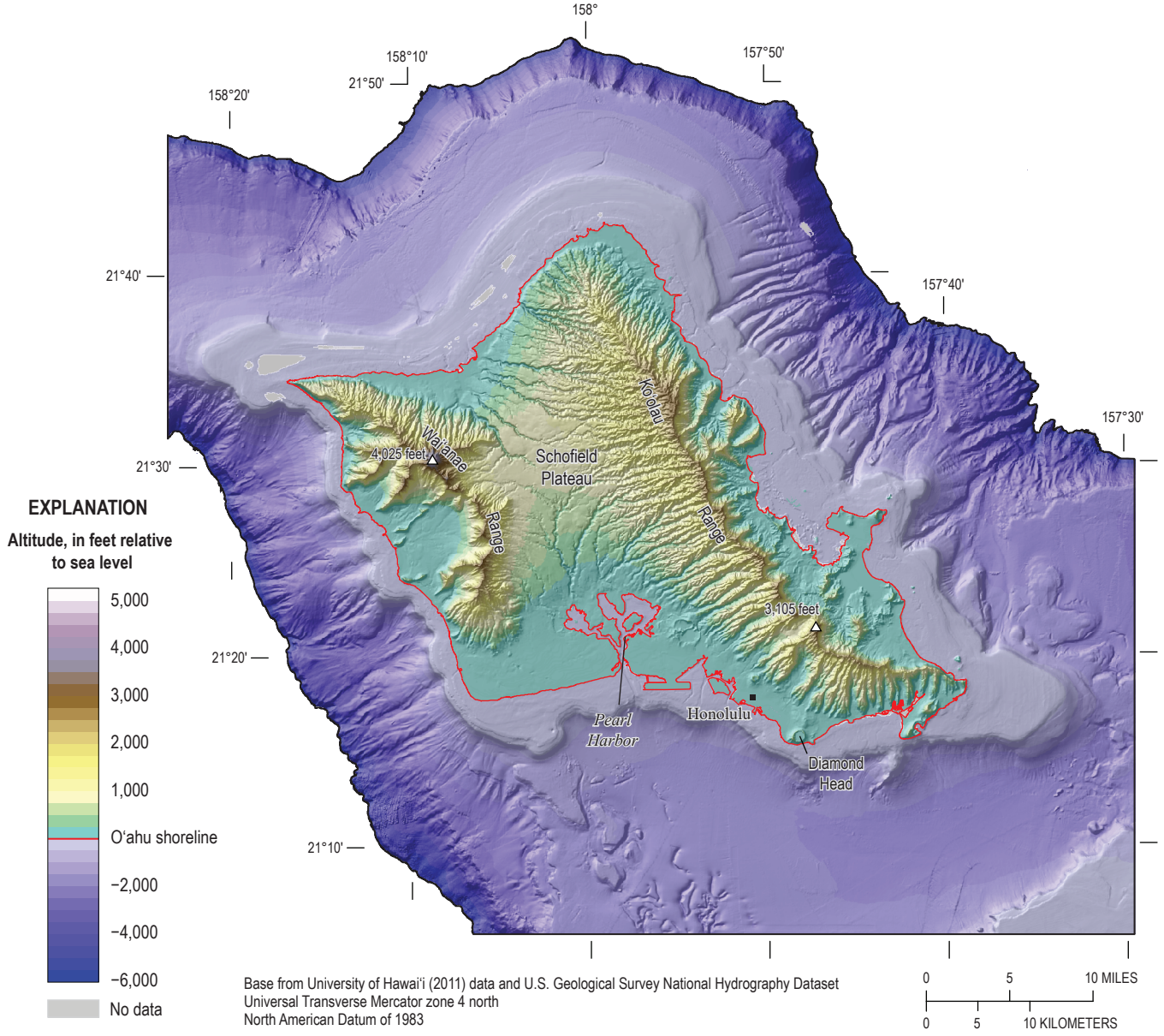

Figure 25. Shaded-relief map of O‘ahu and the surrounding seafloor, Hawai‘i. The base of the groundwater model of O‘ahu is at an altitude of about −6,000 feet. Modified from Izuka and others (2018).

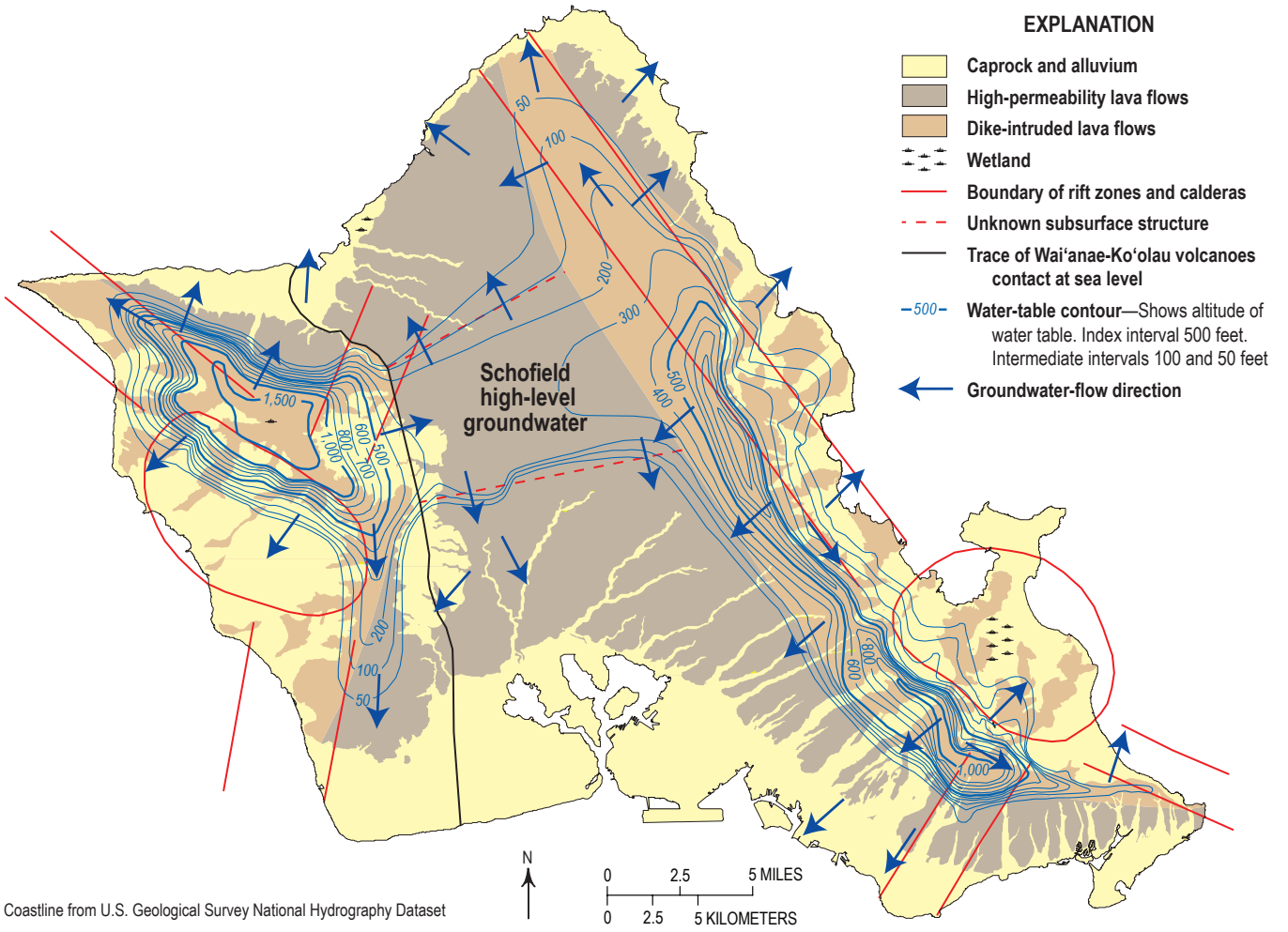

Figure 26. Map showing the water table and its relation to the hydrogeology of O'ahu, Hawai'i. Rift zone and caldera traces modified from Macdonald (1972) and Hunt (1996). Black line shows the O'ahu coastline. Modified from Izuka and others (2018).

in slight (less than about 20 ft) water-level offsets. Measured water levels on either side of the contact between the Wai'anae and Ko'olau volcanoes differ by a few to more than 10 ft as a result of low-permeability weathered basalt and alluvium that resist groundwater flow between the rocks of the two shield volcanoes (Stearns and Vaksvik, 1935). Alluvium and rejuvenation-stage volcanic rocks partly fill stream valleys and form elongate low-permeability barriers that penetrate the freshwater lenses, causing differences in water-table altitudes and lens thickness on either side of the barriers.

Rift zones of O'ahu's shield volcanoes have been identified from dikes exposed by erosion (fig. 26). In the Ko'olau volcano, dikes are concentrated in narrow bands and are aligned subparallel to the rift-zone trend, groundwater flows preferentially in the direction of the trend (Hirashima, 1962), and K_h is greater in the direction of the trend than transverse to it. Estimated K_h from aquifer tests in dike-intruded aquifers on O'ahu vary from less than one to several thousand feet per day (Williams and Soroos, 1973; Hunt, 1996; Rotzoll and El-Kadi, 2008); these estimates probably largely reflect the conductivity parallel to the general dike trend. Values of K_h are between 0.1 and 1.6 ft/d for the dike complex and between 3 and 800 ft/d in the marginal dike zone have been used in numerical models (Meyer and Souza, 1995; Whittier and others, 2004; Rotzoll and El-Kadi, 2007). In the areas of dike intrusion, fresh groundwater exists primarily in the dike-impounded-groundwater setting (figs. 4*A* and 27). Because they typically have the highest water levels and occur in the interior of the island, dike-impounded-groundwater settings receive most of their inflow though the surface from recharge. Much of the groundwater flows through the subsurface into downgradient aquifers, including freshwater lenses in O'ahu's high-permeability coastal aquifers. Where dike compartments have been breached by erosion, some groundwater discharges to springs and streams above sea level.

Some water from the dike-impounded-groundwater settings on O'ahu flows to the Schofield high-level groundwater area (fig. 26). This area has an enigmatically high water table that is not perched, yet exists in an apparently dike-free, high-permeability aquifer (Stearns, 1940; Oki, 1998). Many conceptualizations invoke low-permeability structures—sometimes referred to as "groundwater dams"—along the north and south boundaries (fig. 27), but the geologic nature

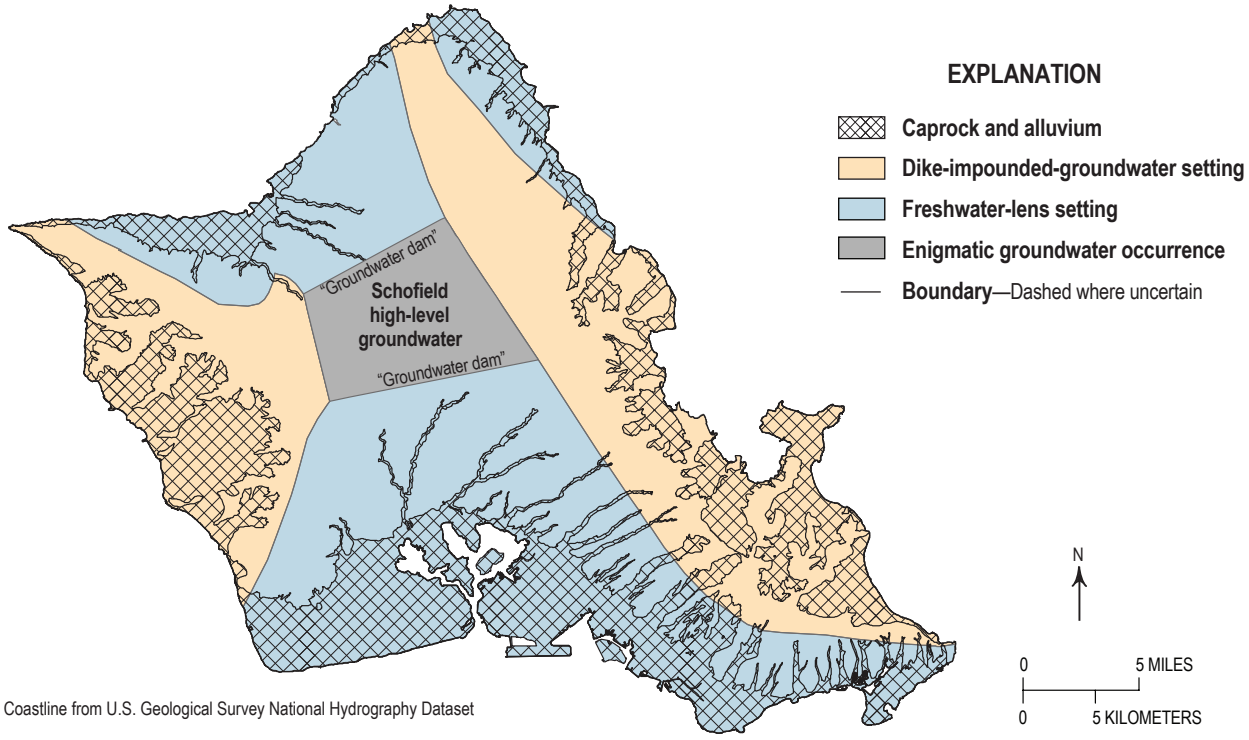

Figure 27. Map showing the principal groundwater settings on O‘ahu, Hawai‘i. Modified from Izuka and others (2018).

of the structures and their precise location are not known. Geophysical and water-level data indicate that the width of the dams differs in the north and south, and that the water table within each dam transitions from the high levels in the Schofield groundwater body to the low water levels in the adjacent freshwater-lens settings (Oki, 1998). Groundwater from the Schofield high-level groundwater body flows to downgradient freshwater-lens settings.

The locations of the calderas of O‘ahu’s two shield volcanoes are interpreted from exposures of thick-bedded lava, breccia, and hydrothermal alteration (Stearns and Vaksvik, 1935) (fig. 26). Gravity anomalies are consistent with these interpretations (Flinders and others, 2013). Caldera rocks are generally considered to have low permeability.

Model Structure

The numerical groundwater model of O‘ahu has a single layer with 448 rows, 352 columns, and 130,429 active cells. The model grid is rotated 28 degrees counterclockwise relative to the cardinal geographic directions (fig. 28) to allow simulation of K_h anisotropy caused by alignment of dikes parallel to the trend of the Ko‘olau rift zone. The rotation aligned the grid’s y direction (parallel to columns) with the general long dimension of the Ko‘olau rift zone. Elsewhere, the value of K_h in the calibrated model was the same in the x and y directions.

The O‘ahu model is divided into 37 *K* zones (fig. 28). In addition to representing regions of rock that have relatively uniform hydraulic properties, the *K* zones include narrow zones that represent low-permeability units, such as low-permeability alluvial valley fill and known or presumed structural barriers. The *K* zones are generally consistent with the hydrogeologic framework and conceptual model presented in figure 26, and those of previous groundwater model studies by Oki (1998, 2005) and Rotzoll and El-Kadi (2007). For this study, the top of the volcanic rocks beneath the coastal plain near Pearl Harbor was modified (on the basis of additional subsurface information) from that given by Izuka and others (2018).

Groundwater recharge totaling 595 Mgal/d was applied to surfaces of the volcanic aquifers above sea level in the O‘ahu model (fig. 29). A total of 198 Mgal/d was withdrawn from the model from wells, shafts, and the six tunnels simulated with the Well package (fig. 30). The withdrawals were averages computed for the calibration period (2001–2010), as described in the Withdrawals section above. For underreported wells in use during 2001–2010, withdrawals for years with missing data were assumed to be equal to the average of reported years. For unreported wells in operation during the calibration period, the proposed withdrawal rate in the well-permit application was used, and if no proposed amount was listed, the rate from CWRM’s water-use permit was used. Discharge from tunnels that feed the Waiāhole Ditch, a long irrigation-water

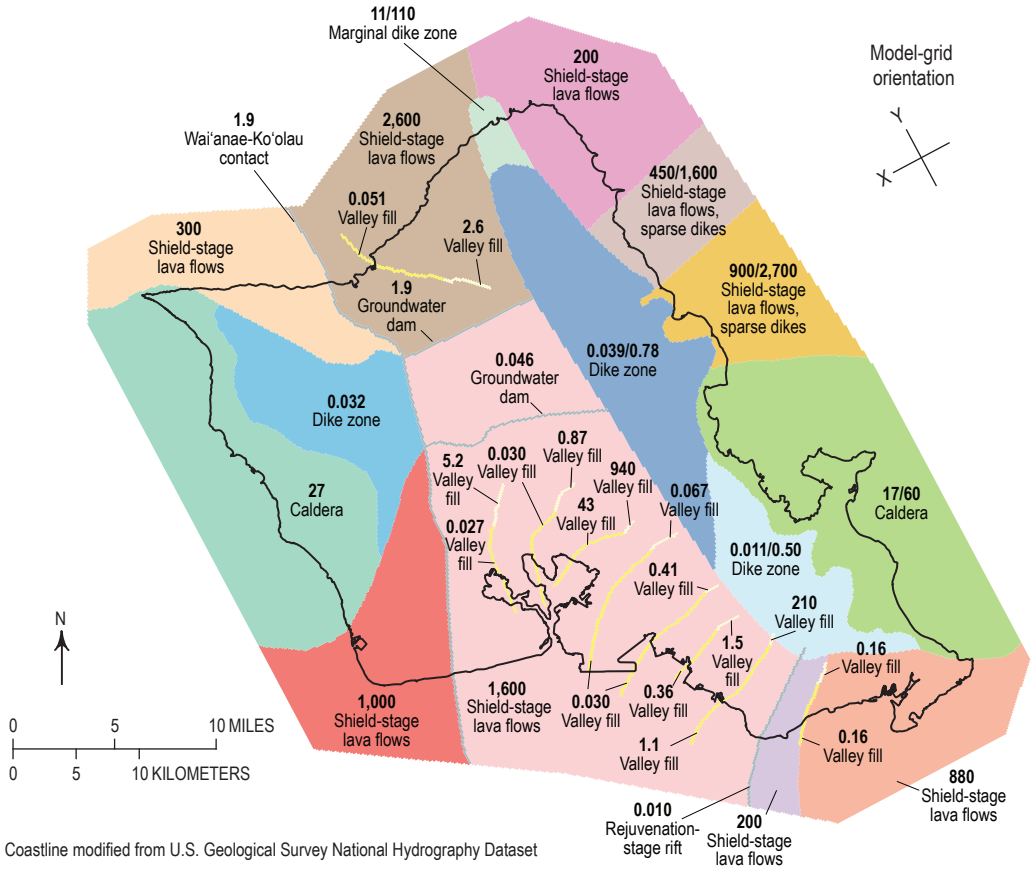

Figure 28. Map of hydraulic-conductivity zones (*K* zones) and values in the numerical groundwater model of O'ahu, Hawai'i. Numbers show horizontal hydraulic conductivity in feet per day. Isotropic *K* zones have one value. Anisotropic *K* zones have two values: the value to the left of the slash is hydraulic conductivity in the x direction, the value to the right is hydraulic conductivity in the y direction. Black line shows the O'ahu coastline.

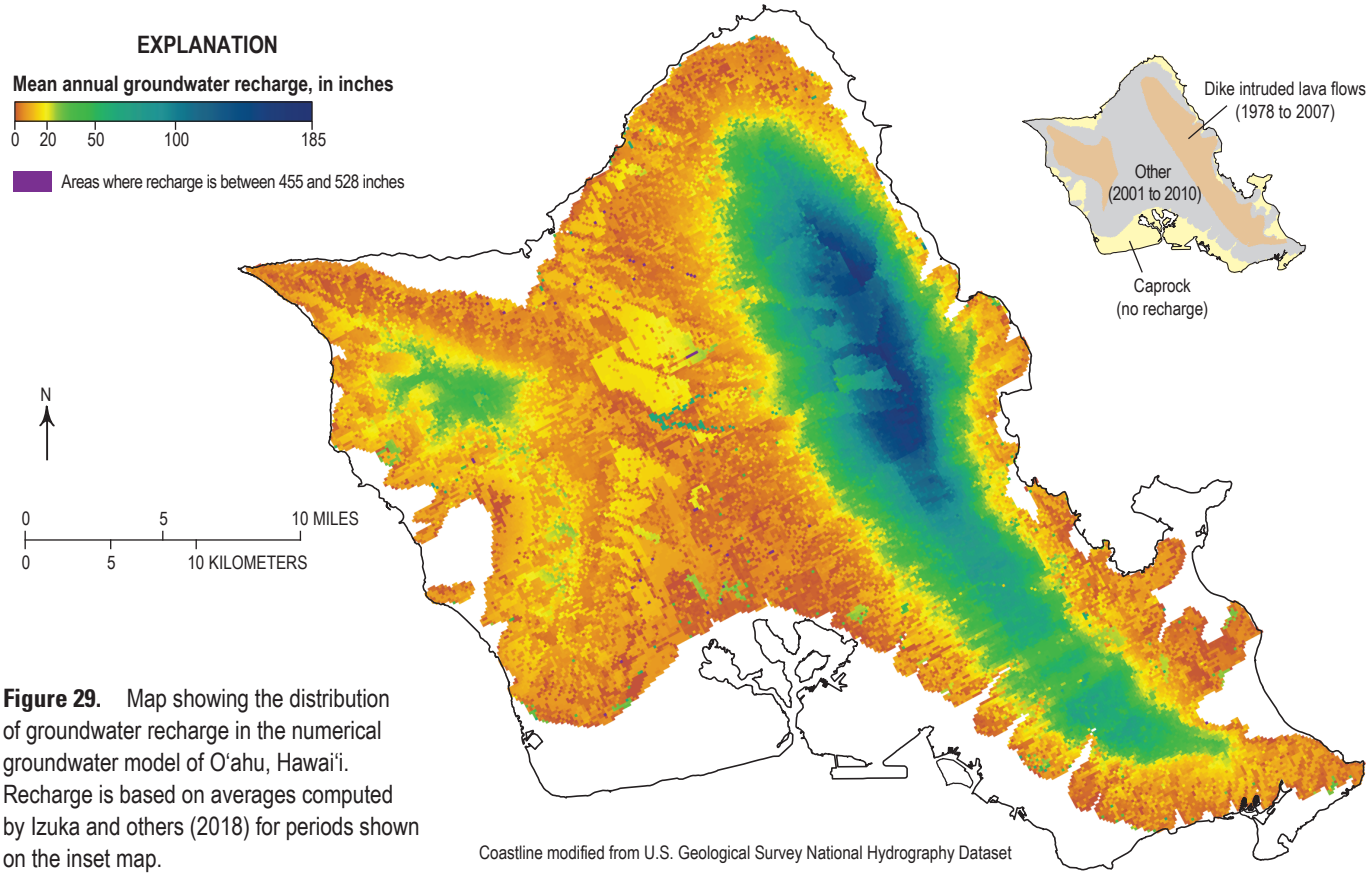

Figure 29. Map showing the distribution of groundwater recharge in the numerical groundwater model of O'ahu, Hawai'i. Recharge is based on averages computed by Izuka and others (2018) for periods shown on the inset map.

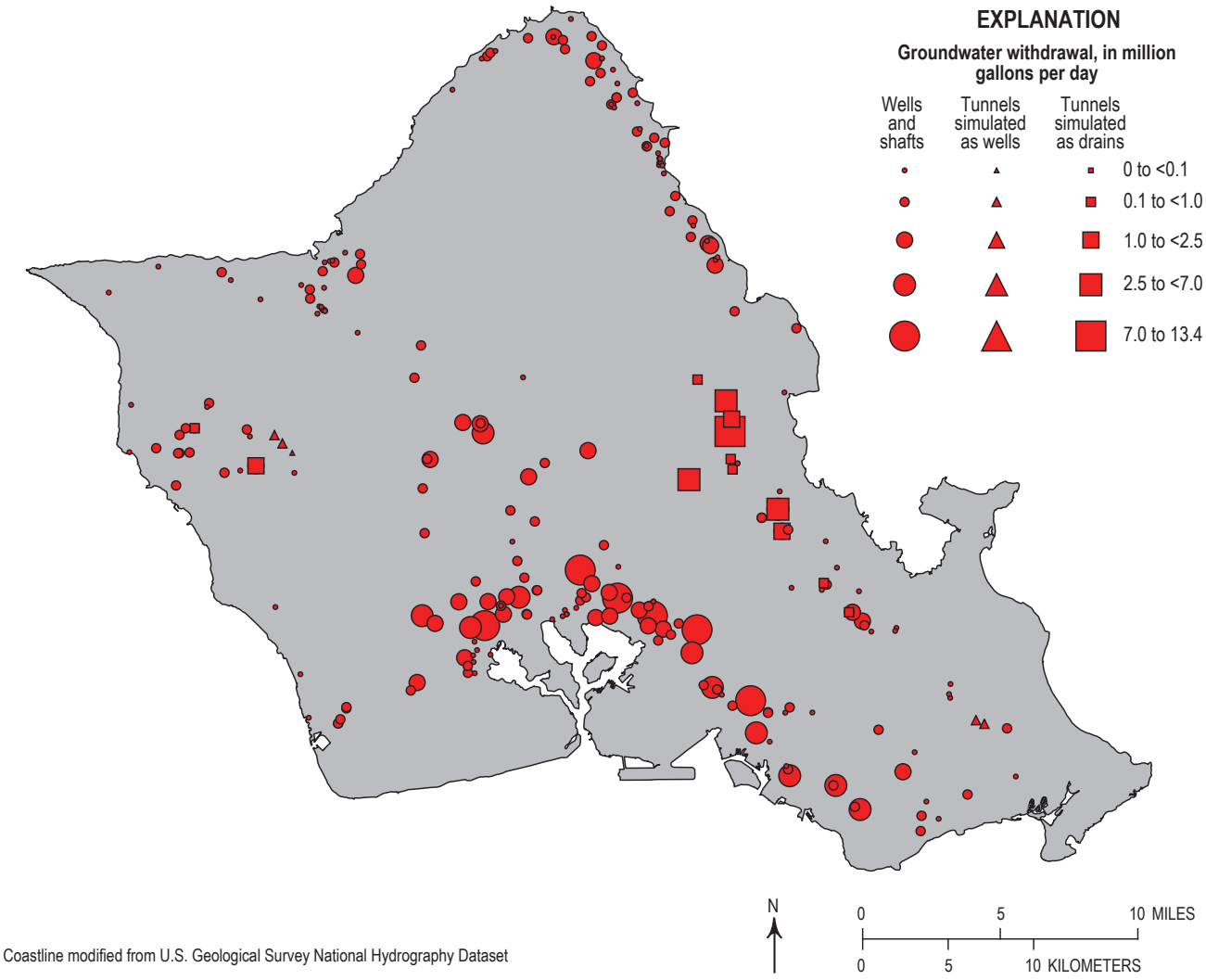

Figure 30. Map showing the distribution of groundwater withdrawals in the numerical groundwater model of O‘ahu, Hawai‘i.

transmission system in the Ko‘olau Range, was estimated by Yeung and Fontaine (2007).

Altitudes for drains that simulate streams and most tunnels (H_{str} in eq. 5) and altitudes for heads used in offshore GHBs (H_{ocean} in eq. 2) (fig. 31) were computed as described in the Flow Boundaries section above. In most places where the caprock is simulated using drains (fig. 9), H_{cpr} was set between 0 and 2 ft on the basis of information reported by Bauer (1996) and Rotzoll and Fletcher (2013). In areas lacking information on caprock head, H_{cpr} (eq. 4) was set to 0 ft.

Hydraulic Properties

In the calibrated model of O‘ahu, *K* zones that represent aquifers composed of shield-stage lavas have K_h values that range from 200 to 2,600 ft/d (fig. 28). These values are consistent with the high K_h typically associated with shield-stage lava-flow aquifers in Hawai‘i.

The main area of dike intrusion in the Ko‘olau volcano (fig. 26) is represented by two dike zones and one marginal dike zone (fig. 28). Values of K_{hy} (parallel to the Ko‘olau rift-zone trend) for these *K* zones in the calibrated model ranged from 0.50 to 110 ft/d; values of K_{hx} (perpendicular to the rift-zone trend) ranged from 0.011 to 11 ft/d. The higher values of K_{hy} relative to K_{hx} are consistent with the preferential flow parallel to the direction of the Ko‘olau rift zone. Hydraulic conductivities along the length of the dike zones are generally lower in the southeast near the caldera of the volcano, and higher in the northwest farther from the caldera. This trend is consistent with the conceptualization that dike frequency diminishes away from the caldera. Two *K* zones on the northeast coast of O‘ahu represent shield-stage lava flows that are mostly dike free, but are sparsely intruded by dikes that impart some horizontal anisotropy; values of K_{hy} for these *K* zones ranged from 1,600 to 2,700 ft/d and values of K_{hx} ranged from 450 to 900 ft/d. A *K* zone representing the former caldera of the Ko‘olau volcano has a K_{hy} value of 60 ft/d and K_{hx} value of 17 ft/d in the calibrated model. The *K* zone representing the dike zone of the Wai‘anae volcano in the calibrated model has a K_h value of 0.032 ft/d, which is consistent with the conceptualization of

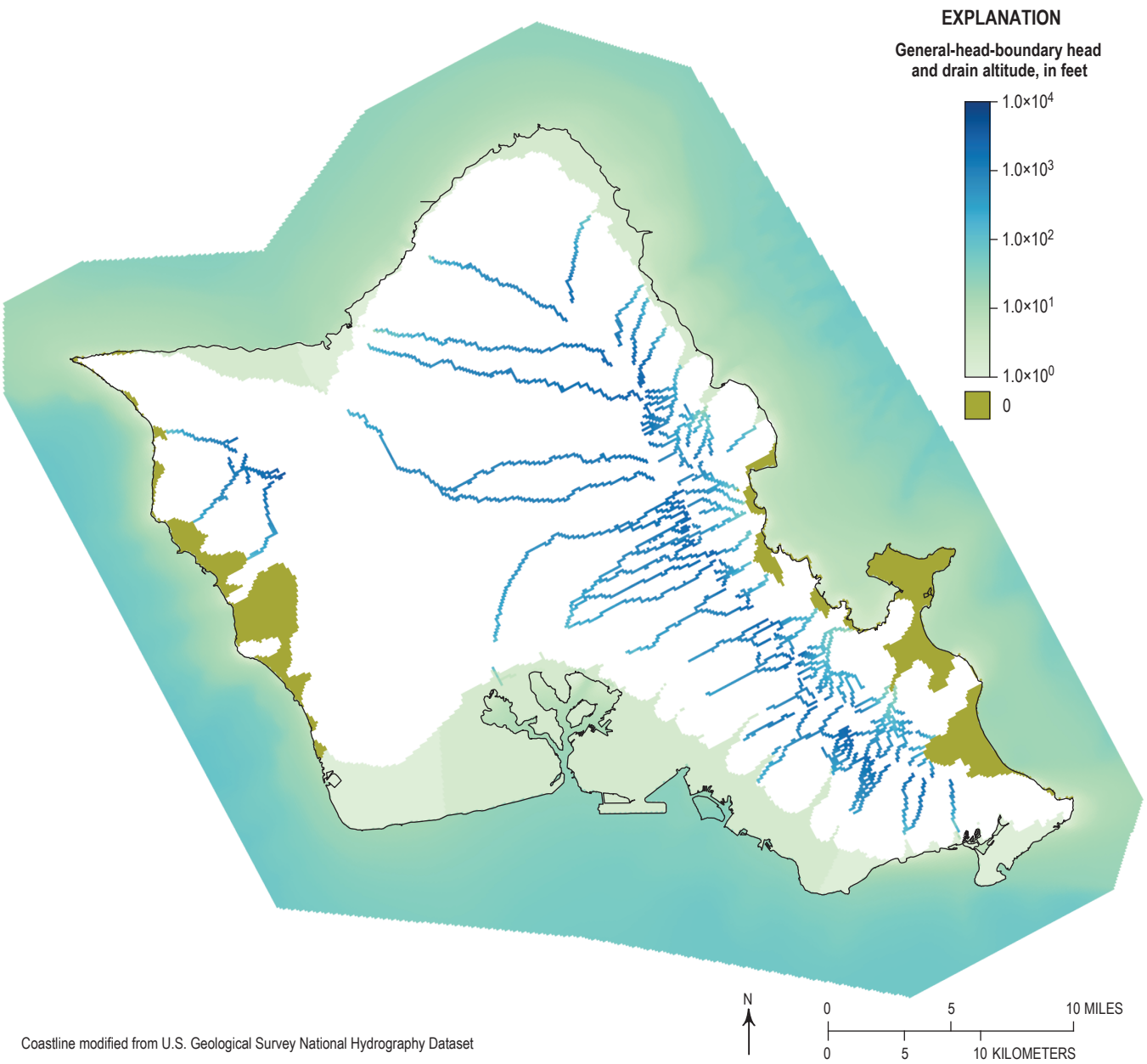

Figure 31. Map of general-head-boundary heads and drain altitudes in the numerical groundwater model of Oʻahu, Hawaiʻi. Black line shows the Oʻahu coastline.

low-permeability dike-intruded areas. A *K* zone representing the caldera of the Waiʻanae volcano has a K_h value of 27 ft/d.

Low-permeability valley-fill barriers (which include alluvium and underlying weathered basalt) that penetrate into the lava-flow aquifer are represented by 18 *K* zones in the Oʻahu model (fig. 28). In reality, a typical valley-fill barrier penetrates deeper in the lower valley than in the upper valley, but in either case probably does not extend to −5,906 ft (the altitude of the bottom of the model). Because the Oʻahu model has a single layer, however, all cells, including those representing valley-fill barriers, are fully penetrating. Simulated hydraulic properties of model cells that represent valley-fill barriers thus integrate the properties of the valley fill and underlying lava-flow aquifers.

To better represent varying ratios of valley fill to lava flows along the length of a valley-fill barrier, each simulated valley-fill barrier is separated into upstream and downstream *K* zones. Values of K_h for *K* zones that represent alluvium/weathered-basalt barriers range from 0.028 to 940 ft/d in the calibrated model. The wide range of values results in part from the variable nature of valley-filling alluvium and in part from the variable penetration depth.

Four *K* zones represent low-permeability structural barriers, including the weathered contact between the Waiʻanae and Koʻolau volcanoes, a rejuvenation-stage rift combined with alluvium/weathered basalt in southeast Oʻahu, and the "groundwater dams" to the north and south of the

Schofield high-level groundwater (figs. 26 and 28). These structural barriers are presumed to extend the entire depth of the model. Values of K_h for these barriers range from 0.010 to 1.9 ft/d in the calibrated model of O‘ahu. The K zones that represent the groundwater dams bounding the Schofield high-level groundwater are narrow and thus cannot simulate the transitional water levels that have been reported in those structures (Oki, 1998), but simulation of this hydrogeologic detail was not needed for the objectives of this study.

Values of C_{str} for stream and tunnel cells range from 2.3 to 10,000 ft^2/d (fig. 32). The wide range of values is consistent with the concept that stream-bed thickness and hydraulic properties vary widely among streams on O‘ahu, but measured values for this parameter are lacking. Values of C_{cpr} for caprock cells range widely from 0.034 to more than 10,000 ft^2/d, which reflects the variability of hydraulic properties and thickness of the caprock in the calibrated O‘ahu model (the highest values are in areas where caprock is absent and offers no resistance to flow). No measured values for C_{cpr} are available for comparison to the model values.

Groundwater Levels and Flow

In the high-permeability lava-flow aquifers that are partly overlain by caprock on O‘ahu (fig. 26), fresh groundwater exists in the freshwater-lens setting (figs. 4*A* and 27). In the calibrated O‘ahu model, simulated heads in this setting vary between 0 and 24 ft, which is consistent with observed water levels (fig. 33*A*).

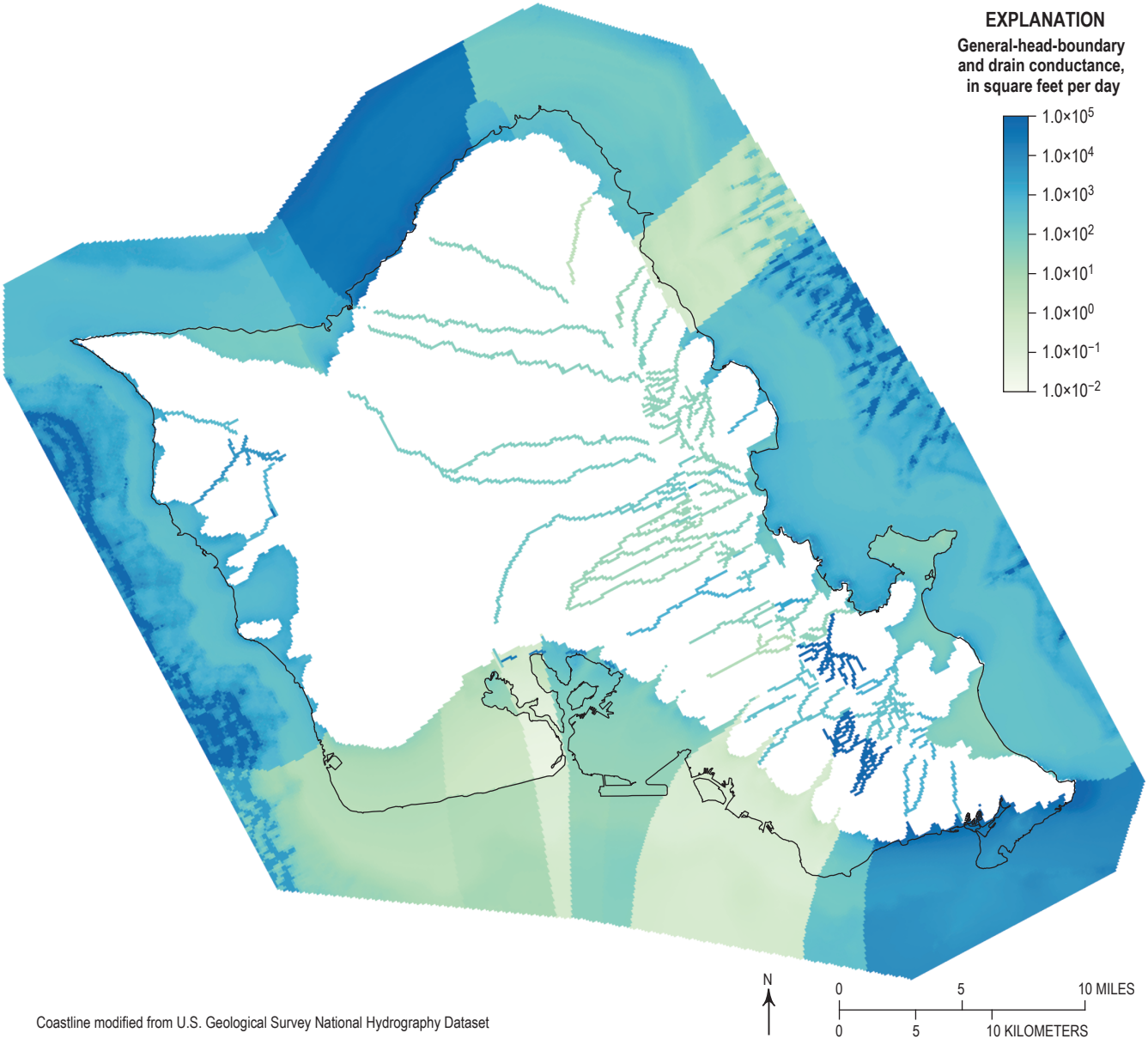

Figure 32. Map showing the distribution of conductance values for head-dependent boundary cells that represent caprock, streams, springs, and tunnels in the calibrated numerical groundwater model of O‘ahu, Hawai‘i. Black line shows the O‘ahu coastline.

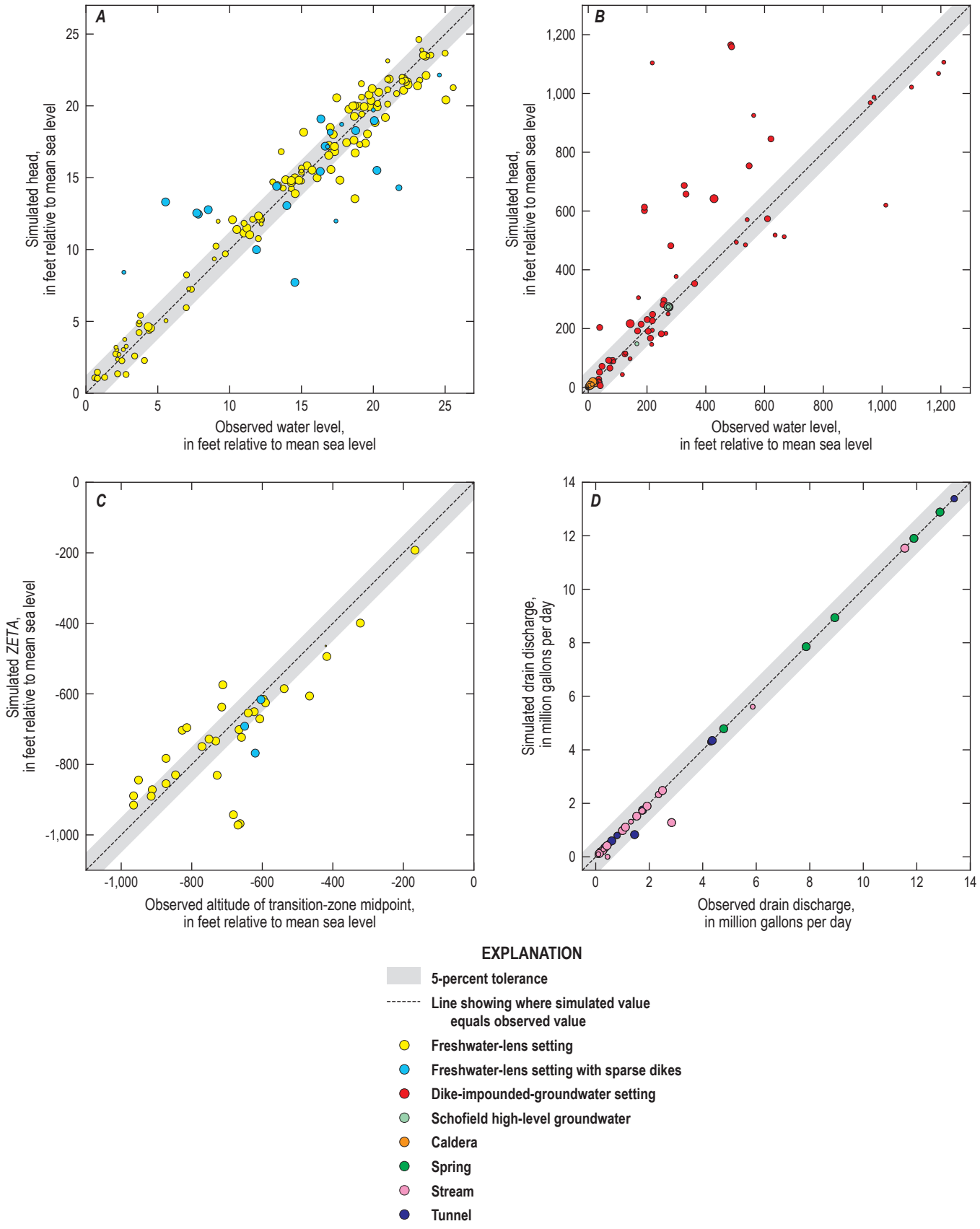

Figure 33. Plots comparing observed and model-simulated values in the calibrated numerical groundwater model of Oʻahu, Hawaiʻi. Symbol diameter indicates relative weight during calibration, with one exception: transition-zone midpoint observations (in *C*) were given zero weight during calibration.

Sixty-nine percent of the simulated heads were within the 5-percent tolerance (table 3). The average absolute residual between simulated head and observed water level was 1.3 ft, and the standard deviation of residuals was 1.9 ft. The ratio of the standard deviation of residuals to the range of observation was 0.08. The distribution of model-simulated heads (fig. 34) generally replicates the gentle seaward gradient of the water table and groundwater flow from inland toward the coast described in the conceptual model (fig. 26). The calibrated model also reproduces the relative differences in head between adjacent freshwater-lens settings separated by low-permeability alluvial valley fill and the weathered contact between the Ko‘olau and Wai‘anae volcanoes.

Simulated heads for the dike-impounded-groundwater setting, calderas, and the Schofield high-level groundwater vary widely between 30 and 1,200 ft, which generally matches water-level observations (fig. 33*B*) and is consistent with the conceptual model (figs. 4*A*, 26, and 27). Although the average residual between simulated and observed values is 69.6 ft and the standard deviation of residuals is 158.5 ft, 76 percent of the simulated values fall within the 5-percent tolerance and the ratio between standard deviation and range of values is 0.13 (table 3). Discrepancies between model-simulated heads and observed water levels result in part from limitations of the model—simulating the dike-intruded areas as a low-permeability unit rather than a combination of high-permeability lava flows and low-permeability sheet-like dikes limits the model’s ability to replicate water-level details that result from dike compartmentalization. Even so, the calibrated model generally replicates the steeply sloping water levels characteristic of these areas (fig. 34). The model also generally replicates the groundwater-flow directions from the conceptual model, including the preferential northwest-southeast flow parallel to alignment of dikes in the Ko‘olau Range and the general flow from high-altitude dike-impounded groundwater in the mountain ridges, to the Schofield high-level groundwater body, and to low-altitude freshwater-lens settings along the coast. In the calibrated model, 70.5 Mgal/d of groundwater flows from the Schofield high-level groundwater body to adjacent freshwater lenses on O‘ahu; 70 percent of this groundwater flows to the south into the freshwater-lens setting near Pearl Harbor.

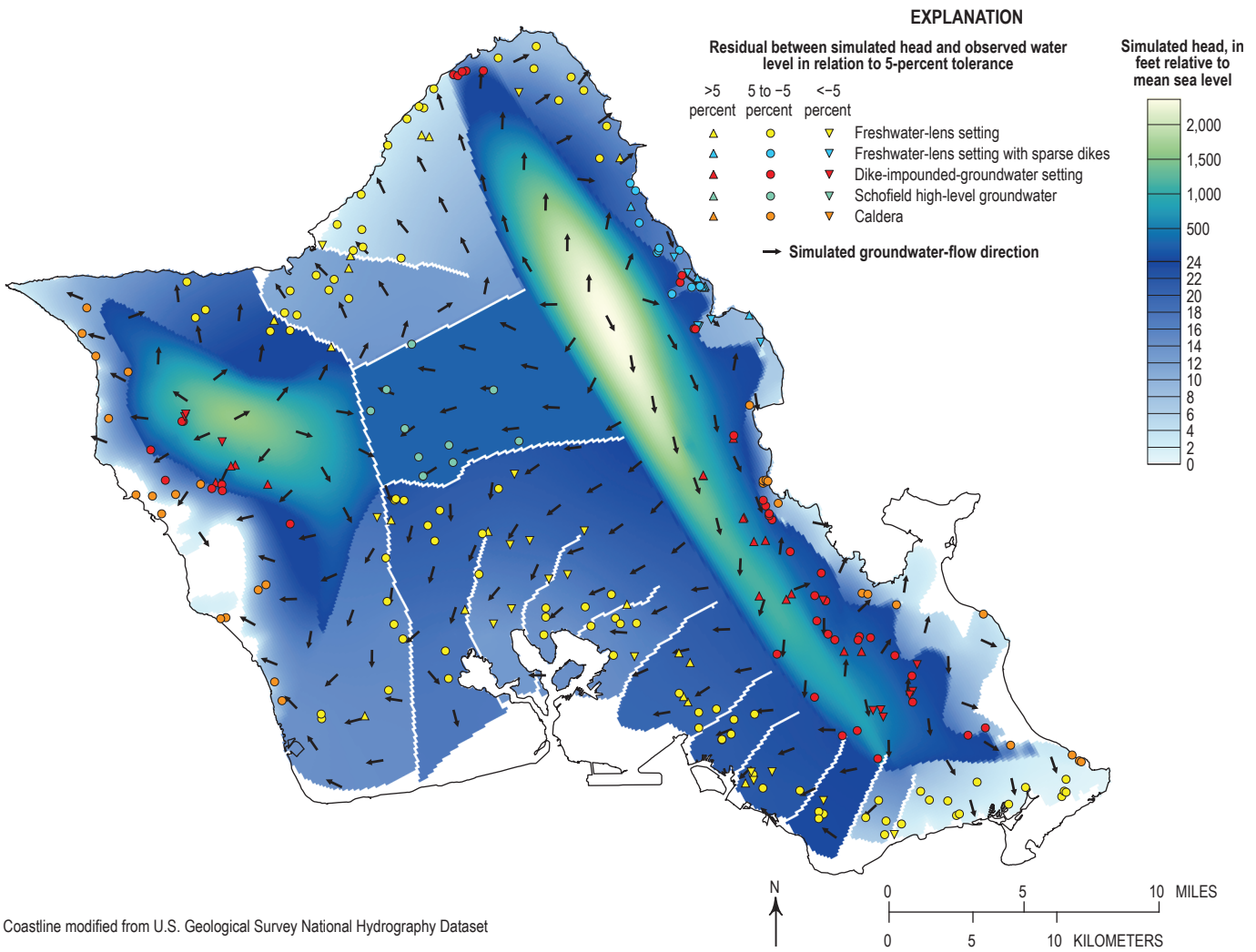

Figure 34. Map of simulated head and groundwater flow in the calibrated numerical groundwater model of O‘ahu, Hawai‘i.

Freshwater-Saltwater Interface

Numerous DMWs on O‘ahu provide observations of the altitude of the transition-zone midpoint for matching *ZETA* during calibration (fig. 35). Simulated *ZETA* generally matches observed midpoints, although at some DMW sites in southern O‘ahu, *ZETA* is as much as a few hundred feet above or below observed midpoints (fig. 33*C*). Discrepancies between simulated *ZETA* and observed midpoints in some DMWs may indicate that the observed transition zone has not reached steady state in response to withdrawal changes that have happened within, and possibly a few decades before, the calibration period. Southern O‘ahu is the site of heavy groundwater development (fig. 30), but withdrawal rates over time have varied (both increases and decreases) with changing agriculture and population. Alternatively, the discrepancies may be due to difficulties in measuring the position of the transition-zone midpoint because of borehole flow in DMWs (Rotzoll, 2012), or the inability of a single-layer model to simulate vertical head gradients that can affect interface position.

Because of the multiple factors that could prevent the model from matching midpoint observations, no weight was given to these observations during PEST calibration.

Cross sections show that freshwater extends to the bottom of the model beneath the Schofield high-level groundwater and most of the dike-impounded-groundwater settings, except near the coast (fig. 36). The cross sections also show that the freshwater is much thinner in the freshwater-lens settings, although freshwater is thicker than it would be without the extensive caprock. These model results are consistent with conceptualizations of the hydrologic settings in Hawai‘i (fig. 4).

Discharge to Streams, Springs, Tunnels, and the Ocean

Base-flow observations for gaged streams were computed as described in the Calibration section (above). Discharge observations for the Pearl Harbor springs were averaged from spring-discharge measurements for five major springs from the

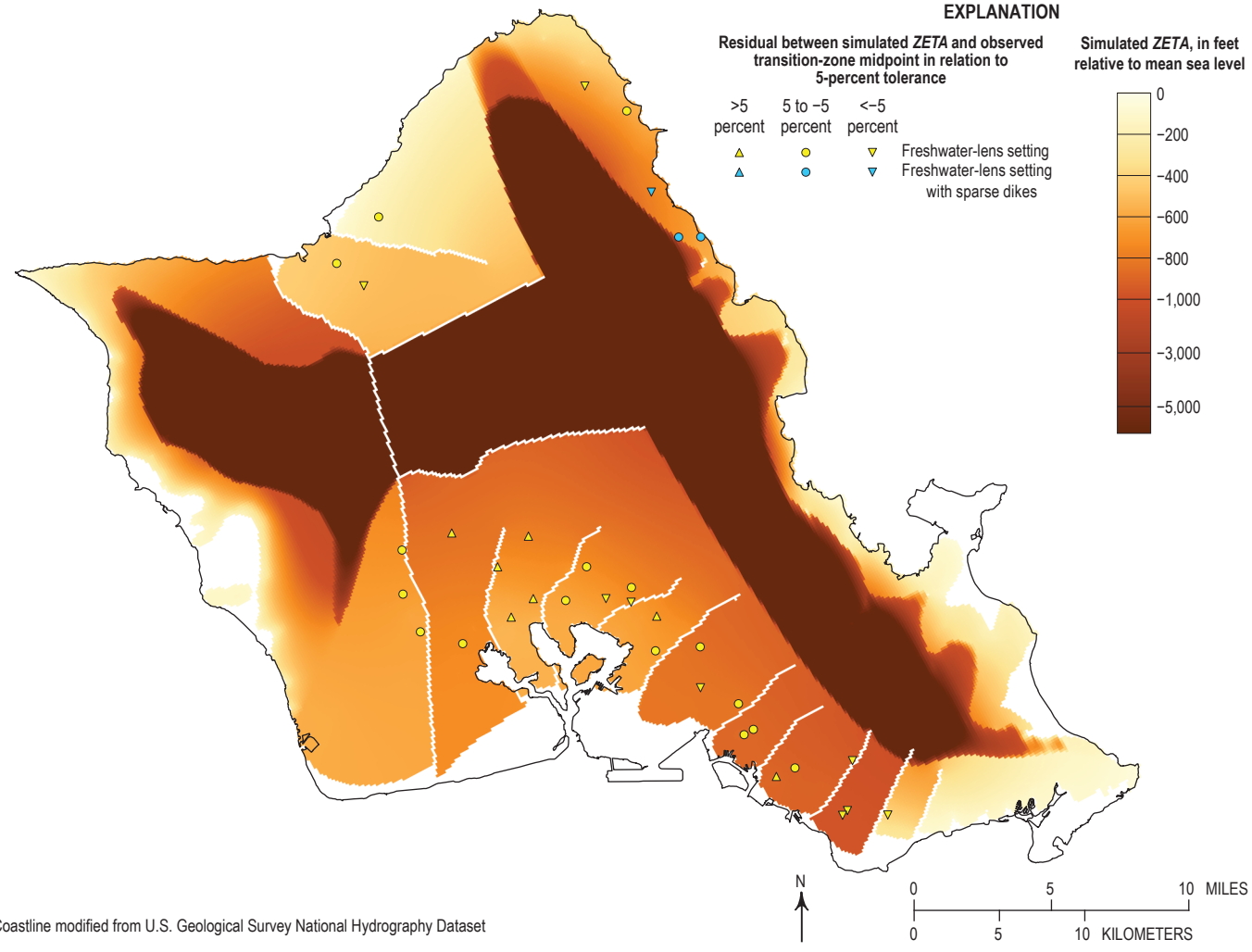

Figure 35. Map of the simulated altitude of the freshwater-saltwater interface (*ZETA*) in the numerical groundwater model of O‘ahu, Hawai‘i.

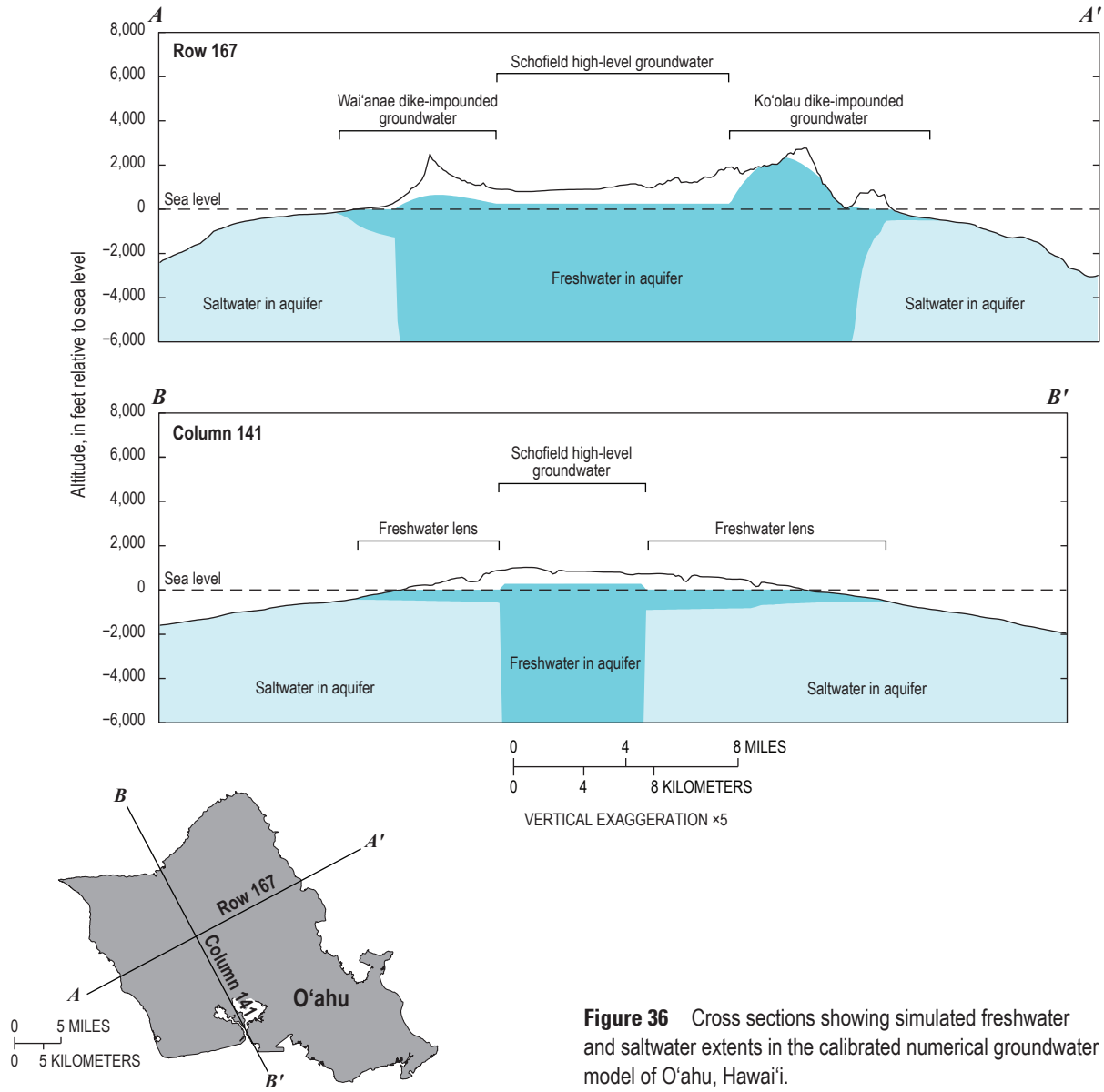

Figure 36 Cross sections showing simulated freshwater and saltwater extents in the calibrated numerical groundwater model of O‘ahu, Hawai‘i.

2001–2010 period information in the USGS NWIS database. The springs occur at the inland contact between the lava-flow aquifer and overlying caprock (figs. 26 and 37). In the model, these springs were simulated using drain boundaries similar to those used to simulate streams, except that simulated spring discharge was only summed from drain cells along the caprock/lava-flow contact.

Simulated groundwater discharge to streams, springs, and tunnels in the calibrated O‘ahu model agree closely with tunnel-draft data and base-flow estimates from analyses of stream-gage data (fig. 33*D*). The average absolute residual was 0.1 Mgal/d, the standard deviation of residuals was 0.3 Mgal/d, and the ratio between standard deviation and range of values was 0.02 (table 3). Ninety-seven percent of simulated discharges are within the 5-percent tolerance. Most of the model-simulated fresh groundwater discharge from the volcanic aquifer above sea level occurs at the springs near Pearl Harbor and from drain cells representing the reaches of streams that incise the dike-impounded groundwater in the Ko‘olau volcano (fig. 37). Most drain cells that represent stream reaches over high-permeability aquifers have no simulated groundwater discharge because heads are below the drain altitude. Simulated discharge to the ocean is mostly diffuse because of the simulated effect of the caprock. This pattern of groundwater discharge to streams is consistent with the conceptual model for O‘ahu (Izuka and others, 2018).

Model Sensitivity to Parameters

The parameter to which the calibrated groundwater model of O‘ahu was most sensitive was C_{str} of springs near Pearl Harbor (fig. 38*B*). Although the parameter applies to only a few cells of the model, adjusting these parameters

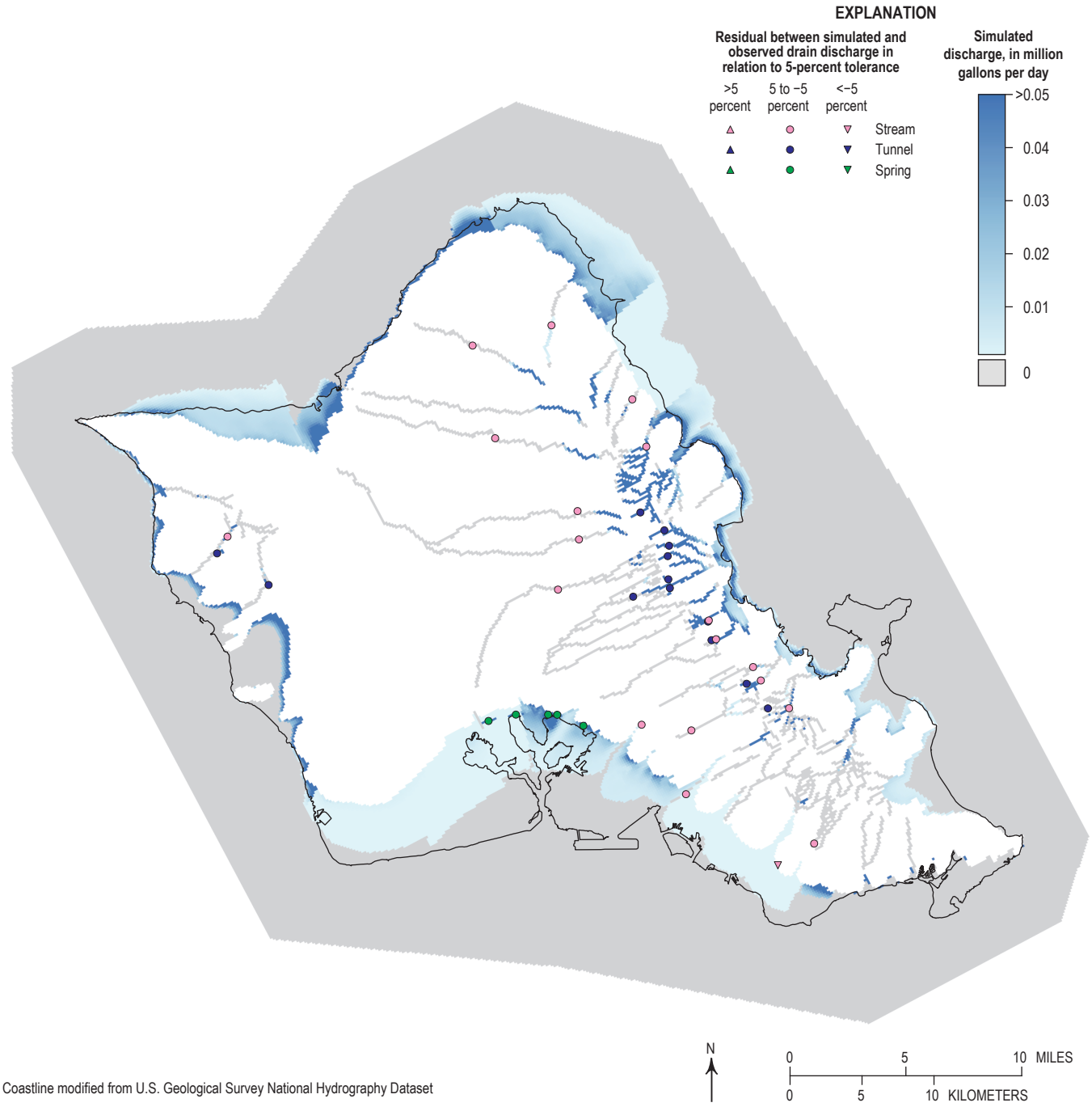

Figure 37 Map of simulated groundwater discharge to streams, tunnels, springs, and the ocean in the calibrated numerical groundwater model of O‘ahu, Hawai‘i. Black line shows the O‘ahu coastline.

during calibration affected the model’s match of numerous observations—including water levels, spring flows, and transition-zone midpoint altitudes—in the upgradient volcanic aquifer (figs. 34 and 35). Among horizontal hydraulic conductivities adjusted during model calibration, the model is most sensitive to properties of *K* zones that represent the dike zone of the Ko‘olau Range and the lava-flow aquifers near Pearl Harbor and Schofield Plateau (fig. 38*A*). The model was also sensitive to the groundwater dams on either side of the Schofield high-level groundwater. Adjusting the properties of these *K* zones affects the model’s match of the numerous observations upgradient of Pearl Harbor (fig. 34). Adjusting the properties of the Ko‘olau Range dike zone affects flow to, and water levels in, adjacent aquifers. The O‘ahu numerical model is much less sensitive to other parameters adjusted during calibration.

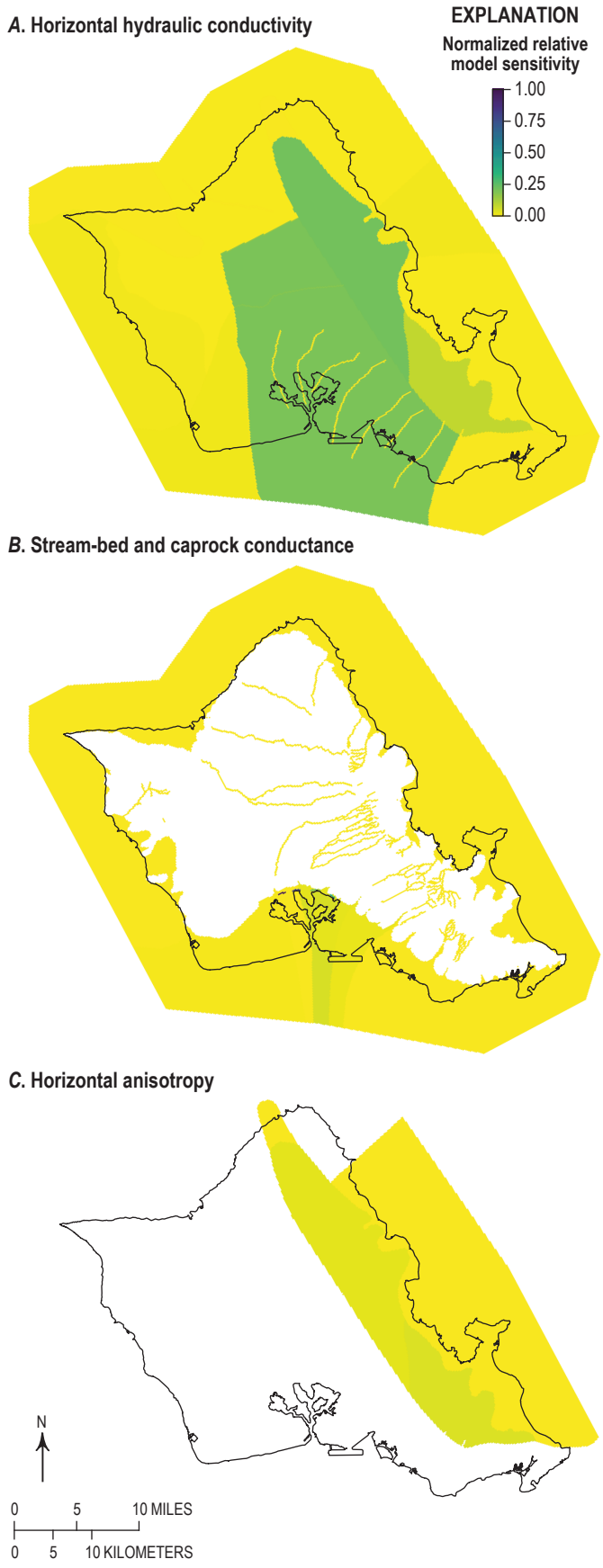

Maui

Maui is the youngest of the islands modeled in this study. It is formed by two shield volcanoes that are connected by an area known as the “isthmus” (fig. 39). The older of the two volcanoes is West Maui; to the east lies the younger, larger Haleakalā. Streams have carved deep valleys in West Maui, whereas stream erosion is less apparent over much of Haleakalā. Both volcanoes are built mostly by thin shield-stage flows that form high-permeability aquifers (fig. 40). Estimates of K_h for shield-stage lava-flow aquifers on Maui vary between about 200 and 11,000 ft/d (Burnham and others, 1977; Hunt, 2007; Rotzoll and others, 2007; Gingerich, 1999b, 2008; Gingerich and Engott, 2012). Postshield-stage rocks on West Maui form a thin veneer over the shield-stage lava flows but are volumetrically small and contain little groundwater. Postshield-stage rocks on Haleakalā, like the shield-stage rocks that underlie them, generally have high permeability (Stearns and Macdonald, 1942), but thicker postshield deposits partly fill and form low-permeability aquifers in large valleys, such as Ke‘anae, Waiho‘i, and Kīpahulu Valleys and Kaupō Gap. Estimates of K_h for postshield-stage lavas on Maui are scant but range from about 0.1 to 4.0 ft/d (Gingerich, 1999b, 2008; Meyer, 2000, and Gingerich and Engott, 2012).

Caldera deposits have been described in West Maui volcano by Stearns and Macdonald (1942). No caldera has been identified in Haleakalā volcano (fig. 40), but the presence of high-density intrusive rocks is indicated by gravity anomalies beneath Haleakalā’s summit (Kinoshita and Okamura, 1965; Flinders and others, 2013). Three rift zones on Haleakalā are identified by postshield-stage eruptive vents (Stearns and Macdonald, 1942). Rift zones have been described on West Maui volcano (Stearns and Macdonald, 1942; Macdonald and others, 1983), but are not clearly defined by the organization of dikes into linear zones. Estimates of bulk K_h for dike-intruded lavas on West Maui volcano are on the order of a few tens of feet per day (Rotzoll and others, 2007; Gingerich and Engott, 2012).

Alluvium partly fills the deep valleys in West Maui (figs. 39 and 40). Alluvium and rejuvenation-stage rocks form caprock along West Maui’s coastal areas. Sedimentary rocks of the isthmus form caprock that resists discharge to the ocean from the underlying volcanic aquifers of Haleakalā and West Maui. Caprock also extends along part of the southwestern

Figure 38. Maps showing normalized relative composite sensitivities of parameters adjusted during calibration of the numerical groundwater model of O‘ahu, Hawai‘i. *A*, Horizontal hydraulic conductivity for isotropic zones and horizontal hydraulic conductivity in the x direction (parallel to model rows) for anisotropic zones; *B*, stream-bed conductance and parameters controlling caprock conductance; and *C*, horizontal anisotropy—the ratio of hydraulic conductivity in the x direction to that in the y direction. Black line shows the O‘ahu coastline.

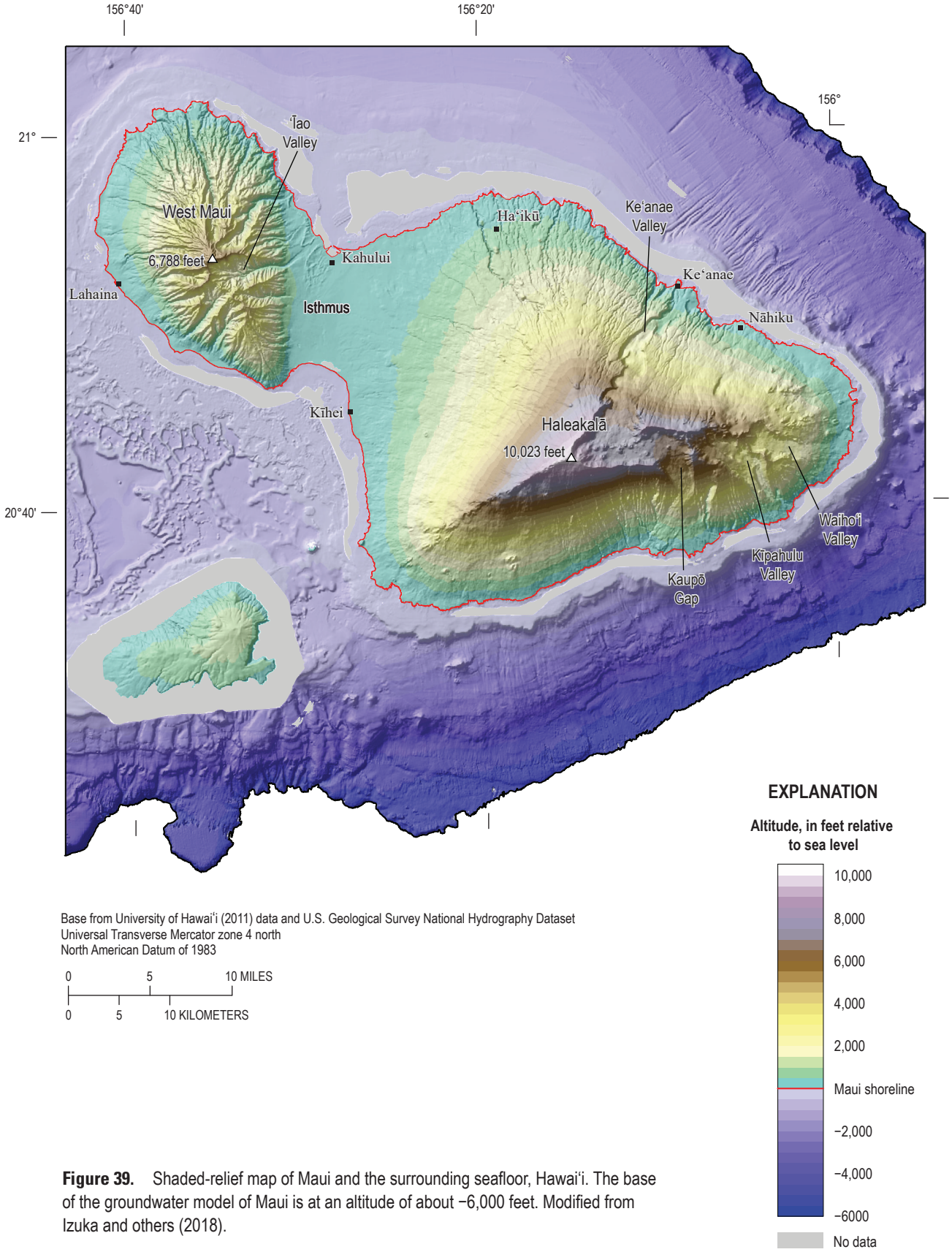

Figure 39. Shaded-relief map of Maui and the surrounding seafloor, Hawaiʻi. The base of the groundwater model of Maui is at an altitude of about −6,000 feet. Modified from Izuka and others (2018).

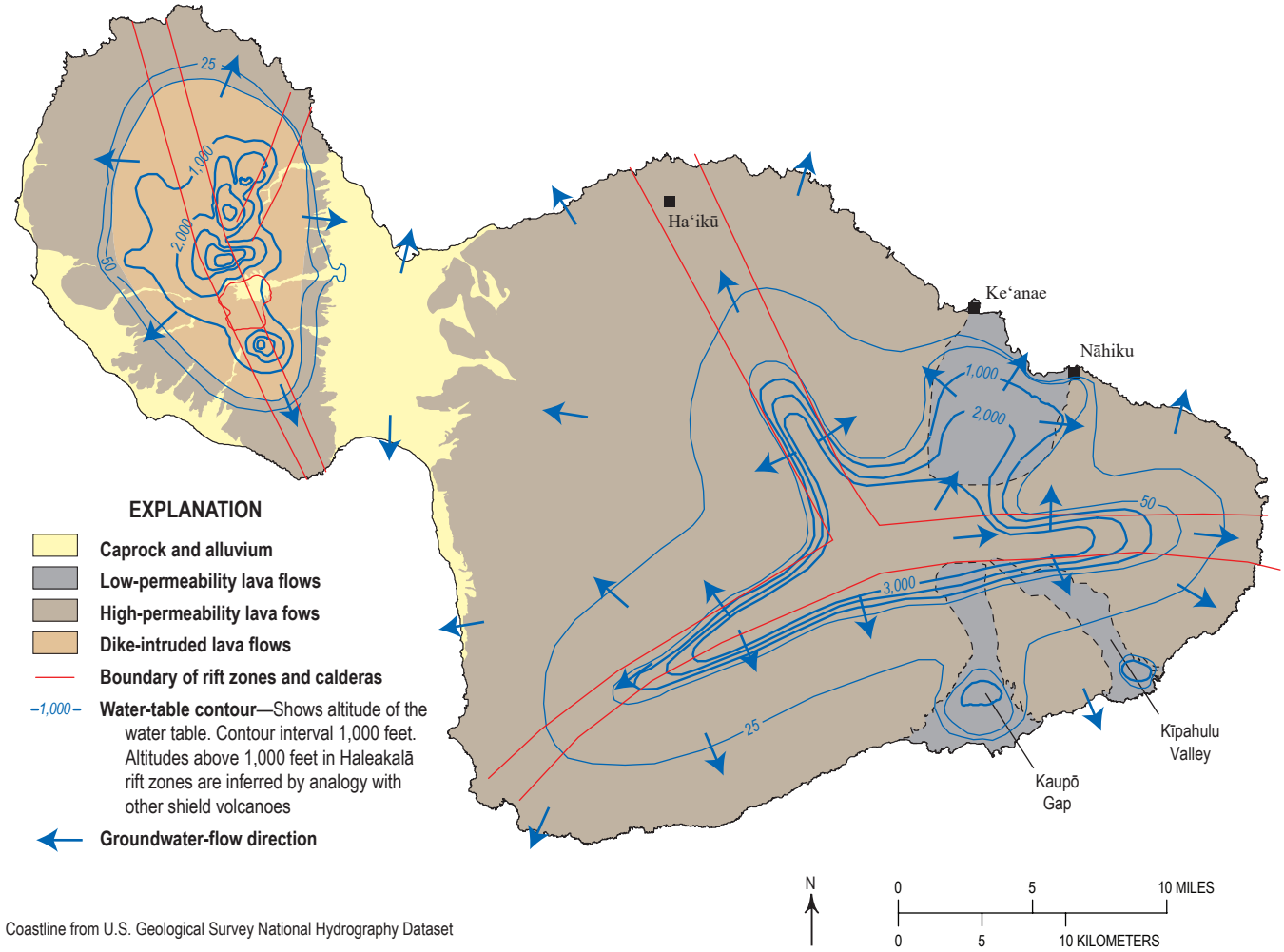

Figure 40. Map showing the water table and its relation to the hydrogeology of Maui, Hawai‘i. Modified from Izuka and others (2018). Approximate rift-zone traces are based on a small-scale illustration by Stearns and Macdonald (1942). Black line shows the Maui coastline.

coast of Haleakalā. Sediments and weathered rock form a low-permeability unit between the volcanic aquifers of West Maui and Haleakalā (Meyer and Presley, 2000).

In West Maui, groundwater levels are highest in the dike-intruded center of the volcano (fig. 40), where fresh groundwater exists in the dike-impounded-groundwater setting (figs. 4*A* and 41). Some groundwater discharges from the dike compartments and feeds springs and streams; draining by streams shapes the water table in West Maui's interior. Water flows through the subsurface from the central dike-impounded-groundwater setting toward high-permeability lava-flow aquifers along the coast. In the coastal aquifers, fresh groundwater exists in the freshwater-lens setting. The water table of the freshwater lens is mostly less than 25 ft above sea level and slopes gently toward the coast. Semiconfining caprock on the southwestern side of West Maui impedes discharge of groundwater from the freshwater lens to the ocean. Caprock also impedes groundwater discharge where the West Maui volcanic rocks meet the isthmus. Caprock is less extensive along the northern coast of West Maui. Some water from West Maui flows into the aquifers of the isthmus, where it encounters the low-permeability sediments that lie between rocks of Haleakalā and West Maui. Flow probably continues eastward beneath the isthmus and merges with flow from Haleakalā, then discharges through caprock along the northern and southern coastlines of the isthmus.

Groundwater-level information is scant for Haleakalā's uplands, summit, and rift zones, but analogy with other shield volcanoes suggests that dikes in Haleakalā's rift zones impound groundwater to altitudes higher than adjacent dike-free aquifers (figs. 40 and 41). Because most dike compartments on Haleakalā have not been exposed by erosion, most groundwater likely flows through the subsurface from dike-impounded-groundwater settings into freshwater lenses in adjacent coastal high-permeability lava-flow aquifers (fig. 4*B*) or discharges to the sea where the rift zones intersect the ocean. Most of Haleakalā's coastal aquifers have no substantial caprock, so freshwater lenses are thin. The water tables of the freshwater lenses are less than 25 ft above sea level throughout much of Haleakalā. Some of the groundwater from Haleakalā flows into

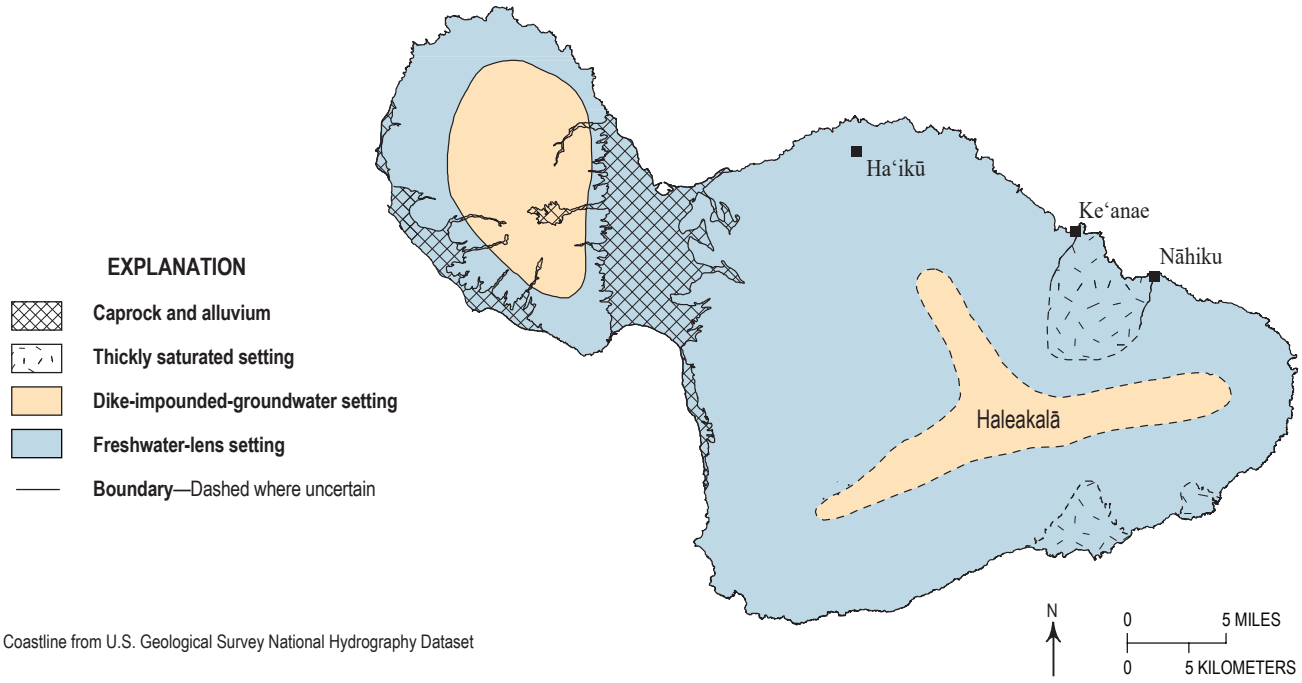

Figure 41. Map of the principal groundwater settings on Maui, Hawai‘i. Modified from Izuka and others (2018).

the isthmus, where it joins water flowing eastward from West Maui before discharging though caprock along the northern and southern coasts of the isthmus.

High groundwater levels in the Ke‘anae-Nāhiku area (fig. 40) are conceptualized as part of a thickly saturated setting in low-permeability aquifers (Meyer, 2000) (figs. 4*C* and 41). Much of the groundwater that flows though this area discharges to streams, although some groundwater likely flows to adjacent freshwater-lens settings or discharges below sea level. High water levels near the coast in Kaupō Gap relative to surrounding areas indicate the possible occurrence of the thickly saturated setting in that area. A relatively high water level was also measured in a well in Kīpahulu Valley, but it has been reported as part of a confined aquifer system (Souza, 1983).

Model Structure

The numerical model of Maui has a single layer with 314 rows, 546 columns, and 107,399 active cells. The model grid is rotated 15 degrees clockwise relative to the cardinal geographic directions to facilitate efficient discretization of the hydrogeologic features (fig. 42). The model is divided into 19 *K* zones that are consistent with structural and stratigraphic relations of Maui’s volcanic aquifers discussed above and those described by Izuka and others (2018), and build upon previous groundwater models by Gingerich (2008) and Gingerich and Engott (2012). In addition to representing regions of volcanic rock that have fairly uniform hydraulic properties, the *K* zones include a section of sediments that represent a low-permeability boundary that lies between the older West Maui volcano and Haleakalā, and narrow zones that represent low-permeability alluvial valley-fill barriers in the West Maui volcano.

Groundwater recharge in the Maui model was applied to surfaces of the volcanic aquifers above sea level (fig. 43); recharge to the model totaled 1,167 Mgal/d. A total withdrawal of 97.5 Mgal/d from wells and shafts was simulated in the model (fig. 44). The withdrawals were computed from reported drafts for the calibration period as described in the section on Withdrawals above. For underreported wells in use in 2001–2010, withdrawal for years of missing data was assumed to equal the average of reported years. For unreported wells in operation during the calibration period, the proposed withdrawal rate in CWRM’s well-permit application was used, and if no proposed amount was listed, the rate from CWRM’s water-use permit was used.

Major stream reaches indicated by the NHD for West Maui are simulated by drains in the model (fig. 45); these streams incise and drain water from the dike-impounded groundwater in the center of West Maui. However, not all streams mapped on Haleakalā were represented by drains in the model because many of these streams are youthful and do not incise the saturated part of the volcano’s aquifers. The exception is between Ke‘anae and Nāhiku (figs. 39 and 45), where streams incise the thickly saturated setting. Altitudes for drains that simulate streams (H_{str} in eq. 5) and heads used in offshore GHBs (H_{ocean} in eq. 2) were computed as described in the Flow Boundaries section above. Altitude for drains that simulate areas where the top of the caprock is above sea level and the top of the volcanic aquifer is below sea level (H_{cpr} in eq. 4) was set to zero.

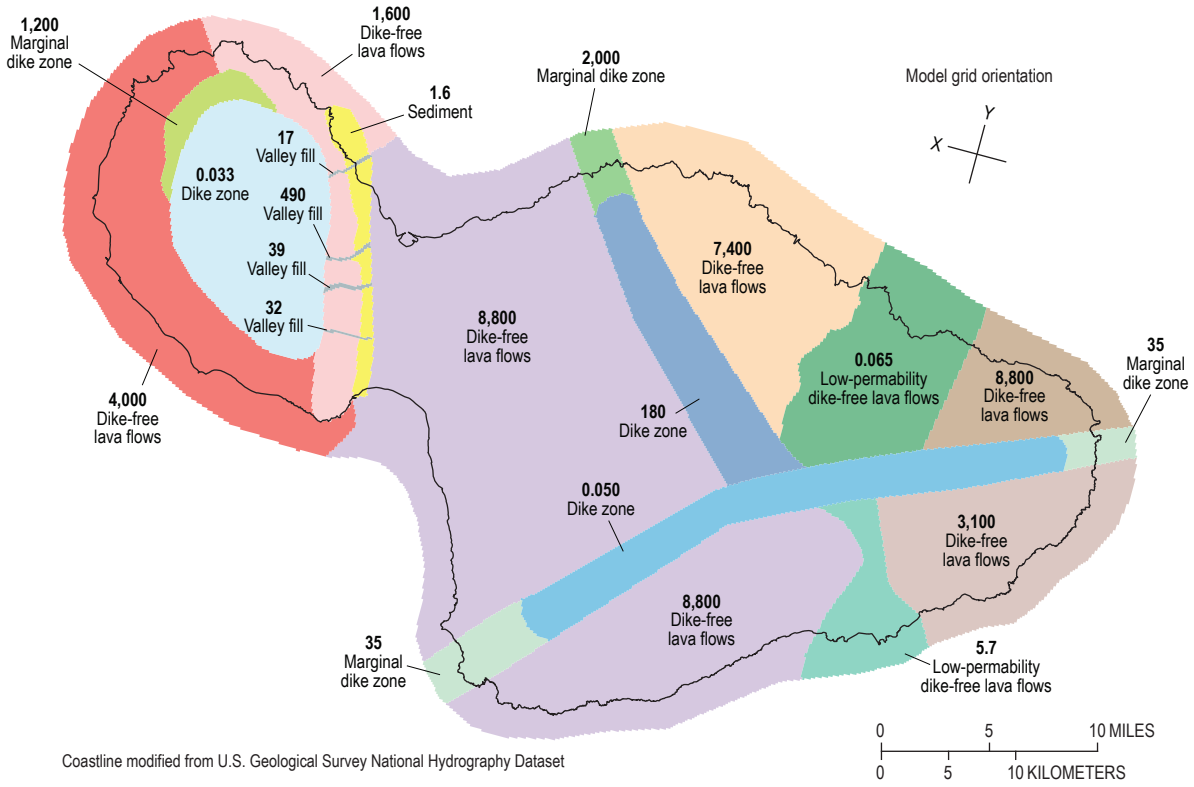

Figure 42. Map of hydraulic-conductivity zones (*K* zones) and values in the numerical groundwater model of Maui, Hawai'i. Numbers show horizontal hydraulic conductivity in feet per day. Black line shows the Maui coastline.

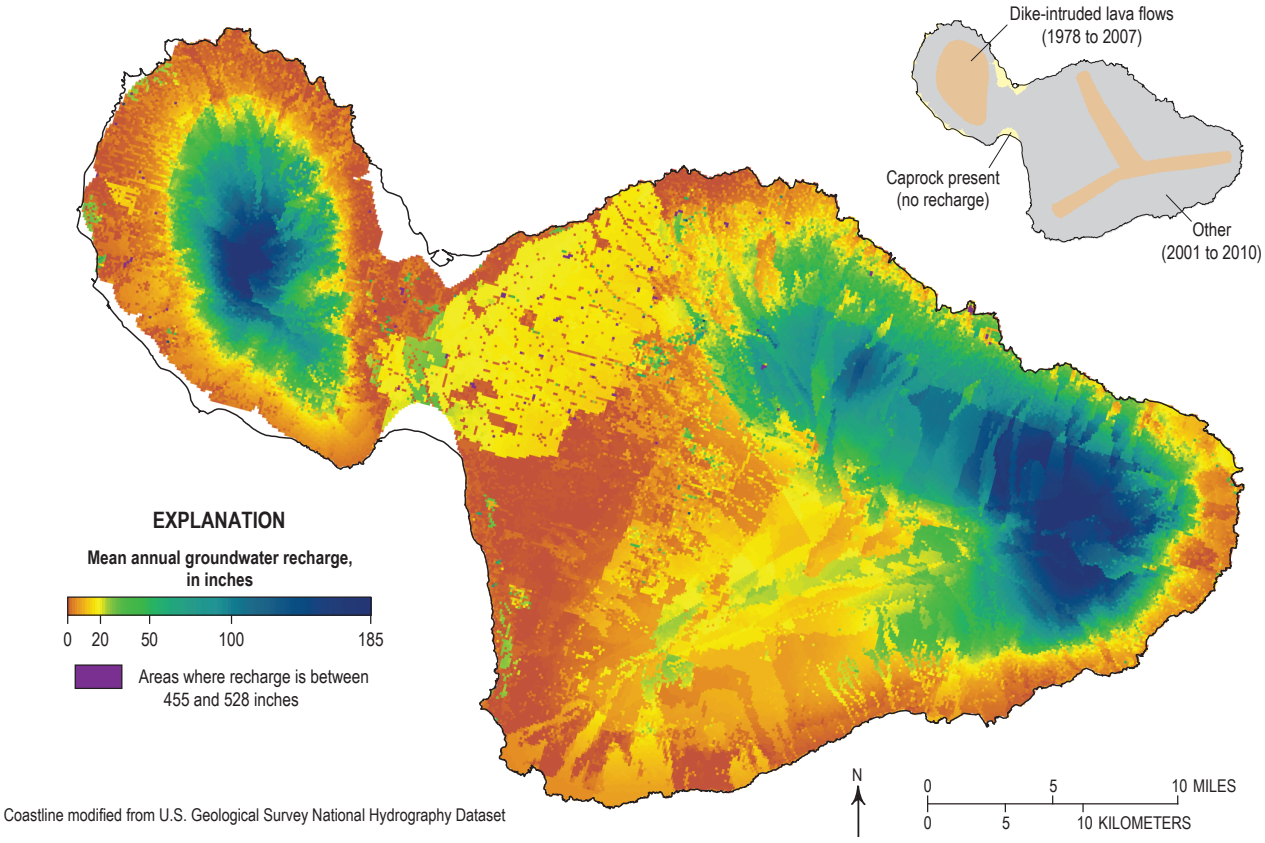

Figure 43. Map showing the distribution of groundwater recharge in the numerical groundwater model of Maui, Hawai'i. Recharge is based on averages computed by Izuka and others (2018) for periods shown on the inset map.

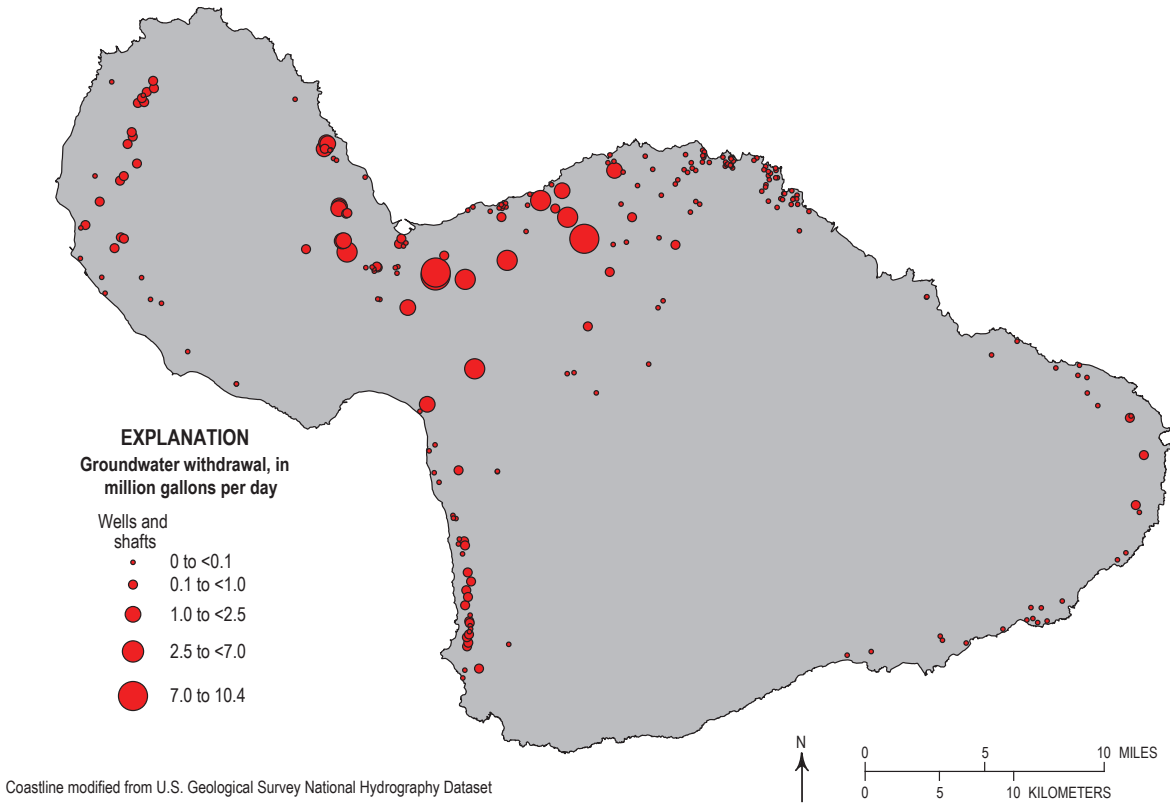

Figure 44. Map showing the distribution of groundwater withdrawals in the numerical groundwater model of Maui, Hawai'i.

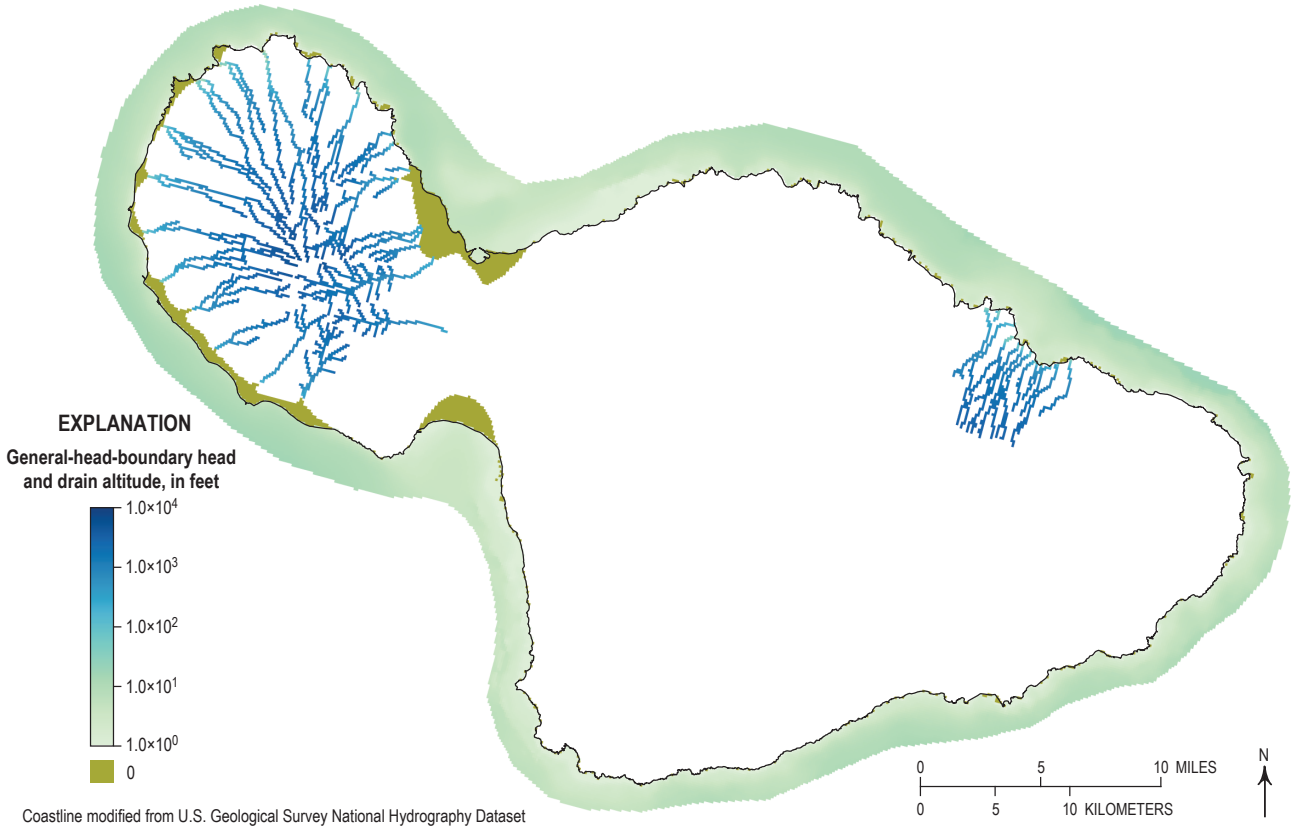

Figure 45. Map of general-head-boundary heads and drain altitudes in the numerical groundwater model of Maui, Hawai'i. Black line shows the Maui coastline.

Hydraulic Properties

In the calibrated model of Maui, the dike-intruded area in the center of the West Maui volcano is represented by two *K* zones. A larger *K* zone in the center of West Maui, representing the main dike zone, has a K_h value of 0.033 ft/d (fig. 42); a smaller *K* zone to the north, representing a marginal dike zone that has fewer dikes, has a higher K_h value of 1,200 ft/d. These values are generally consistent with the principal generalized hydrogeologic units (fig. 40). Dike-free lava flows of West Maui are represented by two *K* zones with K_h values of 4,000 and 1,600 ft/d, which are consistent with the high hydraulic conductivities characteristic of shield-stage lava-flow aquifers in Hawai‘i.

In the eastern part of West Maui, the dike-free *K* zone is dissected by four *K* zones that represent low-permeability valley-fill barriers and have K_h values between 17 and 490 ft/d in the calibrated model (fig. 42). The K_h values vary widely in part because in the single-layer Maui model, simulated hydraulic properties of a valley-fill-barrier cell integrate the properties of the valley-fill barrier and underlying lava-flow aquifer, and the ratio of valley-fill barrier to lava-flow aquifer and underlying lava-flow aquifer can differ substantially from one cell to the next. Even so, the range in K_h values for these sedimentary valley-fill barriers is much lower than dike-free lava-flow aquifers. The *K* zone that represents sediments lying between the West Maui volcano and Haleakalā also has a low K_h value of 1.6 ft/d.

The dike-intruded rift zones of Haleakalā are represented by four *K* zones (fig. 42). In the calibrated Maui model, the *K* zone that represents most of the prominent southwest-northeast trending rift zones has a K_h value of 0.050 ft/d; *K* zones that represent areas of marginal dike intrusion at the west and east ends of the rift zone have a K_h value of 35 ft/d. The *K* zone that represents most of the north-trending rift zone has a K_h value of 180 ft/d, and the *K* zone that represents the area of marginal dike intrusion at the northern end of the rift zone has a K_h value of 2,000 ft/d. The higher K_h values of the north-trending rift zone is consistent with its fewer vents (possibly indicating fewer dikes) compared to the east- and southwest-trending rift zones (Stearns and Macdonald, 1942).

Dike-free high-permeability lava-flow aquifers of Haleakalā are represented by four *K* zones in the calibrated model (figs. 40 and 42). These *K* zones have K_h values of several thousand feet per day, which are consistent with the high hydraulic conductivities characteristic of high-permeability, dike-free lava-flow aquifers.

Two *K* zones represent dike-free low-permeability aquifers on the flanks of Haleakalā (fig. 42). A *K* zone (K_h = 0.065 ft/d) on the northeastern flank represents the low-permeability area near Nāhiku, and a *K* zone (K_h = 5.7 ft/d) on the southeastern flank represents a low-permeability area in the Kaupō Gap. Both of these *K* zones are consistent with the conceptual model (fig. 40).

Values of C_{str} for streams range from 2.3 to 100,000 ft^2/d (fig. 46). The wide range of values is consistent with the

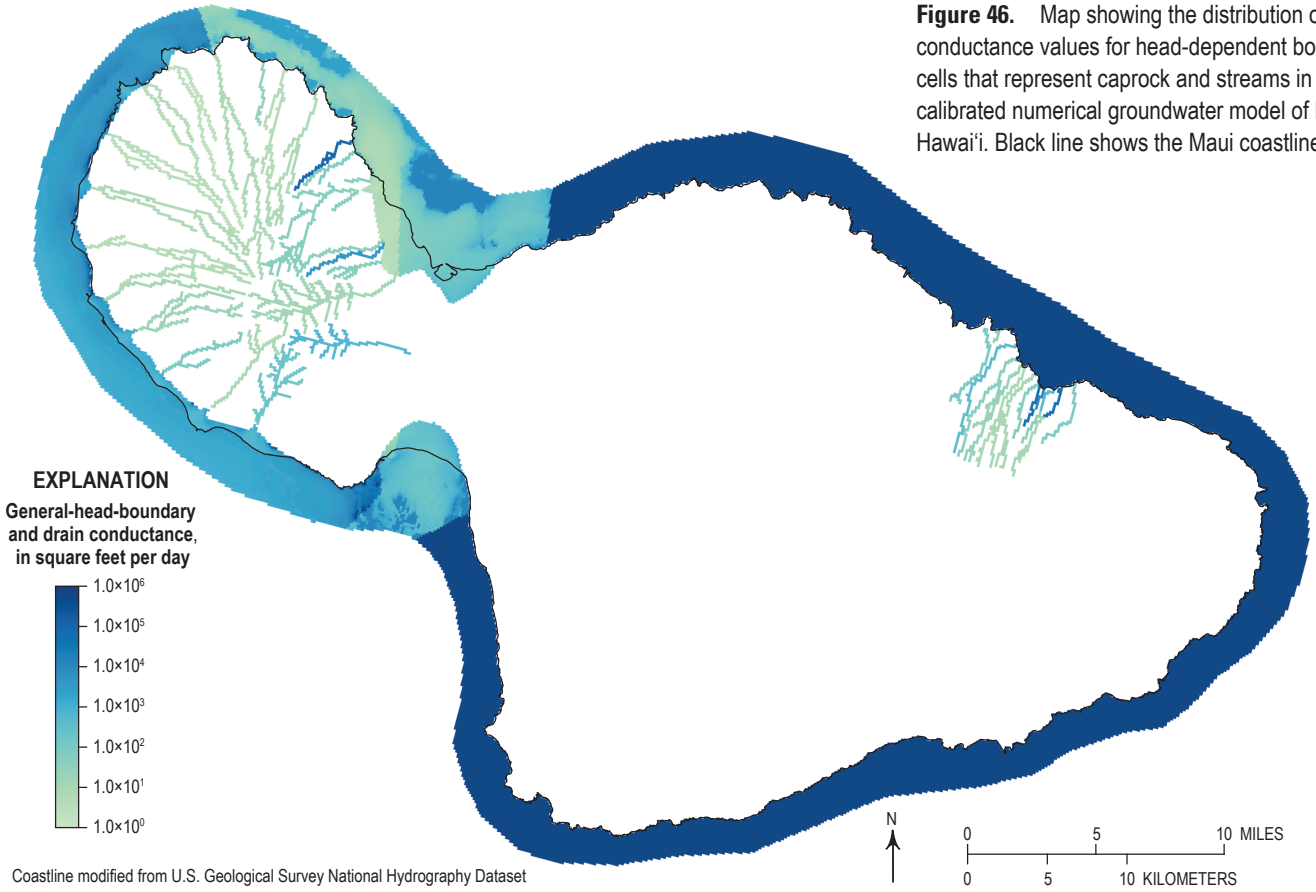

Figure 46. Map showing the distribution of conductance values for head-dependent boundary cells that represent caprock and streams in the calibrated numerical groundwater model of Maui, Hawai‘i. Black line shows the Maui coastline.

conceptualization that stream-bed thickness and hydraulic properties vary widely among the streams on Maui, but measured values for this parameter are lacking.

Values of C_{cpr} also range widely from 2.7 to 630,000 ft/d in the calibrated model, primarily because of the large variability of hydraulic properties and in caprock thickness. Measured values for C_{cpr} are also lacking.

Groundwater Levels and Flow

The calibrated model of Maui generally matches the different ranges of observed water levels among the different groundwater settings present on Maui (fig. 47). In high-permeability aquifers with freshwater lenses, simulated heads vary narrowly between 0 and 13 ft above sea level and generally

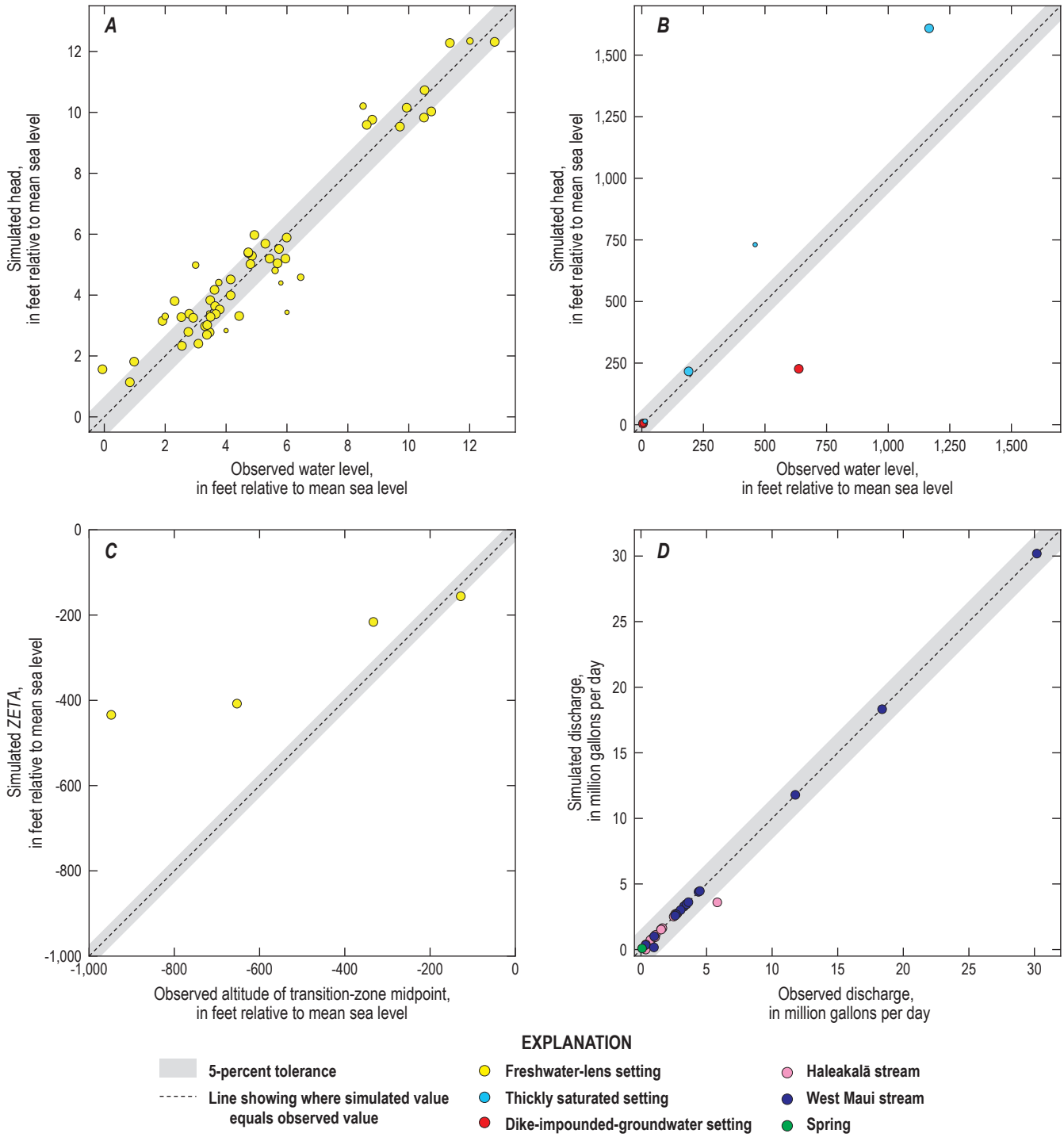

Figure 47. Plots comparing observed and model-simulated values in the calibrated numerical groundwater model of Maui, Hawai'i. Symbol diameter indicates relative weight during calibration, with one exception: transition-zone midpoint observations (in *C*) were given zero weight during calibration.

match the distribution of observed water levels. The average absolute residual between simulated head and observed water level was 0.7 ft and the standard deviation of residuals was 0.9 ft (table 3). The ratio between standard deviation and range of values was 0.07, and 49 percent of the simulated freshwater-lens water levels fall within the 5-percent tolerance. The model generally replicates the low-altitude water levels, gentle gradient, and flow toward the coast that is characteristic of this setting (fig. 48).

Few observed water levels are available from the dike-impounded-groundwater and thickly saturated settings on Maui. The calibrated model of Maui coarsely agrees with the widely varying observed water levels in these settings, but some simulated heads differ from the corresponding observed water levels by a few hundred feet (fig. 47*B*). The average absolute residual is 96.5 ft, the standard deviation of residuals is 189.2 ft, and the ratio between standard deviation and range of values was 0.16 (table 3). Seventy-five percent of the simulated water levels fall within the 5-percent tolerance.

In the thickly saturated low-permeability aquifers on the northeastern flank of Haleakalā, model-simulated water levels were mostly higher than the observed water levels (fig. 47*B*). This discrepancy is likely related to a single-layer model's limited ability to match both water levels and base flows in an area where heads are known to decrease with depth in the aquifer (Meyer, 2000). Stream baseflow is driven by the higher heads in the aquifer near the surface, whereas a water level measured in a well integrates the lower heads deeper in the aquifer.

In dike-impounded-groundwater settings, discrepancies between model-simulated head and observed water levels (fig. 47*B*) result from the model's use of broad *K* zones to represent the compartmentalized groundwater bodies that exist in reality in dike-intruded areas (fig. 4). Water levels in adjacent compartments can differ by hundreds of feet. The simulated heads replicate, however, the steep gradients and thick freshwater saturation of the dike-impounded-groundwater setting (figs. 40 and 48) and result in simulated stream discharges that match observed stream base flows.

Hydraulic properties used in the calibrated model for the dike-impounded-groundwater setting of Haleakalā's rift zones are highly uncertain because of the lack of water-level observations. The high simulated heads in these areas of the

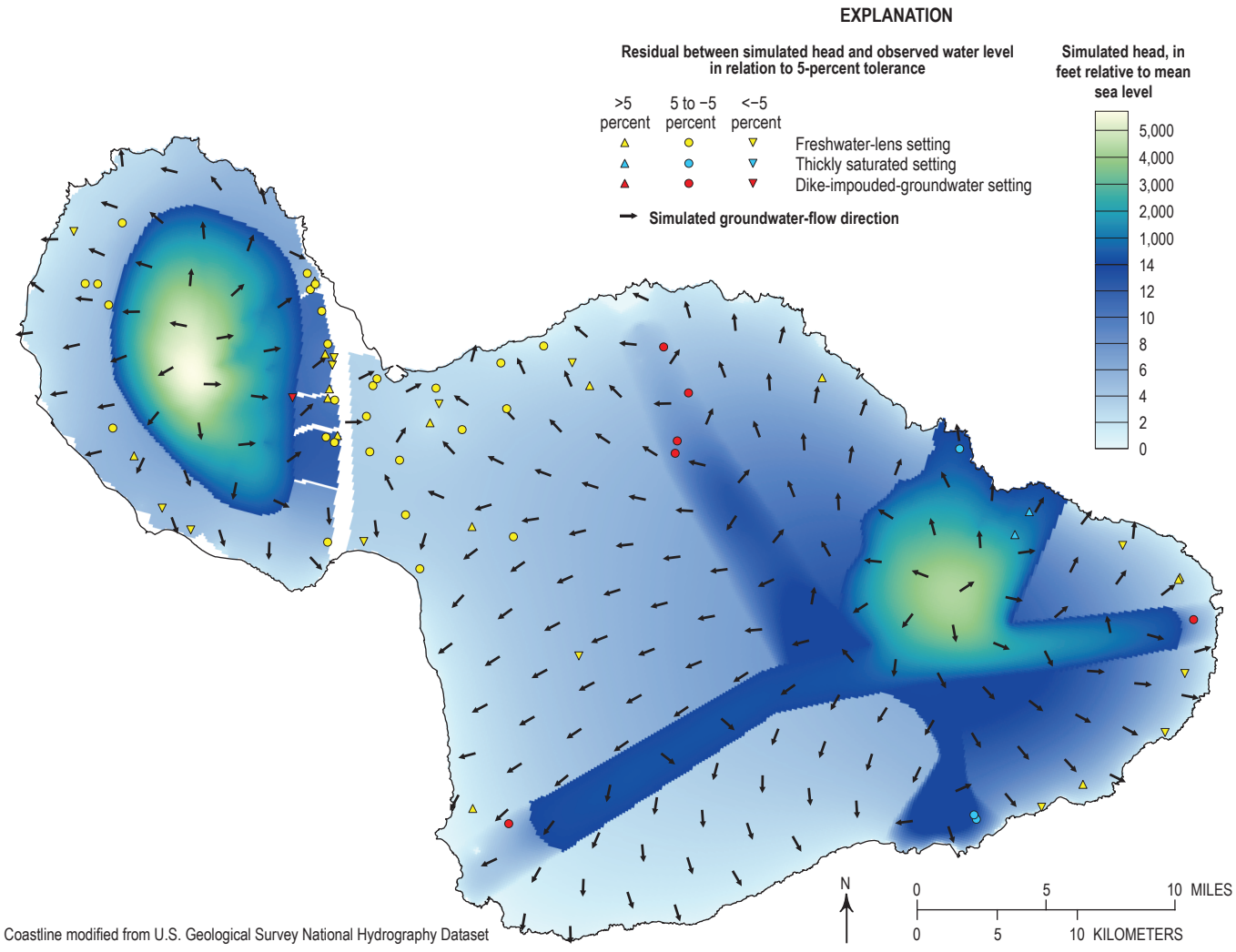

Figure 48. Map of simulated head and groundwater flow in the numerical groundwater model of Maui, Hawai'i.

model are consistent with the conceptual model, but simulated heads in parts of the Haleakalā rift zones are lower—in some cases by thousands of feet—than indicated in the conceptual model (fig. 40). Analogy with the rift zones of other shield volcanoes suggests that water levels in the rift zones of Haleakalā are likely to be high relative to water levels in adjacent areas, but no data exists that indicate the actual water-table altitudes. The differences between the conceptual and numerical models results in differences in groundwater flow near the thickly saturated setting in the low-permeability zone between Keʻanae and Nāhiku. In the conceptual model, water flows north from the rift zone to the low permeability zone, but in the numerical model, some water flows south from the low permeability zone to the rift zone (fig. 48). Given the lack of data, the numerical and conceptual models represent different but equally plausible conditions. Limitations associated with model nonuniqueness are discussed below (see section on Limitations).

Simulated groundwater flow in the calibrated Maui model (fig. 48) is generally consistent with the conceptual model (fig. 40). Water from high-level dike-impounded-groundwater settings in the interiors of the West Maui volcano and Haleakalā flows toward the coast; much of it discharges to streams, some is intercepted by tunnels, and the remainder flows into high-permeability coastal aquifers and the isthmus. Much of the groundwater in the thickly saturated setting on the northeastern flank of Haleakalā discharges to streams, but some discharges to adjacent high-permeability coastal aquifers or to the coast. Most of the groundwater in the coastal aquifers and isthmus ultimately discharges at the coast, except for water that is withdrawn from wells and shafts.

Freshwater-Saltwater Interface

The altitude of the transition-zone midpoint in four DMWs provided observations for comparison with *ZETA* during calibration of the Maui model, although no weight was given to them during PEST calibration. In three of the DMWs, model-simulated steady-state *ZETA* was higher than the observed midpoint depth (fig. 47*C*); these wells are in an area of high groundwater withdrawal on the east side of West Maui (fig. 49). In contrast, model-simulated *ZETA* at the fourth DMW, in an

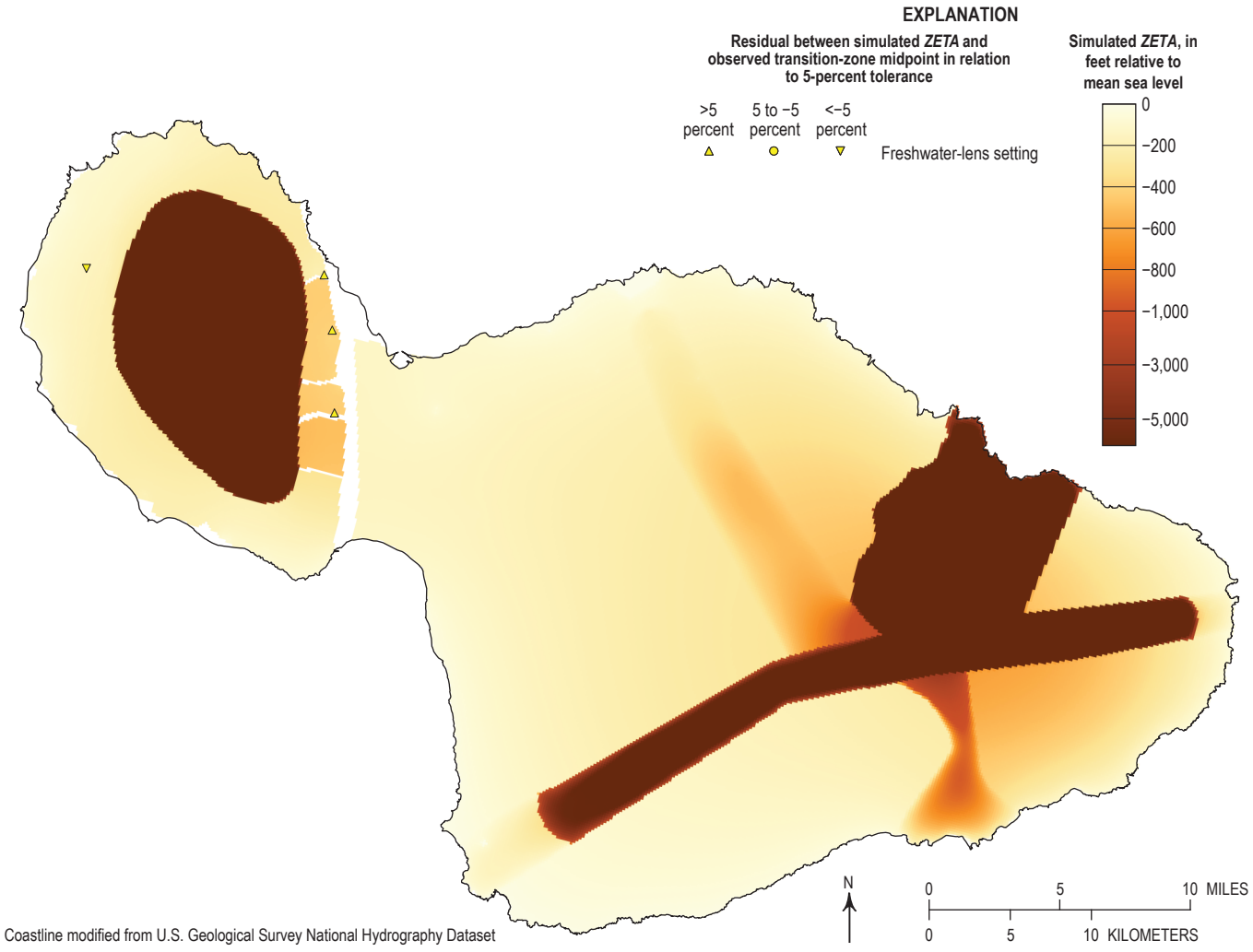

Figure 49. Map of the simulated altitude of the freshwater-saltwater interface (*ZETA*) in the numerical groundwater model of Maui, Hawaiʻi.

area of low groundwater development on the west side of West Maui, more closely matches the observed midpoint depth. These results may indicate that the observed interface depths in eastern West Maui have not yet reached steady state, and the transition zone is still rising in response to large groundwater withdrawals; if so, *ZETA* indicates the altitude to which the transition-zone midpoint will rise in eastern West Maui if conditions are allowed to develop to steady state. The discrepancies may also be due to difficulties in measuring the position of the transition-zone midpoint because of borehole flow in DMWs, as seen in some DMWs on O‘ahu (Rotzoll, 2012), or the inability of a single-layer model to simulate vertical gradients.

Simulated *ZETA* (figs. 49 and 50) in the calibrated Maui model is consistent with the conceptual model of groundwater in oceanic islands (figs. 4 and 41). Fresh groundwater extends down to the bottom of the model in most of the dike-impounded-groundwater settings at the center of West Maui and in the rift zones of Haleakalā. Fresh groundwater also extends to the bottom of the model in the thickly saturated setting in the northeastern slope of Haleakalā, but the simulated freshwater thickness may be greater than in reality because the single-layer model cannot simulate vertical head gradients. However, freshwater in these low-permeability settings is so thick that saltwater rise is not likely to limit fresh groundwater availability except near the coast. Elsewhere, the model-simulated fresh groundwater forms thin lenses in the high-permeability lava-flow aquifers, especially where substantial caprock is absent.

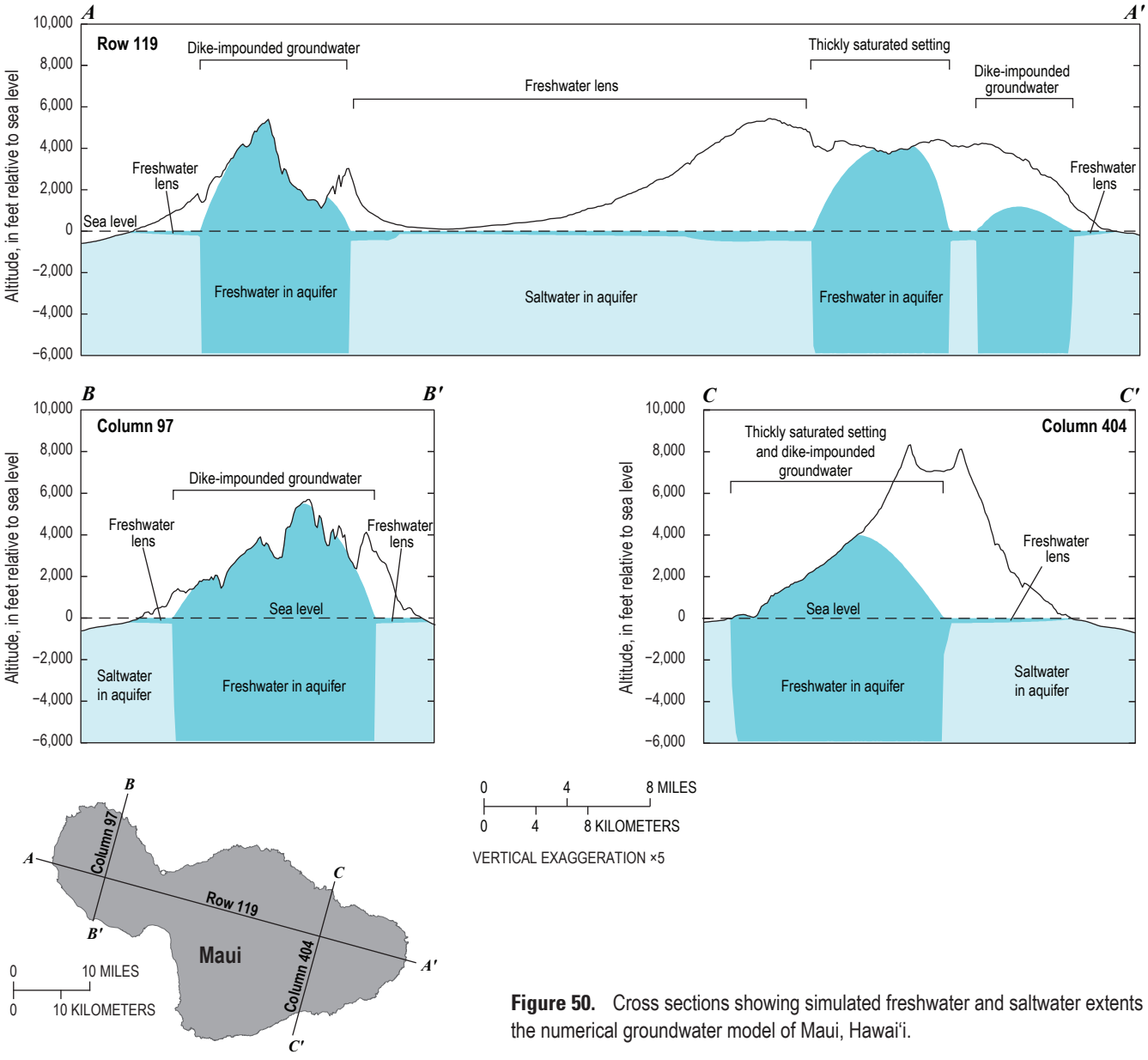

Figure 50. Cross sections showing simulated freshwater and saltwater extents in the numerical groundwater model of Maui, Hawai‘i.

Discharge to Streams and the Ocean

Simulated groundwater discharge to streams in the calibrated Maui model agrees closely with base-flow estimates from analyses of stream-gage data (fig. 47*D*). The average absolute residual is 0.1 Mgal/d, the standard deviation of residuals is 0.4 Mgal/d, and the ratio between standard deviation and range of values is 0.01 (table 3). All but one of the simulated discharge rates are within the 5-percent tolerance. All base-flow observations used to calibrate the Maui model come from gages in one of two areas of low-permeability rocks: (1) the dike-intruded lava flows in West Maui and (2) low-permeability lava flows on the northeastern flank of Haleakalā (figs. 40 and 51). The model results are consistent with the conceptualizations of the dike-impounded-groundwater and thickly saturated settings that occur in these areas (figs. 4*A*, 4*C*, and 41).

Groundwater discharge to the ocean is voluminous in the Maui model (see discussion below in Comparison of Model Water Budgets for Kaua‘i, O‘ahu, and Maui), but it is difficult to see in figure 51 because the discharge, particularly from Haleakalā, is concentrated at cells near the shoreline. The concentrated discharge results because there is little or no caprock to resist discharge from the coastal aquifers of the young Haleakalā volcano. In the isthmus and parts of West Maui, where caprock is more substantial, the discharge of groundwater to the ocean is spread diffusely over a wider area of cells. Groundwater that may discharge to streams from perched aquifers that are postulated to exist in the Ha‘ikū area of Haleakalā (Gingerich, 1999a, b) is not simulated in the model.

Model Sensitivity to Parameters

The parameter to which the calibrated Maui model is most sensitive is K_h of the *K* zone that represents the dike zone in the center of West Maui (figs. 42 and 52). Adjustment of this parameter during calibration affects the base-flow of West Maui streams, where about half of the stream base-flow observations used in calibration are located (fig. 51). Adjusting this parameter also affects groundwater flow toward the coast, which, in turn, affects water levels in the coastal aquifers in West Maui and the

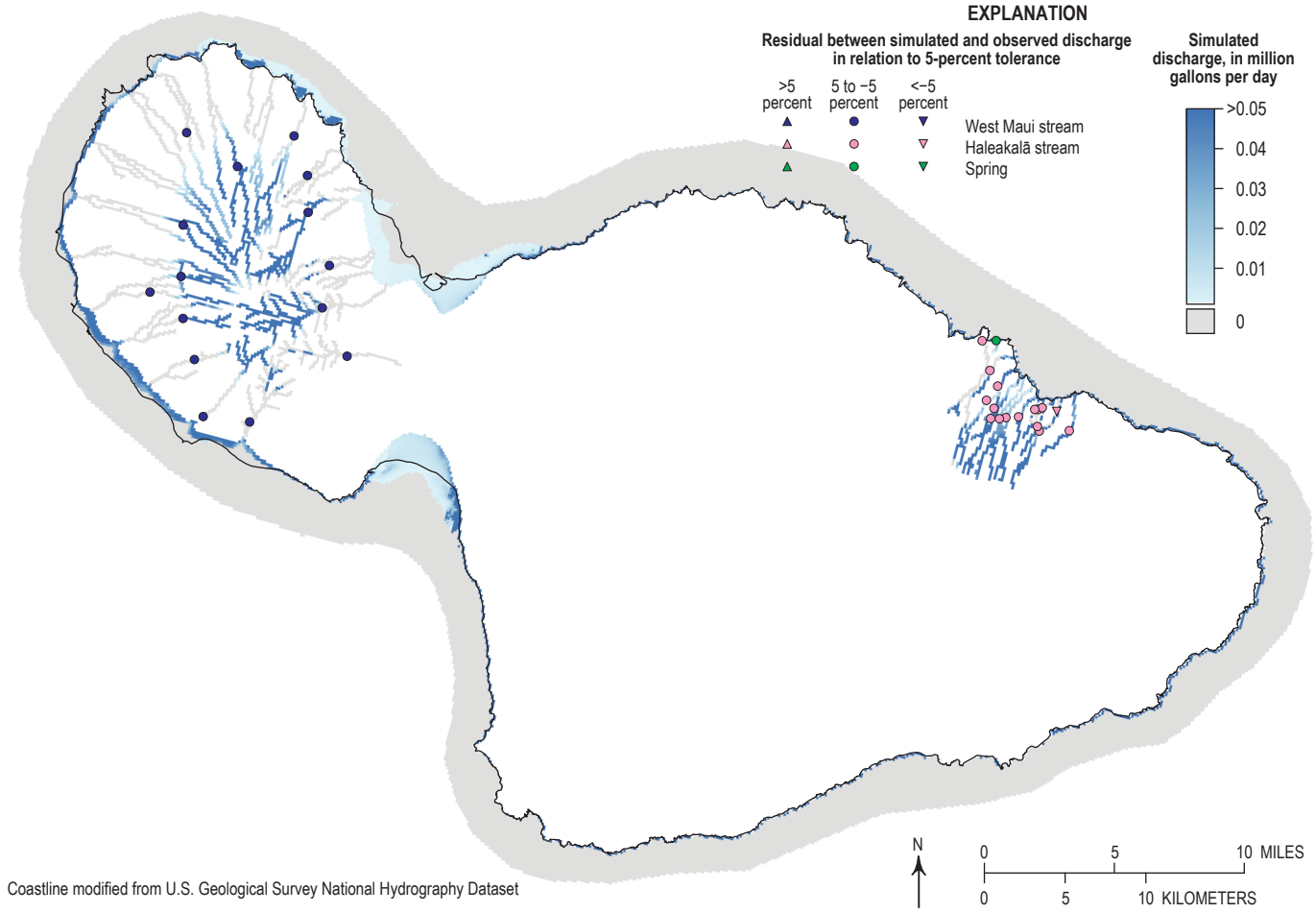

Figure 51. Map showing simulated groundwater discharge to streams and the ocean in the calibrated numerical groundwater model Maui, Hawai‘i. Black line shows the Maui coastline.

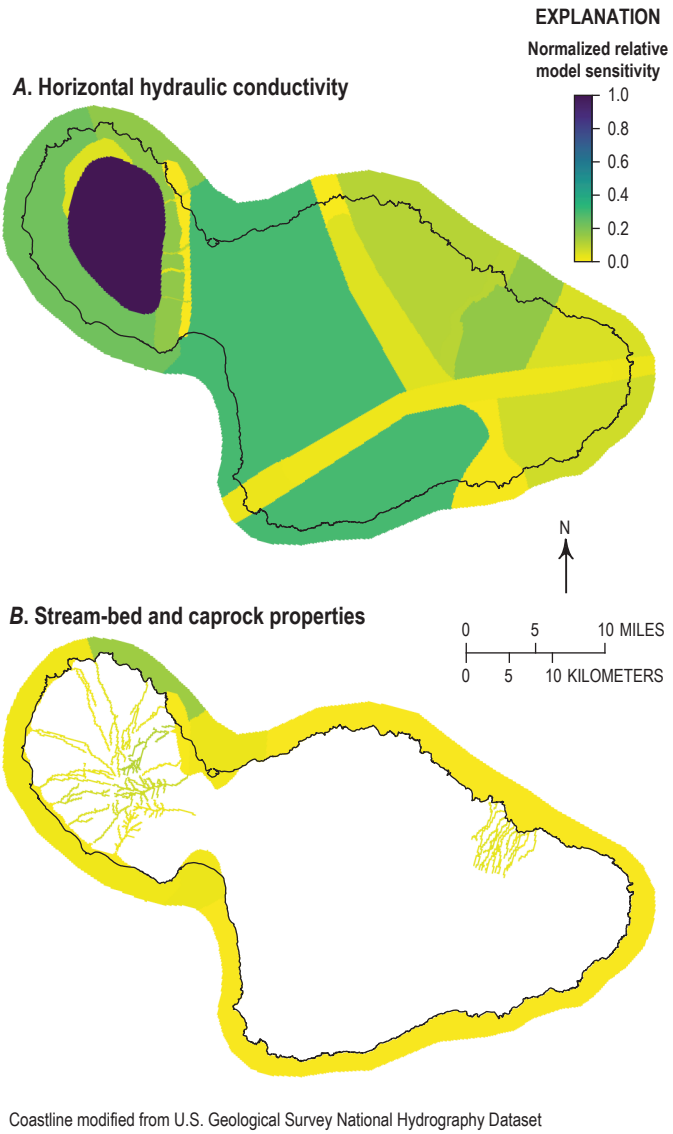

Figure 52. Map showing normalized relative composite sensitivities of parameters adjusted during calibration of the numerical groundwater model of Maui, Hawai‘i. *A*, horizontal hydraulic conductivity; *B*, hydraulic properties of stream beds and caprock. Black line shows the Maui coastline.

isthmus, where most of the water-level observations used in calibration are located (fig. 48). The Maui model is moderately sensitive to K_h values of other K zones, including the zone that represents the lava-flow aquifers of western Haleakalā and the zone that represents lava-flow aquifers in the west coast of West Maui. Model hydraulic properties of these areas affect the model's match of the numerous water-level observations in eastern West Maui, western Haleakalā, and the isthmus. Calibration of the Maui model was less sensitive to hydraulic properties of the rift zones of Haleakalā, caprock, and streams.

Comparison of Model Water Budgets for Kaua‘i, O‘ahu, and Maui

In steady-state models, the total of all groundwater inflow components is balanced by the total of all outflow components. As discussed above, freshwater inflow to each of the models in this report comes from groundwater recharge through the surface. Freshwater outflow components include withdrawals (from wells, shafts, and tunnels) for human use, and groundwater discharge to the ocean, streams, and springs. The Kaua‘i, O‘ahu, and Maui models show substantial differences in the relative distribution of discharge among these outflow components (fig. 53). The differences reflect the different groundwater settings and anthropogenic effects among the islands. The differences also indicate that consequences that limit the availability of fresh groundwater for human use are likely to differ among the three islands.

On the basis of percentage of an island's fresh groundwater discharge, withdrawals are highest in the O‘ahu model (37 percent or 221 Mgal/d) (fig. 53), which is commensurate with the distribution of population among the islands of Hawai‘i. In contrast, withdrawals are 6 percent (50 Mgal/d) and 9 percent (109 Mgal/d) of total freshwater discharge on the less-populated islands of Kaua‘i and Maui, respectively.

The percentage of an island's fresh groundwater discharge that goes to streams and springs is highest in the Kaua‘i model (80 percent or 701 Mgal/d) (fig. 53). The high percentage is due largely to the extensive area of dike-impounded groundwater that has been dissected by streams on Kaua‘i (figs. 13 and 23), the oldest of the islands modeled in this study. Substantial groundwater discharge to streams is also typical of the thickly saturated setting that predominates eastern Kaua‘i. Discharge to streams and springs in the O‘ahu model is much less (21 percent or 128 Mgal/d) than in the Kaua‘i model. In the O‘ahu model, most discharge to streams and springs occurs in the dike-impounded-groundwater setting (figs. 27 and 37), but a substantial fraction comes from springs at the inland boundary of O‘ahu's caprock. Discharge to streams and springs constitutes an even smaller percentage of total fresh groundwater discharge in the Maui model (13 percent), although the volumetric rate (157 Mgal/d) exceeds that of the O‘ahu model. In the Maui model, most of this water discharges to streams that incise the dike-impounded groundwater in West Maui, and some discharges to streams dissecting the thickly saturated setting on Haleakalā. Model-simulated dike-impounded groundwater in Haleakalā's rift zones does not contribute to simulated discharge to streams and springs because the rift zones of this young volcano have not been exposed by erosion; instead, groundwater from the rift zones flows into the downgradient freshwater-lens settings from which it ultimately discharges to the ocean. Because the models in this study do not simulate perched groundwater, simulated discharge to streams does not include discharge from perched aquifers, which has been postulated in some areas, such as parts of the north slope

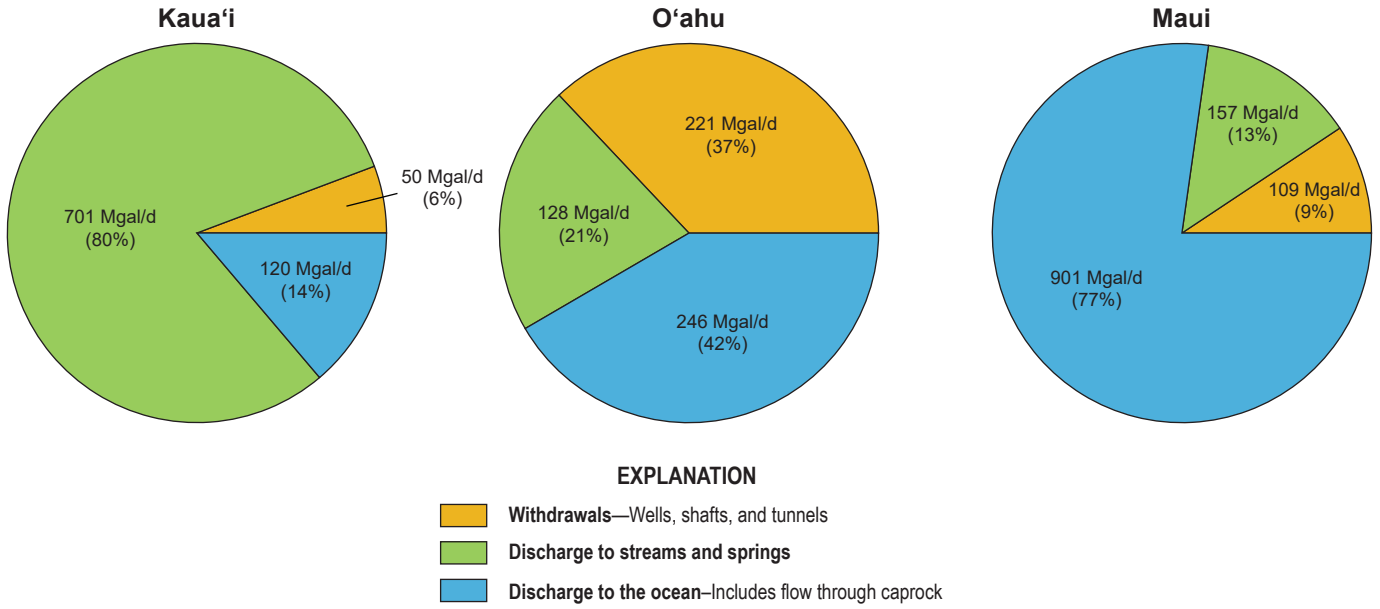

Figure 53. Pie diagrams showing the distribution of simulated discharge of fresh groundwater in million gallons per day (Mgal/d) and as a percentage of the island total (%) for the calibrated groundwater models of Kaua'i, O'ahu, and Maui, Hawai'i. Percentages may not add to 100 because of rounding.

of Haleakalā (Gingerich, 1999a, b). The totals also do not include direct surface runoff that can constitute a substantial component of the average stream flow in high-rainfall areas.

The percentage of an island's fresh groundwater discharge that goes to the ocean, either through the caprock or directly from the volcanic aquifers, is by far the highest in the Maui model (77 percent or 901 Mgal/d) (fig. 53), which is consistent with the extensive freshwater-lens settings on the island (fig. 41). Discharge to the ocean is also high in the O'ahu model (42 percent or 246 Mgal/d), which also has extensive freshwater-lens settings (fig. 27), but the discharge to the ocean is reduced by the high rate of withdrawals. Also, O'ahu's extensive caprock causes some water in the freshwater lens to discharge to springs above sea level (fig. 4*A*). In contrast, discharge to the ocean in the Kaua'i model, which has less extensive freshwater-lens settings, is only 14 percent (120 Mgal/d) of the total fresh groundwater discharge for the island.

Limitations

The numerical groundwater models described in this report were created specifically for the purpose of quantifying consequences that can limit the availability of fresh groundwater for human use from the volcanic aquifers of Hawai'i. These consequences include changes in the volume of fresh groundwater and the rates of natural groundwater discharge to streams, nearshore areas, and adjacent groundwater areas, that can result from changes in groundwater withdrawal and recharge. Use of the models outside this purpose may be limited, or require modification of the models.

All numerical models are limited by spatial discretization. Each cell in the models described in this report represents a volume that has horizontal dimensions of 500 ft by 500 ft. This level of discretization limits the models' ability to resolve small geologic features, such as individual dikes, narrow stream reaches, and thin flow barriers. Because the O'ahu and Maui models each have only one layer, they cannot simulate variations of hydraulic properties with depth or vertical flow in the aquifer. The two-layer Kaua'i model can simulate some vertical flow and variations of hydraulic properties with depth, but is still limited by the small number of model layers. Also, the models' *K* zones and *C* zones, within which parameter values were uniform, are a simplification of the diverse hydraulic properties that may exist in these zones in nature. Simplification of geologic structure was necessary to facilitate the island-wide models; thus, not all known hydrogeologic details have been simulated. Although the level of discretization and hydrogeologic detail simulated in the models is sufficient for the island-wide assessment objectives established in this report, finer discretization and inclusion of greater geologic detail may be required for models that assess groundwater flow at finer scales—for example to study local effects of groundwater development or the movement of contaminants.

The models were constructed to be used for steady-state simulations only. Although using SWI2 with *ZETA* requires models to be run in the transient mode, model parameters that affect the transient response of a groundwater system (such as effective porosity and specific storage [Harbaugh, 2005]) were assigned reasonable values from the literature without calibration and may not be an accurate representation of these values in nature. As a result, the model-simulated rates of

change (for example, the rate of rise of the interface that results from increased withdrawal) are not discussed in this report. The models described in this report are intended to evaluate the ultimate magnitude of changes that would result under a given set of stresses, not the rate at which those changes would develop.

In this study, model results (*ZETA*, head, and discharge through drains and GHBs) from the last two time steps of the final runs for each model were averaged to mitigate the effect of oscillation of *ZETA* at some model cells, particularly those at boundaries between *K* zones that have sharply contrasting hydraulic properies (see discussion in Calibration section). This approach provided adequate accuracy for the island-scale purposes of the models in this report but may not be adequate for studies that require greater precision in simulations of flow, interface depth, or head near these boundaries.

The models' sharp-interface representation of the freshwater-saltwater transition zone allows broad assessment of volumetric changes in groundwater storage resulting from the movement of the underlying saltwater in response to changes in withdrawals and recharge, but cannot quantify changes in the salinity of water pumped at specific wells. Also, because the sharp interface is a simplified representation of a transition zone that has variable thickness, the modeled fresh groundwater thickness is not a precise indicator of the actual thickness of potable fresh groundwater. The actual thickness of potable groundwater is less than the models indicate. Other limitations to groundwater availability that may result from poor water quality, such as anthropogenic contamination, are not considered in this study.

The models described in this report do not simulate perched groundwater. If a well in reality withdraws water from a perched system whose water would otherwise flow to an underlying non-perched saturated aquifer, the effect will be accounted for in the models as withdrawal from the underlying non-perched saturated aquifer. However, if a well in reality withdraws water from a perched system whose water would otherwise discharge to a stream, the model may not accurately account for the resulting reduction in stream base flow. This limitation may be particularly relevant for the Maui model, where perched groundwater may be discharging to streams in some areas on the north slope of Haleakalā (Gingerich, 1999a, b). In addition, not all stream reaches indicated by the NHD for the northern flank of Haleakalā are simulated by drains in the Maui model. Omitted are youthful streams, particularly between Ha‘ikū and Ke‘anae on Maui (fig. 39), whose incision does not reach the non-perched saturated part of the Haleakalā aquifers. This stream-groundwater relation is consistent with the conceptual model, but little groundwater-level information is available to inform the conceptual model in that area. Additional water-level data and a better understanding of perched conditions is needed to assess the effect of groundwater withdrawals in this part of Maui.

Simulating the effect of caprock using head-dependent boundaries (drains and GHBs) was appropriate for the models in this report because the study focuses on the volcanic aquifers of the islands. This simplifying approach, however, limits the models' ability to simulate stresses and effects on and within the caprock. Groundwater withdrawals from the caprock are not simulated, nor are changes in the volume of freshwater resources of the caprock. Also, groundwater discharge to streams that flow over caprock in the real world is counted as discharge to the ocean in the models.

The numerical models in this study are nonunique because of uncertainties. Even though the calibrated models were constrained by available data and are generally consistent with conceptual models based on current understanding of the hydrogeology of Kaua‘i, O‘ahu, and Maui, alternative values and distributions of hydraulic properties may result in calibration that is as satisfactory as that in this study. Some model uncertainties are related to the limited available data. Observation data were not equally available for the three models described in this report (table 2), and not equally distributed spatially within a model. Areas of the models with little or no observation data have greater uncertainty than areas with abundant observation data. Maps showing locations of water-level (figs. 20, 34, and 48), transition-zone-midpoint (figs. 35 and 49), and base-flow (figs. 23, 37, and 51) observations used in calibration, and the residuals associated with these observations (figs. 19, 33, and 47), indicate where model representativeness is more or less certain. Additional uncertainties stem from the limitations in available information on geologic structure (for example, structures related to the enigmatic Schofield high-level groundwater) and the ranges of some hydraulic properties used in the models (for example, streambed and caprock conductances).

Some uncertainties are related to the assumption that inflows, outflows, and water levels are at a reasonably steady state. Although the 2001–2010 period was considered the best period for steady-state calibration in this study, some wells show downward or upward trends (fig. 7) that indicate gradual change over time. The models' inability to match both observed water levels and some transition-zone midpoints may also be an indication that some areas are not truly in steady state. Uncertainties may also be inherited from uncertainties of externally computed estimates, such as recharge and base flows, used as input to, or calibration targets for, the models. Under the premise that response to changes in recharge is slower in low-permeability aquifers than in high-permeability aquifers, recharge applied to dike-intruded areas of the models in this study was based on an average from 1978–2007, rather than the average from the 2001–2010 calibration period used in other areas of the models; this generalized method is one approach to address the premise as it relates to the steady-state assumptions, given the availability of recharge estimates for Hawai‘i.

Summary

Three numerical groundwater models that represent the movement and storage of groundwater on the islands of Kaua‘i, O‘ahu, and Maui were created with the objective of assessing

groundwater availability. The consequences of groundwater withdrawal by humans include lowering of the water table; rise of the saltwater underlying freshwater in aquifers near the coast; reduction of natural groundwater discharge to streams, springs, and submarine seeps; and reduction in flow to adjacent groundwater bodies. These consequences can lead to limitations on availability of groundwater for human use. The three numerical models described in this report were designed to quantify the consequences.

Kauaʻi, Oʻahu, and Maui share some broad hydrogeologic similarities. Groundwater in these islands include freshwater and saltwater. Most fresh groundwater exists in one of three principal groundwater settings—the freshwater-lens, dike-impounded-groundwater, and thickly saturated settings. Kauaʻi, Oʻahu, and Maui each have different combinations of these settings. The freshwater-lens setting is present in high-permeability aquifers on all of the islands, but the freshwater lenses on Oʻahu are thicker because the island has extensive caprock that resists groundwater discharge to the ocean. Caprock is present but less areally extensive or thick on Kauaʻi and Maui. The dike-impounded-groundwater setting is present on all the islands, but groundwater-saturated dike compartments on Kauaʻi, Oʻahu, and West Maui have been breached by erosion and discharge substantial groundwater to streams, whereas dike-impounded groundwater in Haleakalā is mostly buried beneath the surface. The thickly saturated setting is most evident on eastern Kauaʻi, where thick rejuvenation-stage lava flows accumulated in eroded and faulted depressions form low-permeability aquifers. Thickly saturated low-permeability aquifers are also present on Maui, but the geologic reason for the low permeability has not been clearly established. High water levels beneath the Schofield Plateau of Oʻahu are enigmatic—they do not fit definitively into any of the principal groundwater settings.

The three models were created using the USGS finite-difference groundwater-modeling program MODFLOW-2005 with the SWI2 package. In the models, water tables are simulated by heads, the boundary between freshwater and saltwater in the aquifer was simulated by a sharp interface whose altitude is represented by *ZETA* in SWI2, and groundwater discharge to springs, streams, and submarine seeps is simulated using head-dependent boundaries. The models in this study were created and calibrated in the steady-state mode. Well withdrawals in the models were based on average reported and estimated withdrawal rates for the period 2001–2010. Recharge in the models was based on average rates for 2001–2010 in most areas, and 1978–2007 for dike-impounded-groundwater settings. Models were calibrated to achieve a reasonable representation of the groundwater systems in the volcanic aquifers of Kauaʻi, Oʻahu, and Maui. Model hydraulic conductivities and head-dependent-boundary conductances were adjusted during calibration until residuals between model-simulated and observed values for groundwater levels, stream base flows, spring flows, and tunnel flows were small.

In the calibrated numerical models of Kauaʻi, Oʻahu, and Maui, horizontal hydraulic-conductivity values for high-permeability aquifers with freshwater lenses varied between 100 and 8,800 ft/d. Horizontal hydraulic-conductivity values for the dike-impounded-groundwater setting varied between 0.011 and 180 ft/d for the main dike-intruded areas, and between 1.5 and 2,000 ft/d for marginal dike zones. Horizontal hydraulic-conductivity values for thickly saturated low-permeability aquifers ranged from 0.065 to 5.7 ft/d. These values are consistent with the ranges typically associated with these settings in conceptual models and published literature. The models generally replicate the shapes of the water tables depicted in maps generated from water-level data, base flows measured at stream gages, and flow directions in conceptual models.

Model-simulated *ZETA* agrees with some observed transition-zone midpoint altitudes but differs from other observed transition-zone midpoints by as much as several hundred feet. The discrepancies indicate that the observed transition zone may not have reached steady state and is still slowly adjusting in response to changes in withdrawals that have happened within, and possibly a few decades before, the calibration period. Alternatively, the discrepancies may be due, in part, to difficulties in measuring the position of the transition-zone midpoint because of borehole flow in DMWs, or the inability of a single-layer model to simulate vertical gradients. On a broad scale, however, *ZETA* indicates freshwater thicknesses that are consistent with the conceptual models—fresh groundwater forms thin lenses in the high-permeability coastal aquifers but extends to great depths in the dike-impounded-groundwater and thickly saturated settings.

The Kauaʻi, Oʻahu, and Maui models show substantial differences in the relative distribution of simulated fresh groundwater discharge to the ocean, streams, and springs and withdrawals (wells, shafts, and tunnels) for human use. On the basis of percentage of a model's fresh groundwater discharge, withdrawals are highest in the Oʻahu model, which is commensurate with population distribution among the islands of Hawaiʻi. The percentage of discharge to streams is highest in the Kauaʻi model, which has large areas of dike-impounded-groundwater and thickly saturated settings that are dissected by streams. Discharge to the ocean, either through the caprock or directly from the volcanic aquifers, is highest in the Maui model, which has extensive freshwater-lens settings. Discharge to the ocean is also high in the Oʻahu model, which also has extensive freshwater-lens settings, but natural discharge to the ocean is reduced by the high rate of withdrawals, and Oʻahu's extensive caprock causes some water in the freshwater lens to discharge to springs above sea level. The differences among the models indicate that consequences that limit the availability of fresh groundwater for human use are likely to differ among the three islands.

The numerical groundwater models described in this report provide tools to assess groundwater availability. Comparing steady-state simulations for different groundwater-withdrawal rates can quantify the effects of changing groundwater use by humans; comparing results for different recharge rates can quantify the effects of changing climate and land cover.

References Cited

Bakker, M., Post, V., Langevin, C.D., Hughes, J.D., White, J.T., Starn, J.J., and Fienen, M.N., 2016, FloPy v3.2.4: U.S. Geological Survey Software Release, 08 February 2016, http://doi.org/10.5066/F7BK19FH.

Bakker, M., Schaars, F., Hughes, J.D., Langevin, C.D., and Dausman, A.M., 2013, Documentation of the seawater intrusion (SWI2) package for MODFLOW: U.S. Geological Survey Techniques and Methods, book 6, chap. A46, 47 p., http://pubs.usgs.gov/tm/6a46/.

Bauer, G., 1996, Reevaluation of the ground-water resources and sustainable yield of the Ewa caprock aquifer—Final report: State of Hawaii, Department of Land Natural Resources Commission on Water Resource Management, 57 p.

Burnham, W.L., Larson, S.P., and Cooper, H.H., 1977, Distribution of injected wastewater in the saline lava aquifer, Wailuku-Kahului wastewater treatment facility, Kahului, Maui, Hawaii: U.S Geological Survey Open File Report 77-469, 58 p.

Cheng, C.L., 2016, Low-flow characteristics for streams on the Islands of Kaua‘i, O‘ahu, Moloka‘i, Maui, and Hawai‘i, State of Hawai‘i: U.S. Geological Survey Scientific Investigations Report 2016-5103, 36 p., http://doi.org/10.3133/sir20165103.

Clague, D.A., and Dalrymple, G.B., 1987, The Hawaiian-Emperor volcanic chain, Part 1—Geologic evolution, *in* Decker, R.W., Wright, T.L, and Stauffer, P.H., eds., Volcanism in Hawaii: U.S. Geological Survey Professional Paper 1350, v. 1, p. 5–54.

Clague, D.A., and Sherrod, D.R., 2014, Growth and degradation of Hawaiian volcanoes, *in* Poland, M.P., Takahashi, J.T., and Landowski, C.M., eds., Characteristics of Hawaiian Volcanoes: U.S. Geological Survey Professional Paper 1801, p. 97–146.

Doherty, J., 2010, PEST—Model-Independent Parameter Estimation User Manual (5th ed.): Watermark Numerical Computing, 333 p.

Flinders, A.F., Ito, G., Garcia, M.O., Sinton, J.M., Kauahikaua, J., and Taylor, B., 2013, Intrusive dike complexes, cumulate cores, and the extrusive growth of Hawaiian volcanoes: Geophysical Research Letters, v. 40, p. 3,367–3,373, www.doi.org/10.1002/grl.50633.

Furumoto, A.S., Campbell, J.F., and Hussong, D.M., 1970, Seismic studies of subsurface structure in the Ewa coastal plain, Oahu, Hawaii: Pacific Science, v. 24, p. 529–542.

Giambelluca, T.W., Chen, Q., Frazier, A.G., Price, J.P., Chen, Y.-L., Chu, P.-S., Eischeid, J.K., and Delparte, D.M., 2013, Online rainfall atlas of Hawai‘i: Bulletin of the American Meteorological Society, www.doi.org/10.1175/BAMS-D-11-00228.1.

Giambelluca, T.W., Nullet, M.A., and Schroeder, T.A., 1986, Rainfall atlas of Hawai‘i: Hawai‘i Department of Land and Natural Resources Division of Water and Land Development Technical Report R76, 267 p.

Giambelluca, T.W., and Schroeder, T.A., 1998, Climate, *in* Juvik, S.P., and Juvik, J.O., eds., Atlas of Hawai‘i (3d ed.): Honolulu, University Press of Hawai‘i, 333 p.

Gingerich, S.B., 1999a, Ground-water occurrence and contribution to streamflow, Northeast Maui, Hawaii: U.S. Geological Survey Water-Resources Investigations Report 99–4090, 69 p., 1 plate.

Gingerich, S.B., 1999b, Ground-water and surface water in the Haiku area, East Maui, Hawaii: U.S. Geological Survey Water-Resources Investigations Report 98–4142, 38 p.

Gingerich, S.B., 1999c, Estimating transmissivity and storage properties from aquifer tests in the Southern Lihue Basin, Kauai, Hawaii: U.S. Geological Survey Water-Resources Investigations Report 99–4066, 33 p.

Gingerich, S.B., 2008, Ground-water availability in the Wailuku area, Maui, Hawai‘i: U.S. Geological Survey Scientific Investigations Report 2008–5236, 95 p.

Gingerich, S.B., and Engott, J.A., 2012, Groundwater availability in the Lahaina District, west Maui, Hawai‘i: U.S. Geological Survey Scientific Investigations Report 2012–5010, 90 p.

Harbaugh, A.W., 2005, MODFLOW-2005, The U.S. Geological Survey modular ground-water model—the Ground-Water Flow Process: U.S. Geological Survey Techniques and Methods 6-A16, variously p.

Hirashima, G.T., 1962, Effect of the Haiku Tunnel on Kahaluu Stream, Oahu, Hawaii, *in* Short papers in geology and hydrology, articles 60–119: U.S. Geological Survey Professional Paper 450–C, p. C118–C117.

Hunt, C.D., Jr., 1996, Geohydrology of the Island of Oahu, Hawaii: U.S. Geological Survey Professional Paper 1412–B, 54 p.

Hunt, C.D., Jr., 2007, Ground-water nutrient flux to coastal waters and numerical simulation of wastewater injection at Kihei, Maui, Hawaii: U.S. Geological Survey Scientific Investigations Report 2006–5283, 69 p.

Izuka, S.K, 2006, Effects of irrigation, drought, and groundwater withdrawals in ground-water levels in the southern Lihue Basin, Kauai, Hawaii: U.S. Geological Survey Scientific Investigations Report 2006–5291, 42 p.

Izuka, S.K., Engott, J.A., Bassiouni, M., Johnson, A.G., Miller, L.D., Rotzoll, K., and Mair, A., 2018, Volcanic aquifers of Hawai‘i—hydrogeology, water budgets, and conceptual models (ver. 2, March 2018): U.S. Geological Survey Scientific Investigations Report 2015–5164, 158 p.

Izuka, S.K., and Gingerich, S.B., 1998, Groundwater in the southern Lihue basin, Kauai, Hawaii: U.S. Geological Survey Water-Resources Investigations Report 98–4031, 71 p.

Izuka, S.K., and Gingerich, S.B., 2003, A thick lens of fresh groundwater in the southern Lihue Basin, Kauai, Hawaii, USA: Hydrogeology Journal, v. 11, p. 240–248.

Izuka, S.K., and Oki, D.S., 2002, Numerical simulation of ground-water withdrawals in the southern Lihue Basin, Kauai, Hawaii: U.S. Geological Survey Water-Resources Investigations Report 01-4200, 54 p.

Juvik, J.O., and Nullet, D., 1995, Relationships between rainfall, cloud-water interception, and canopy throughfall in a Hawaiian montane forest, chap. 11 *of* Hamilton, L.S., Juvik, J.O., and Scatena, F.N., eds., Tropical montane cloud forests: New York, Springer-Verlag, p. 165–182.

Kauahikaua, J., 1993, Geophysical characteristics of the hydrothermal systems of Kilauea volcano, Hawai‘i: Geothermics, v. 22, no. 4, p. 271–299.

Kinoshita, W.T., and Okamura, R.T., 1965, A gravity survey of the island of Maui, Hawaii: Pacific Science, v. 19, p. 341–342.

Kuniansky, E.L., Gómez-Gómez, F., and Torres-González, S., 2004, Effects of aquifer development and changes in irrigation practices on ground-water availability in the Santa Isabel area, Puerto Rico: U.S. Geological Survey Water-Resources Investigations Report 2003–4303, 65 p.

Lau, L.S., and Mink, J.F., 2006, Hydrology of the Hawaiian Islands: Honolulu, University of Hawai‘i Press, 274 p.

Macdonald, G.A., 1972, Volcanoes: Englewood Cliffs, N.J., Prentice-Hall, 510 p.

Macdonald, G.A., Abbott, A.T., and Peterson, F.L, 1983, Volcanoes in the sea—The geology of Hawaii (2d ed.): Honolulu, University of Hawaii Press, 517 p.

Macdonald, G.A., Davis, D.A., and Cox, D.C., 1960, Geology and groundwater resources of the island of Kauai, Hawaii: Hawaii Division of Hydrography Bulletin 13, 212 p.

Macdonald, G.A., and Katsura, T., 1964, Chemical composition of Hawaiian lavas: Journal of Petrology, v. 5, part 1, p. 82–133.

Meyer, W., 2000, A reevaluation of the occurrence of ground water in the Nahiku area, East Maui, Hawaii: U.S. Geological Survey Professional Paper 1618, 81 p.

Meyer, W., and Presley, T.K., 2000, The response of the Iao aquifer to ground-water development, rainfall, and land-use practices between 1940 and 1998, island of Maui, Hawaii: U.S. Geological Survey Water-Resources Investigations Report 00–4223, 60 p.

Meyer, W., and Souza, W.R., 1995, Factors that control the amount of water that can be diverted to wells in a high-level aquifer, *in* Hermann, R., Back, W., Sidle, R.C., and Johnson, A.I., eds., Water resources and environmental hazards—Emphasis on hydrologic and cultural insight in the Pacific Rim: Proceedings of the American Water Resources Association Annual Summer Symposium, June 25–28, p. 207–216.

Mink, J.F., and Lau, L.S., 1980, Hawaiian groundwater geology and hydrology, and early mathematical models: University of Hawaii, Water Resources Research Center Technical Memorandum Report 62, 74 p.

Moore, J.G., 1987, Subsidence of the Hawaiian Ridge, *in* Decker, R.W., Wright, T.L, and Stauffer, P.H., eds., Volcanism in Hawaii: U.S. Geological Survey Professional Paper 1350, v. 1, p. 85–100.

Moore, R.B., and Trusdell, F.A., 1993, Geology of Kilauea volcano: Geothermics, v. 22, p. 243–254.

Nichols, W.D., Shade, P.J., and Hunt, C.D., 1996, Summary of the Oahu, Hawaii, Regional Aquifer-System Analysis: U.S. Geological Survey Professional Paper 1412–A, 61 p.

Oki, D.S., 1998, Geohydrology of the central Oahu, Hawaii, ground-water flow system and numerical simulation of the effects of additional pumping: U.S. Geological Survey Water-Resources Investigations Report 97–4276, 132 p.

Oki, D.S., 1999, Geohydrology and numerical simulation of the ground-water flow system of Kona, Island of Hawaii: U.S. Geological Survey Water-Resources Investigations Report 99–4070, 49 p.

Oki, D.S., 2005, Numerical simulation of the effects of low-permeability valley-fill barriers and the redistribution of ground-water withdrawals in the Pearl Harbor Area, Oahu, Hawaii: U.S. Geological Survey Scientific Investigations Report 2005–5253, 111 p.

Palmer, H.S., 1927, The geology of the Honolulu artesian system: Supplement to the Report of the Honolulu Sewer and Water Commission, 68 p.

Reilly, T.E., Dennehy, K.F., Alley, W.M., and Cunningham, W.L., 2008, Ground-Water Availability in the United States: U.S. Geological Survey Circular 1323, 70 p., http://pubs.usgs.gov/circ/1323/.

Rotzoll, K., 2012, Numerical simulation of flow in deep open boreholes in a coastal freshwater lens, Pearl Harbor Aquifer, O‘ahu, Hawai‘i: U.S. Geological Survey Scientific Investigations Report 2012–5009, 39 p.

Rotzoll, K., and El-Kadi, A.I., 2007, Numerical ground-water flow simulation for Red Hill fuel storage facilities, NAVFAC Pacific, Oahu, Hawaii: University of Hawaii, Water Resources Research Center [prepared for TEC Inc.], 74 p.

Rotzoll, K., and El-Kadi, A.I., 2008, Estimating hydraulic conductivity from specific capacity for Hawaii aquifers, USA: Hydrogeology Journal, v. 16, p. 969–979.

Rotzoll, K., El-Kadi, A.I, and Gingerich, S.B., 2007, Estimating hydraulic properties of volcanic aquifers using constant-rate and variable-rate aquifer tests: Journal of the American Water Resources Association, v. 43, p. 334–345.

Rotzoll, K., and Fletcher, C.H., 2013, Assessment of groundwater inundation as a consequence of sea-level rise: Nature Climate Change, v. 3, no. 5, p. 477–481.

Rotzoll, K., and Izuka, S.K., 2021, MODFLOW-2005 and SWI2 models for assessing groundwater availability in volcanic aquifers on Kaua‘i, O‘ahu, and Maui, Hawai‘i: U.S. Geological Survey data release, https://doi.org/10.5066/P9K4DK2P.

Rotzoll, K., Oki, D.S., and El-Kadi, A.I., 2010, Changes of freshwater-lens thickness in basaltic island aquifers overlain by thick coastal sediments: Hydrogeology Journal, v. 18, p. 1425–1436.

Scholl, M.A., Gingerich, S.B., and Tribble, G.W., 2002, The influence of microclimates and fog on stable isotope signatures used in interpretation of regional hydrology—East Maui, Hawaii: Journal of Hydrology, v. 264, p. 170–184.

Sherrod, D.R., Sinton, J.M., Watkins, S.E., and Brunt, K.M., 2007, Geologic map of the State of Hawai‘i: U.S. Geological Survey Open-File Report 2007–1089, 83 p., 8 plates, scales 1:100,000 and 1:250,000, with GIS database.

Soroos, R.L., 1973, Determination of hydraulic conductivity of some Oahu aquifers with step-drawdown test data: Honolulu, University of Hawaii, M.S. thesis, 239 p.

Souza, W.R., 1983, Exploratory drilling and aquifer testing at the Kipahulu District Haleakala National Park, Maui, Hawaii: U.S. Geological Survey Water-Resources Investigations Report 83–4066, 21 p.

Souza, W.R., and Voss, C.I., 1987, Analysis of an anisotropic coastal aquifer system using variable-density flow and solute transport simulation: Journal of Hydrology, v. 92, p. 17–41.

Stearns, H.T., 1940, Supplement to the geology and groundwater resources of the island of Oahu, Hawaii: Hawaii Division of Hydrography Bulletin 5, 164 p.

Stearns, H.T., 1946, Geology of the Hawaiian Islands: Hawai‘i Division of Hydrography Bulletin 8, 106 p.

Stearns, H.T., 1966, Geology of the State of Hawaii: Palo Alto, California, Pacific Books, 266 p.

Stearns, H.T., and Macdonald, G.A., 1942, Geology and ground-water resources of the island of Maui, Hawaii: Hawai‘i Division of Hydrography Bulletin 7, 344 p.

Stearns, H.T., and Vaksvik, K.N., 1935, Geology and groundwater resources of the Island of Oahu, Hawaii: Hawaii Division of Hydrography Bulletin 1, 479 p.

Takasaki, K.J., and Mink, J.F., 1985, Evaluation of major dike-impounded ground-water reservoirs, Island of Oahu: U.S. Geological Survey Water-Supply Paper 2217, 77 p.

U.S. Census Bureau, 2011, 2010 Census—Hawaii Profile: U.S. Census Bureau web page, accessed February 10, 2012, at http://www2.census.gov/geo/maps/dc10_thematic/2010_Profile/2010_Profile_Map_Hawaii.pdf.

U.S. Geological Survey, 2012, The National Map national hydrography dataset: U.S. Geological Survey web page, accessed February 12, 2013, at http://nhd.usgs.gov/data.html;ftp://nhdftp.usgs.gov/DataSets/Staged/States/FileGDB_C/.

U.S. Geological Survey, 2019, National Water Information System: U.S. Geological Survey web interface, accessed June 20, 2019, at http://doi.org/10.5066/F7P55KJN.

University of Hawai‘i, 2011, Main Hawaiian Islands Multibeam Bathymetry Synthesis: Hawaii Mapping Research Group, School of Ocean and Earth Science and Technology, University of Hawai‘i at Mānoa, accessed March 22, 2013, at http://www.soest.hawaii.edu/hmrg/multibeam/grids.php.

Wahl, K.L., and Wahl, T.L., 1995, Determining the flow of Comal Springs at New Braunfels, Texas, *in* Proceedings of Texas Water ’95, A Component Conference of the First International Conference on Water Resources Engineering [August 16–17, 1995, San Antonio, Texas]: American Society of Civil Engineers, p. 77–86.

Walker, G.P.L., 1987, The dike complex of Koolau volcano, Oahu—Internal structure of a Hawaiian rift zone, *in* Decker, R.W., Wright, T.L, and Stauffer, P.H., eds., Volcanism in Hawaii: U.S. Geological Survey Professional Paper 1350, v. 2, p. 961–993.

Wang, H.F., and Anderson, M.P., 1982, Introduction to groundwater modeling—Finite difference and finite element methods: New York, W.H. Freeman and Company, 237 p.

Watermark Numerical Computing, 2014, Groundwater Data Utilities Part B: Program Descriptions, 381 p, accessed November 15, 2015, at http://www.pesthomepage.org/Downloads.php#hdr7.

Wentworth, C.K., 1928, Principles of stream erosion in Hawaii: Journal of Geology, v. 36, no. 5, p. 385–410.

Whittier, R.B., Rotzoll, K., Dhal, S., El-Kadi, A.I., Ray, C., Chen, G., and Chang, D., 2004, Hawaii source water assessment program report—Volume II, Island of Hawaii source water assessment program report: Honolulu, University of Hawai‘i at Mānoa Water Resources Research Center, 65 p.

Williams, J.A., and Soroos, R.L., 1973, Evaluation of methods of pumping test analysis for application to Hawaiian aquifers: University of Hawaii Water Resources Research Center Technical Report 70, 159 p.

Wolfe, E.W., and Morris, J., 1996, Geologic map of the Island of Hawaii: U.S. Geological Survey IMAP Series I–2524–A, scale 1:100,000.

Wong, M.F., 1994, Estimation of magnitude and frequency of floods for streams on the island of Oahu, Hawaii: U.S. Geological Survey Water-Resources Investigations Report 94–4052, 37 p.

Wu, I.-P., 1969, Hydrograph study and peak discharge determination of Hawaiian small watersheds; Island of Oahu: University of Hawai‘i Water Resources Research Center Technical Report no. 30, 85 p.

Yeung, C.W., and Fontaine, R.A., 2007, Natural and diverted low-flow duration discharges for streams affected by the Waiāhole Ditch System, windward O‘ahu, Hawai‘i: U.S. Geological Survey Scientific Investigations Report 2006–5285, 75 p.

Moffett Field Publishing Service Center, California
Manuscript approved October 30, 2020
Edited by Monica Erdman
Illustration support by Cory Hurd and JoJo Mangano
Layout by JoJo Mangano

ISSN 2328-0328 (online)
https://doi.org/10.3133/sir20205126